University of Kentucky
UKnowledge

Theses and Dissertations--Chemical and Materials Engineering

Chemical and Materials Engineering

2012

NOVEL DESIGN OF FUNCTIONALIZED CARBON NANOTUBE ELECTRODES AND MEMBRANES FOR FUEL CELLS AND ENERGY STORAGE

Xin Su
University of Kentucky, suxin81@gmail.com

Right click to open a feedback form in a new tab to let us know how this document benefits you.

Recommended Citation
Su, Xin, "NOVEL DESIGN OF FUNCTIONALIZED CARBON NANOTUBE ELECTRODES AND MEMBRANES FOR FUEL CELLS AND ENERGY STORAGE" (2012). *Theses and Dissertations--Chemical and Materials Engineering*. 5.
https://uknowledge.uky.edu/cme_etds/5

This Doctoral Dissertation is brought to you for free and open access by the Chemical and Materials Engineering at UKnowledge. It has been accepted for inclusion in Theses and Dissertations--Chemical and Materials Engineering by an authorized administrator of UKnowledge. For more information, please contact UKnowledge@lsv.uky.edu.

STUDENT AGREEMENT:

I represent that my thesis or dissertation and abstract are my original work. Proper attribution has been given to all outside sources. I understand that I am solely responsible for obtaining any needed copyright permissions. I have obtained and attached hereto needed written permission statements(s) from the owner(s) of each third-party copyrighted matter to be included in my work, allowing electronic distribution (if such use is not permitted by the fair use doctrine).

I hereby grant to The University of Kentucky and its agents the non-exclusive license to archive and make accessible my work in whole or in part in all forms of media, now or hereafter known. I agree that the document mentioned above may be made available immediately for worldwide access unless a preapproved embargo applies.

I retain all other ownership rights to the copyright of my work. I also retain the right to use in future works (such as articles or books) all or part of my work. I understand that I am free to register the copyright to my work.

REVIEW, APPROVAL AND ACCEPTANCE

The document mentioned above has been reviewed and accepted by the student's advisor, on behalf of the advisory committee, and by the Director of Graduate Studies (DGS), on behalf of the program; we verify that this is the final, approved version of the student's dissertation including all changes required by the advisory committee. The undersigned agree to abide by the statements above.

Xin Su, Student

Dr. Bruce J Hinds, Major Professor

Dr Stephen E. Rankin, Director of Graduate Studies

NOVEL DESIGN OF FUNCTIONALIZED CARBON NANOTUBE ELECTRODES AND MEMBRANES FOR FUEL CELLS AND ENERGY STORAGE

DISSERTATION

A dissertation submitted in partial fulfillment of the
requirements for the degree of Doctor of Philosophy in the
College of Business and Economics
at the University of Kentucky

By
Xin Su

Lexington, Kentucky

Director: Dr. Bruce J Hinds, Professor of Material Engineering

Lexington, Kentucky

2011

Copyright © Xin Su 2011

ABSTRACT OF DISSERTATION

NOVEL DESIGN OF FUNCTIONALIZED CARBON NANOTUBE ELECTRODES AND MEMBRANES FOR FUEL CELLS AND ENERGY STORAGE

A novel electrochemical method to generate nm-scale bubbles at the tips of CNTs can temporarily block the membrane. A 92% blocking efficiency is achieved when the bubbles are stabilized in 30-60 nm diameter 'wells' at the tips of CNTs. This well is formed by the electrochemical oxidation of the conductive CNTs partially into the polymer matrix of the membrane. Meanwhile, the nanoscale bubbles can be removed with 0.004 atm pressure to recover the transport through the CNT membrane. The CNT membrane with nanoscale bubble valve system was used to demonstrate electrochemical energy storage.

Uniform ultrathin Pt films were electrodeposited onto an aligned array of carbon nanotubes (CNTs) for high-area chemically stable methanol fuel cell anodes. Electrochemical treatment of the graphitic CNT surfaces by diazonium benzoic acid allowed for uniform Pt electroplating. The mass activity of the Pt thin film can reach 400 A/g at a scan rate of 20 mV/s and in a solution of 1 M CH_3OH/0.5 M H_2SO_4. A novel programmed pulse potential at 0 V was also seen to nearly eliminate the effects of carbon monoxide poisoning on catalyst Pt. Furthermore, the Pt monolayer was deposited on buckypaper by replacing the precursor Cu monolayer coated on CNTs by the underpotential deposition. The electrochemical surface modification of graphite CNTs by fluorinated benzoic acid was critical to coordinate Cu ions for monolayer formation. The mass activity of the monolayer can be improved to the record value of 2711 A/g. This is about 13 times higher than that of the ~10 nm thick Pt film coated on MWCNTs. Besides the high mass activity, the Pt monolayer coated on buckypaper can be used as catalyst for fuel cells with several advantages such as low cost, high surface area, flexibility, mechanical robustness and enhanced pressure flow.

Finally, a new strategy has been developed toward electrochemical water oxidation with Ir complexes catalyst, which was grafted on buckypaper by direct binding to enhance catalyst activity. The TOF (turn over frequency) of the Ir catalyst for water splitting was 7.9 s^{-1} at the constant potential of 1.4 V vs Ag/AgCl.

KEYWORDS: Pt, monolayer, fuel cell, CNT membrane, energy storage

Xin Su

NOVEL DESIGN OF FUNCTIONALIZED CARBON NANOTUBE ELECTRODES AND MEMBRANES FOR FUEL CELLS AND ENERGY STORAGE

By

Xin Su

Dr Bruce J. Hinds
Director of Dissertation

Dr Stephen E. Rankin
Director of Graduate Studies

7th December 2011

Dedicated to my parents who always guide and support me in my whole life

ACKNOWLEDGEMENTS

At first of all, all of my gratitude goes to my advisor Dr. Bruce J Hinds, for his excellent guidance, support during my whole Ph.D. work. I would like to thanks the funding provided by the Department of Energy (DOE), National Science Foundation (NSF), and National Institutes of Health (NIH).

I am thankful to faculties Dr. John Balk, Dr. Chuck May and stuffs Mr. Larry Rice, Dr. Alan Dozier, Dr. Jia Ye, Mr. Brian Wajdyk of Electron Microscopy Center and Center for Nanoscale Science and Engineering (CeNSE) for training and providing access to the all of facilities during my PhD work. I would like to thank faculty Dr. Rodney Andrews and staff Dr. Dali Qian from Center for Applied Energy and Research (CAER) for supporting to the carbon nanotube for the research work.

The helpful discussion from our group mates and cooperators including Dr. Ji Wu, Dr. Xinhua Sun, Xin Zhan, Dr. Mainak Majumder, Dr. Qingliu Wu, Dr. Karin Keis are appreciated here. I also thank the help and training from Dr. Ji Wu on CNTs membrane fabrication and synthesis of diazonium salt.

I would like to appreciate my entire advisory committee members: Dr. Yang Tse Cheng, Dr. John Balk, Dr Stephen E. Rankin, Dr. John P. Selegue for the interests, smart advises, support on my whole Ph.D. work.

My friends Fang Tang, Dr Fuqian Yang, Dr Yang Liu, Xin Hua, Lingbo Lu, Ping Yi and Yan Li *et al.* who I made in Lexington let my Ph.D. life here are not only valuable and but also wonderful and memorable.

TABLE OF CONTENTS

ACKNOWLEDGEMENTS iii

LIST OF TABLES vii

LIST OF FIGURES viii

Chapter 1: Introduction 1

1.1 Historical development and future of renewable energy 1

1.2 CNTs membrane for energy storage 4

1.2.1 Simulations about mass transport in CNT membrane 4

1.2.2 The advantages of the CNT membrane 6

1.2.3 The CNT membrane for chemical energy conversion and storage 8

1.2.4 The observations and applications of nanoscale bubbles 9

1.2.5 The membranes for electrochemical energy storage 10

1.3 Catalytic conversion for fuel cell 12

1.3.1 The methanol fuel cell 12

1.3.2 The catalyst Pt for fuel cell 14

1.3.3 The monolayer deposition by underpotential method 20

1.4 Catalytic conversion for water splitting 22

1.5 Goals of the Ph.D. work 24

Chapter 2 Nanoscale bubble valves on CNT membranes for chemical energy storage 39

2.1 Introduction 39

2.2 Experimental details and characterization methods 40

2.3 Results and discussion..... 43

2.4 Conclusion..... 47

Chapter 3: The MWCNT membrane used for electrochemical energy storage..... 61

3.1 Introduction 61

3.2 Experimental details and characterization methods 63

3.3 Results and discussion..... 65

3.4 Conclusion..... 69

Chapter 4: Catalytic activity of ultrathin Pt films on aligned carbon nanotube arrays 80

4.1 Introduction 80

4.2 Experimental details and characterization methods 82

4.3 Results and discussion..... 85

4.4 Conclusion..... 88

Chapter 5: Pt monolayer deposition onto carbon nanotube mats with high electrochemical activity 94

5.1 Introduction 94

5.2 Experimental details and characterization methods 96

5.3 Results and discussion..... 98

5.4 Conclusion..... 103

Chapter 6: Electrochemical catalytic water oxidation by buckypaper grafted Ir complexes 110

6.1 Introduction 110

6.2 Experimental details and characterization methods 111

6.3 Results and discussion 113

6.4 Conclusion 116

Chapter 7: Conclusion and future research direction 125

Reference 129

Vita 144

LIST OF TABLES

Table 2.1 A series of blocking efficiencies of nanoscale bubbles generated by the different potentials on a MWCNTs membrane, which is pretreated by electrochemical oxidization (5 mM $[Ru(bipy)_3]^{2+}$/0.05 M H_2SO_4 in feed side; deionized water in permeate side). 57

Table 2.2 A series of block efficiencies before/after that nanoscale bubbles on pretreated MWCNTs membrane, are removed by pressure gradient from bottom to top of membrane. (5 mM $[Ru(bipy)_3]^{2+}$/0.05 M H_2SO_4 in feed side; deionized water in permeate side)..... 60

Table 3.1 Ka for reaction equations: $Cl_2+H_2O=HCl+HClO$ and $H_2O+HClO=H_3O^{+}+ClO^{-}$ and the related concentrations of molecules and ions under the experimental conditions 72

Table 3.2 The related diffusion coefficient and the flux rate of HClO and $[Fe(CN)_6]^{3-}$ transport through the MWCNT membrane 73

Table 3.3 The related parameters for the Nernst equations for the cell reactions: 1) $HClO+H^{+}+Fe=Fe^{2+}+Cl^{-}+H_2O$ and 2) $Fe(CN)_6^{3-}+e=Fe(CN)_6^{4-}$ 74

Table 5.1 The relative parameters between the Pt monolayer coated on MWCNTs and porous Au 109

LIST OF FIGURES

Figure 1.1 The global population (a) and GDP (b) in last three centuries from 1700 to 2000 (The data adapted from the reference [5]) 25

Figure 1.2 The history and tendency of global energy demand from 1920 to 2050 (The figure adapted from reference [10]) 26

Figure 1.3 The total global CO_2 emissions in the last three centuries from 1700 to 2000 (The data adapted from [21]) 27

Figure 1.4 The percentage of renewable energy in total global energy consumption (The permission from reference of [27]) 28

Figure 1.5 Simulated flux of methane across a10 μm thick membrane as a function of the upstream pressure. The pressure difference maintains at 1.38 bars. (Adapted from the reference [45]) 29

Figure 1.6 The simulation results of water density distribution in carbon nanotube (red, sp^2 carbon parameters; blue, modified carbon-water interactions). (The permission from reference [39]) 30

Figure 1.7 SEM of aligned CNTs and schematic picture of CNT membrane (The figures adapted from reference [55]) 31

Figure 1.8 The schematic process of micro cutting for the CNT membrane fabrication . 32

Figure 1.9 The schematic pictures for charging and discharging process of electrochemical flow battery (Adapted from reference of [92]) 33

Figure 1.10 Schematic picture and related reactions of direct methanol fuel cell (a) and indirect methanol fuel cell (b) 34

Figure 1.11 The surface modification of CNTs for the improvement on dispersion of Pt nanoparticles 35

Figure 1.12 The schematic pictures for the surface modification of CNTs by electrochemical diazonium grafting 36

Figure 1.13 The schematic picture of Pt monolayer coated on porous Au(Reprinted with the permission from reference [159]) 37

Figure 1.14 The schematic process about the storage of solar energy by converting the solar energy to oxygen and hydrogen fuel 38

Figure 2.1 The schematic of the setup (a) for the electrochemical oxidation of MWCNTs to produce polymer wells and (b) testing approach for demonstrating nanoscale bubble blocking the diffusion through CNTs membrane 49

Figure 2.2 The mechanism about the nanoscale bubbles blocking the transport through MWCNTs membrane. (b), (c) the SEM top view images of the MWCNTs membrane before and after electrochemical oxidization 50

Figure 2.3 Optical images of MWCNTs membrane with and without electrochemical oxidization 51

Figure 2.4 The UV-vis spectra of the MWCNTs membrane before and after electrochemical oxidization with the air as the reference 52

Figure 2.5 Optical images of the big bubbles generated on the MWCNT membrane at constant potential of -1.2 V vs Ag/AgCl 53

Figure 2.6 The calibration curve for the relationship between the concentration of $[Ru(bipy)_3]^{2+}$ and the absorbance of the UV 54

Figure 2.7 The relationship between the total amounts of $[Ru(bipy)_3]^{2+}$ transported through membrane and screening time, when the constant potential (-1.2 V vs Ag/AgCl) is applied on the membrane. 55

Figure 2.8 Cyclic voltamograms of the MWCNTs membrane in a solution of 0.05 M H_2SO_4/5 mM $[Ru(bipy)_3]^{2+}$, at a scan rate of 100 mv/s and with set up shown in figure 2.1b..... 56

Figure 2.9 The schematic picture for the surface modification of polymer wells for the control experiment 58

Figure 2.10 The blocking efficiencies of nanoscale bubbles depend on the time of sine potential applied on CNTs membrane..... 59

Figure 3.1 The schematic set up and mechanism of MWCNT membrane for the redox flow battery 71

Figure 3.2 (a) (b) SEM image of membrane bottom (CNTs sputtered with Au) and top (porous polymer wells sputtered with Au). The cross section image of CNT membrane before/after electrolessly depositing Au into polymer wells. 75

Figure 3.3 The self discharge rate of the battery by storing $HClO/Cl_2$ (Δ) in reservoir and by storing Fe^{2+} (□) in the reservoir..... 76

Figure 3.4 The self discharge rate of the battery by storing $HClO/Cl_2$ (Δ) in reservoir and by storing $Fe(CN)_6^{3-}$(□) in the reservoir from the calculations and the experiments. 77

Figure 3.5 The current vs time during charging process of the CNT membrane at 1.2 V with the feed solution of 5 mM $FeCl_2$ and deionized water in permeate side. 78

Figure 3.6 The self discharge of the flow battery with (□)/without (▲) nanoscale bubble as valve under the diffusion conditions 79

Figure 4.1 Schematic of the process for preparing the aligned CNT array electrodes 89

Figure 4. 2 SEM images of aligned CNT electrodes after epoxy transfer (a) top view; (b) cross sectional view. 90

Figure 4. 3 (a) SEM image of Pt particles electrodeposited on the untreated CNTs; (b) HRTEM image of CNT away from large Pt particles showing absence of thin Pt layer; (c) SEM image of Pt electrodeposited onto the CNTs with surface treatment of carboxyl groups from electrochemical diazonium grafting; (d) HRTEM image of uniform ~2 nm thick Pt coating on treated CNTs. 91

Figure 4.4 (A) Cyclic Voltammogram of Pt nanofilm deposited on CNTs grafted with carboxyl groups in a solution of 0.5 M H_2SO_4 and at a scan rate of 100 mV/s; (B) Cyclic Voltammogram of Pt nanofilm (blue) and Pt nanoparticles (red) on untreated CNTs in a solution of 1 M CH_3OH/0.5 M H_2SO_4 and at a scan rate of 20 mV/s. Insert figure is the experiment (red) and calculation (blue) showing Randles–Sevcik behavior of peak currents ratios vs scan rates from 20 mv/s to 100 mv/s. 92

Figure4. 5 (A) The steady state current densities of methanol oxidation vs time (i) applying programmed pulse potential， with a recovery time of t=7 s, (ii) applying constant potential of 0.7 V (vs Ag/AgCl) on the sample; (B) Diagram of programmed pulse potentials with recovery pulses for Pt catalyst activity; (C) Steady state current densities of methanol oxidation vs. the recovery time of programmed pulse potentials.. 93

Figure 5.1 Schematic illustration of the fabrication procedure for Pt monolayer coating onto MWCNT mats..... 104

Figure 5.2 Cyclic Voltammograms on buckypaper in the ethanol solution of 0.1 M $LiClO_4$/ 3 mM 4-amino-2,3,5,6-tetrafluorobenzoic acid, the 1st (■), 14th (□),17th (●) and 20th scans (○) cycles at the scan rate of 20 mV/s. The reaction equation for surface modification. 105

Figure 5.3 Cu stripping current vs applied potentials. The samples are Cu deposited MWCNTs with/without surface modification under different conditions(at 0 V 480 s (■), at 0 V 2400 s (○), at -0.1 V 480 s (Δ), background (▲) on MWCNTs with surface modification, 0 V 480 s on bare MWCNTs (●)) 106

Figure 5.4 (a) SEM image and (b) TEM image of Pt film coated on MWCNTs by repeating coating, (c) SEM image,(d) TEM image in bright field and (e) STEM image in dark field of the Pt monolayer coated on MWCNTs, (f) EDS of Pt thick film coated on MWCNT, (g) XPS of Pt monolayer coated on MWCNTs. 107

Figure 5.5 (a) Cyclic Voltammogram of Pt monolayer (■) coated on MWCNTs of buckypaper/ bare MWCNTs (○) in a solution of 0.5 M H_2SO_4 and at a scan rate of 100 mV/s; (b) Cyclic Voltammogram of Pt monolayer (■) and film (○) coated on MWCNTs of buckypaper in a solution of 1 M CH_3OH/0.5 M H_2SO_4 and at a scan rate of 20 mV/s 108

Figure 6.1 The schematic processes of direct binding and indirect binding for loading the Ir catalyst on glassy carbon..... 118

Figure 6.2 the CVs for catalyst activity of the Ir complex catalyst, which is directly diazonium grafting on buckypaper (▲) and CV of the Ir complex catalyst which is indirectly binding to buckypaper by EDC coupling (■) in buffer solution pH=5, I=0.1 M CH_3COOH/CH_3COONa 119

Figure 6.3 XPS full spectra of glassy carbon electrodes loaded with 1 by EDC coupling (a) and diazonium grafting (b). (This was done by UNC) 120

Figure 6.4 Current vs time during electrochemical diazonium grafting the 1st Ir complex catalyst on buckypaper..... 121

Figure 6.5 The CVs for catalyst activity of the Ir complex catalyst, which is directly diazonium grafted on buckypaper (▲) and CV of bare buckypaper (□) in buffer solution pH=5, I=0.1 M CH_3COOH/CH_3COONa..... 122

Figure 6.6 (a) Current during constant potential electrolysis at 1.4 V vs Ag/AgCl in buffer solution pH=5, I=0.1 M CH_3COOH/CH_3COONa and (b) the accompanying generation of O_2 detected in solution for 1 loaded onto CNTs by diazonium grafting. The amount of O_2 corresponding to 100% saturation is generated at 129% current efficiency, based on integration of the current up to this point..... 123

Figure 6.7 The CV of bare CNTs, initial CV of CNTs with grafted Ir complex and the CV the of CNTs with grafted Ir complex after 17 h time test at 1.4 V vs Ag/AgCl in buffer solution pH=5, I=0.1 M CH_3COOH/CH_3COONa. 124

Chapter 1: Introduction

1.1 Historical development and future of renewable energy

Due to the limited reserves of fossil fuels, the increasing demand of human society for energy and the environmental protection, renewable energy has been considered as the solution for the challenge of human society on growing energy demand.[1, 2] It is well known that the fossil fuels take million years to form and thus have limited reserves. However, their consumption rate is much faster than their generation rate in the age of industry, which started after industry revolution at late 18th century.[3] During the 20st century the global energy demand increases 3% annually, due to the rapid growth of global population and economy.[4] As shown in figure 1.1 (a),(b), in last three centuries, the global population and GDP are growing at a much faster rate than before.[5] As a result, the global energy demand in 2000 is more than 10 times of that in 1920.[6, 7] The global energy demand will continue to increase in the future.[3, 8, 9] The history and tendency of global energy demand from 1920 to 2050 is shown in figure 1.2.[10] The major oil companies claimed that there were enough fossil oil reserves for decades.[11, 12] What can humans do after such reserves are depleted? In addition, to sustain a decent life for a fast growing population, extra fossil resources are required to secure sufficient food and organic raw materials. It is a definite myopia for human beings to obtain 'cheap energy' just by burning the limited fossil fuel. This will be disastrous to the human society after the reserves of fossil fuels are depleted after decades without any substitutes or alternatives. Thus the technologies on renewable energy have attracted intensive research attention since several decades ago, especially after energy crisis in 1970s.[1, 2, 13-17] Furthermore the environmental problems like 'global warming' request human beings

to replace fossil fuels with renewable energy to limit the total emission of greenhouse gas such as CO_2.[18, 19] From 1880 to 2000, the global land-ocean average temperature has already increased by 0.8 ℃ and will continue to increase at a very rapid rate.[20] This is mainly due to human activities on deforestation and fossil fuels burned for energy, which will generate more and more CO_2 in air. As shown in figure1.3, the total global emission of greenhouse gas CO_2 increases faster and faster in last three centuries.[21] The global warming can result in various environmental and climate problems like an increase of the sea level, more extreme weather events and change of water distribution. These will bring significant impact on the global economy, agriculture and wild species.[22] For example, if the sea level increased, the prosperous metropolises like New York, Los Angeles, Tokyo Shanghai etc. around the coast of world would have seriously flooding. Extreme weather conditions will dramatically reduce the agricultural harvest and significantly increase foods' cost. The wild species will be extinct and the desert will expand due to the rapid change of water distribution. Meanwhile burning the fossil resource to get energy can also cause serious atmospheric and water pollutions. For example, chemicals like sulfur oxide, nitride oxide generated during burning the fossil resource to get energy can cause acid rain.[23] It will lead to the damage of plants, decay of statues, sculptures and building, and harm to human health.

Due to the above-mentioned reasons, the research on renewable energy has been significantly promoted and attracted much more attention than ever before. For instance, the wind power, one type of clean renewable energy resources, grows at ~30% annually in the past five years.[24-26] As shown in figure 1.3, 19% of global final energy consumption is from renewable energy in 2008.[27] However, 68% of renewable energy is

from traditional biomass, most of which has relative lower efficiency of energy conversion and also emits lots of greenhouse gas during burning them. The new clean renewable energy with relative high efficiency on the conversion like solar/wind/biomass/geothermal/hydro power generation only accounts for 32% of the renewable energy. Therefore, much more improvement needs to be done for expanding the applications of clean renewable energy like solar energy/wind energy/biomass and hydro power generation. Only by doing so, the renewable energy can finally replace the fossil fuel energy in the future when the limited fossil fuel reserve runs out or human beings need to reduce total emission of CO_2. Boosted by the fast advancing technologies and its strong demand, the global market of renewable energy for electricity grow at 20~30% per year recently and it is predicted to supply 60% of the demand on electricity by 2050.[28-31]

Referred to science and engineering for renewable energy, improving the technologies for conversion and storage of renewable energy is highly demanded. The development of the human society and environmental protection requests clean and cheap energy. However, the instability and low reliability of clean renewable energy like wind power and solar energy limit its practical applications.[32-37] For example, the solar energy from 1h sunshine to earth is enough for the whole energy consumed by human in the entire year. However the distribution of solar energy is varied by day of year, latitude, orientation and intermittency of day/night cycles etc. [38] This is similar to the wind power. It is well known that the energy for industry and other application require a stable and convenient supply. Thus cheap and convenient energy conversion and storage for the solar energy, which can convert the daytime solar energy to a continuous stable

electricity supply for industry, is obviously important for large scale application. Due to the reasons above, technologies related to renewable energy conversion and storage are of critical importance. The research focus of this dissertation is on applying carbon nanotube (CNT) membranes and CNT array coated with catalysts for energy storage and conversion. CNTs have unique physical properties of fast mass transport, chemical inertness, high electrical conductivity, and chemical surface modification that make them unique platforms for electrochemical energy conversion.

1.2 CNTs membrane for energy storage

1.2.1 Simulations about mass transport in CNT membrane

Carbon nanotubes (CNTs) are allotropes of carbon with the interesting nanostructure which has a high length over diameter ratio. Due to their novel properties of extraordinary strength, unique electrical properties, efficient heat conductivity, there is extensive research focused on them. Another interesting property of CNTs is the atomically smooth and hydrophobic interface of the nanotubes. Scientists are very interested in the mass transport like gas, DNA, water, etc. in this type of nanotube. Therefore, a series of the related simulation with the corresponding experiments have been done [39-44].

From the simulation of mass transport through the CNTs, it was shown that light gases (H_2,CH_4) could transport orders of magnitude faster through CNTs than other traditional pores like zeolite pores.[45] The predicted flux rate of methane transport through the CNTs and zeolite under 1.38 bar of pressure difference is shown in Figure 1.5. According to the simulations of Newsome *et al.* and Verweij *et al.*, other gases like

Ar, N_2 and CO_2 were also transported very quickly in CNT.[46, 47] The fast gas transport in CNTs is mainly due to the frictionless surface of CNT, which is highly rigid graphene plane with non-polar carbon network. Because of the fast transport of gas in CNTs, the surface resistance for gas to enter and leave nanotubes is more important for the whole process of gas transport through CNTs than through traditional pores like zeolite. The related simulation indicated that surface resistance for gas molecules to enter and leave the tubes was much smaller for long tubes (5~10 μm) than short ones.[46] For other factors that influence the transport rate of gas transport through CNTs, Lee *et al.* performed the simulation on the flux rate of gas through the different types of single wall carbon nanotubes. They found that the transport rate of CH_4 through the single wall carbon nanotube depended on the diameter of the CNT but not on the helical symmetry of the CNT. The movement of the molecules in CNT was a bouncing motion.[48] Meanwhile the transport rates of gas through rigid and flexible CNT under pressure of 1 bar were found to be similar in the simulation of Chen et al..[49] All of these simulations concluded that transport rates of gases through the CNTs were much faster comparing with those through the conventional nanopores. The result of these simulations about enhancement of gas transport CNTs has been confirmed by the corresponding experimental result. In these experiments, the gas transport rate in CNTs is much faster than that predicted by classic Knudsen diffusion model for gas transport in traditional material pores.[47, 50] Even the simulation of long chain polymer molecule through the CNT demonstrated that the transport rate of the molecule in CNT is a few magnitude orders larger than that in zeolite pore.[51] Not only have the simulations about the gas transport through the CNTs been done,[46, 52, 53] but also the simulations about liquids like

water transport CNTs have been done.[39, 54] Hummer *et al.* demonstrated that the transport of water in CNTs was a pulse-like transmission through the nanotube due to the tight hydrogen-bonding network inside the tube. From the simulation results shown in Figure 1.6, the rigid nonpolar structure of carbon nanotube could reduce the attraction between the tube wall and water to minute levels. This would result in the sharp, two-state transitions between empty and filled states on a nanosecond scale. Water would slip in the CNTs, which was much faster than the traditional transport of water in nano-channels.[39] The velocity of water flow in a single wall nanotube was about 90 cm/s.[40] Another simulation confirmed that the fluid flow in a carbon nanotube under pressure could get a large slip length when the pressure was applied along the axis of the nanotube.[44] The slip velocity of fluid in a carbon nanotube with the diameter of 1.2 nm could reach 120 m/s. Therefore, from the simulations, the mass transport of water and light gases through CNTs can be enhanced due to CNTs' atomically smooth and hydrophobic interface.

1.2.2 The advantages of the CNT membrane

The best physical system to test whether there are enhanced fluid flow effects in CNTs is the membrane geometry. In this geometry a large number of CNTs can pass across an impermeable structure allowing macroscopically measurable quantities of analyte to pass only through the cores of CNTs. The first report of CNT membranes was published by Hinds' group.[55] Chopra *et al.* used polystyrene to fill up the gap between the aligned CNTs, and then plasma etching to open the tip of CNTs to form the membrane.[40, 55] The aligned CNTs and schematic structure of CNT membrane is shown in figure 1.7. The CNT membranes show dramatically (>10,000 Xs) enhanced

fluid flow/mass transport.[40] This is mainly due to the atomically smooth and hydrophobic interior surface of CNTs as predicted by theory.

Holt et al. later independently confirmed the pressure-driven transport of water through the sub-2nm CNTs was enhanced. The transport rate is about 3 magnitude orders faster than that of no-slip hydrodynamic flow.[42] Whitby *et al.* reported that the flow of water through carbon nanopipes with a diameter of 43nm is about the 34 times theoretical prediction.[56] Meanwhile Kim *et al.* reported a fast and simple method to fabricate the CNT membrane with the combination of self-assembling and filtration.[50] Then a significant improvement in fabrication of CNT membrane was achieved by Hinds' group again. The schematic process about the new facile way for membrane fabrication with micro cutting is shown in figure1.8. To describe it briefly, aligned CNTs were prepared via a chemical vapor deposition (CVD).[57] Next, epoxy resin and hardener were thoroughly mixed, which was employed to fabricate epoxy/CNTs composite using a casting method. As-prepared CNTs-Epoxy composite was then appropriately cured before being cut into CNTs membranes using a microtome equipped with a glass blade. Finally, the residual epoxy on the tips of CNTs was removed by H_2O plasma oxidation. Thousands of CNT membranes could be fabricated per day by this new method, the size of membrane is on the order of 0.1 cm^2, thus requiring significant advances in scale-up process.[58] Furthermore, with advancement of CNT membrane fabrication methods, a series of the reports about their applications in drug delivery, water desalination and bio separation have been published.[58-63]

The extensive research has been done based on CNT membranes are due to their unique and fantastic properties for great potential in application. In summary, there are

three major advantages of the CNT membranes. 1) Atomically smooth interface of CNT enhance fluid flow through the membrane by 3-4 orders of magnitude. 2) The CNTs in the membrane are conductive. The CNT membranes can be used as an electrode for electrochemical reactions and pore entrances of the CNTs can be electrochemical modified for selective transport. 3) The process of cutting CNTs means that chemistry can be precisely placed at the entrance to pores. For example, the pores of CNT membrane were modified with charged groups, which can be gatekeepers for the transport of ion through the membrane.[58, 64] By having only a monolayer of gatekeeper chemistry and mass enhanced transport, the CNT membranes offer an opportunity to solve the long-standing trade-off between selectivity and flow rate.

1.2.3 The CNT membrane for chemical energy conversion and storage

The three unique features of CNT membrane mentioned above can be applied to develop broad new applications from drug delivery to bio separations.[58, 60, 63] For this dissertation work, a novel device design is to use the membrane as an active element in electrochemical storage system. Briefly a low-energy chemical can be electrochemically converted to a high energy chemical at the storage side of the membrane. The reservoir side of the membrane can be closed by an active gatekeeper or bubble generation for long-term energy storage. Finally the flow can be reversed and the electrochemical energy recovered. There are two fundamental questions to address in this dissertation to realize such a devise. 1) Can a reversible blockage scheme be developed to stop diffusion of high energy chemicals across the membrane while the energy is stored for long periods of time? In particular, can stable bubbles be formed at CNT entrances and thus block the transport through the CNT membrane? 2) Can the CNTs be modified with catalyst to

electrochemically convert chemicals from low energy state to high energy state at a high catalytic activity? With demonstration of the concepts and qualified modeling, the efficiency of the device can be further improved. This dissertation of energy storage will focus on issues relating to the fundamental questions.

1.2.4 The observations and applications of nanoscale bubbles

For the first question, an effective valve to turn off the CNT membrane during energy storage time needs to be developed. As mentioned before, the mass transport through CNTs is much faster than that through conventional material pores. The gate keeper at entrance of CNTs can let the CNT membrane reach the goal of ideal membrane for separation, which has fast transport with high selectivity.[65] The carboxyl functional groups on CNT entrances have been generated during the fabrication process of the CNT membrane. Thus the molecular gate keepers such as straight chain alkanes, anionically charged dye molecules and aliphatic amine elongated by polypeptide spacers have been grafted on CNTs with EDC coupling. [58, 65-67] However, the molecular gate keepers, which have been developed for CNTs membrane, can not completely turn on/off CNTs membrane.[58, 64] However bubbles at entrances to CNT pores can be used as a nearly ideal valve to completely turn on or off the transport through channels, without any solid mechanical moving part. This will reduce the complexity in fabrication and integration of the whole system for storage and pump. Thus, there is extensive research focused on the application and observation of microscale bubbles and nanoscale bubbles.[68-73] Micron-scale bubbles have been used as valves for micropumps in microchannels.[68] These bubbles were generated by several methods such as water electrolysis, thermal vapor generation, chemical reactions and inert gas injection. The most controllable and energy

efficient method is water electrolysis. By water electrolysis, the H_2 and O_2 microscale bubbles can be continually generated. The power efficiency of water electrolysis for micropump is 10 to 100 times higher than that of thermal methods. For the nanoscale bubbles, according to the Laplace equation $P_v-P_l=2\mu\pi r\delta/\pi r^2=2\delta/r$, they are hard to maintain stable due to the high pressure inside them (140 atm for nanoscale bubbles in diameter of 20 nm).[70] However, nanoscale bubbles have been observed with unexpected stability on hydrophobic surface due to small contact angle.[71-75] It is found that the average pressure in the flat nanoscale bubbles (large radius of curvature) is only about 1 atm.[75, 76] This is the reason for long term stability of nanoscale bubbles. Furthermore nanoscale bubbles are prone to form inside of the nanochannels.[76] The formation and growth of hydrogen nanoscale bubble can be controlled by electrochemical method.[77] Meanwhile these nanscale bubble can be used to tune the nanofluid.[78] Thus nanoscale bubbles formed on entrances of CNTs in the membrane can be used as the controllable valve for the membrane. Due to the good conductivity of CNTs, these bubbles can be generated on CNTs membrane by electrochemical method.[40, 42, 55, 58] Therefore, we hypothesize that the CNTs membranes with nanoscale bubbles as valve are excellent candidates for energy storage.

1.2.5 The membranes for electrochemical energy storage

Electrochemical energy storage offers a promising and convenient strategy for smart grid of renewable energy. It can build a direct conversion between the electrical and chemical energy.[32-34] Many kinds of the electrochemical energy storage platforms have been developed including lead-acid battery, nickel-cadmium battery, sodium-sulfur battery, redox flow battery, lithium ion battery, etc..[79, 80] The batteries are the efficient

electrochemical energy storage.[80-82] They can be applied in the energy storage system for solar energy, emergence power supply and even the electric vehicles. The membranes/separators are the critical parts for batteries for converting the chemical energy to electrical energy. For example, for the redox flow battery, they should prevent the transport of active chemicals but allow the transport of charge carriers.[83] Extensive research works have focused on modification of the membrane by preventing the cross contamination/reaction of chemicals in two sides of the membrane for redox flow battery.[84-89] For the rechargeable flow battery, the membranes/separators usually allow the reactive ions to transport through them during the charging process. After the charge process, the membrane should block the transport of reactive chemicals as redox flow battery.[90, 91] The schematic process of the whole system for the rechargeable electrochemical flow battery is shown in figure 1.9. During the charging process, the active chemical anion Cl^- was electrochemical oxidized to Cl_2, which was transported to reservoir for storage. After the battery is fully charged, the active chemical was stored in the reservoir with the valve close. For discharging the battery, the valve was open and the active chemical was transported into reactive area to generated the electrical power.[92]

It was reported that the CNT membrane could be an exciting platform for energy storage since the mass transport through CNT cores is a thousand fold faster than pores of conventional materials, which can enhance charge/discharge rate for the energy sotrage.[58, 60] The CNT membrane with nanoscale bubbles as valves can be used as a smart membrane for controlling the transport (on/off) through the membrane. Meanwhile graphite is highly conductive and stable and CNT surfaces can be functionalized with catalyst metals or complexes for a low overpotential.[40, 42, 47, 55, 93] The conductivity of

CNTs can also allow high current efficiency across the membrane. Owing to all the properties mentioned above, the pretreated CNT membrane has potentials to be an ideal membrane for the electrochemical energy storage.

Finally for the second question whether the CNTs modified with catalyst can electrochemically convert chemicals from low energy state to high energy state at a high efficiency and mass activity, Pt catalyst and Ir complex were chosen to be electrochemically deposited onto CNTs. Pt catalyst is critical for methanol fuel cells,[94-96] and Ir complex is an important catalyst for the water splitting,[97, 98] which is the critical process for the storage of solar energy. Pt is a very active catalyst due to non-corroding surface but ability to coordinative bonds for electron transfer. However it is very expensive metal, needed is a method to form just one monolayer of catalyst on a high area stable conductor.

1.3 Catalytic conversion for fuel cell

1.3.1 The methanol fuel cell

With increasing energy demand and significant bio-mass conversion to methanol, there are extensive research works on methanol fuel cells.[94-96, 99-101] There are two kinds of methanol fuel cell: direct methanol fuel cell and indirect methanol fuel cell. The direct methanol fuel cell was firstly invented by Dr Prakash and Dr Olah in the early 1990s, which could directly convert the methanol into electricity.[102, 103] The schematic structure and related reaction of the direct methanol fuel cell is shown in Figure 1.10 (a). The methanol with water is fed into the anode electrode and methanol is oxidized there to generate the CO_2, protons and electrons. The protons can be transported through the

membrane (usually Nafion film), which is selectively transport the protons and block transport of the electrons, to the cathode electrode. Then the protons combine with the oxygen and electrons on the cathode electrode surface to form the water. The common operating temperature of direct methanol fuel cell is in range from 50 ℃ to 120 ℃.[104, 105] The methanol is liquid from 97 ℃ to 65 ℃. So when the methanol fuel cell is operated in high temperature, it is usually with high pressure. The efficiency of direct methanol fuel cell is relative higher in high temperature and pressure.[106, 107] The only waste the direct methanol fuel cell is water and carbon dioxide. Therefore, the methanol fuel cell is friendly to the environment with consuming methanol which is renewable. The advantages of direct methanol fuel are following. First of all, the methanol is liquid at room temperature and atmospheric pressure. Thus it is much more convenient for transport and storage of fuel than that for hydrogen fuel cell. The energy density of methanol fuel cell is one magnitude order higher than those of the compressed hydrogen fuel cell and lithium ion battery. [106, 108] Therefore the methanol fuel cell with same weight has more power and can support longer time power supply for civil applications like mobile phone, laptop or digital camera or for military applications like portable power supply for soldiers.[109] Furthermore, one more advantage of methanol fuel cell over the rechargeable battery is the methanol fuel cell can be refilled immediately for continual power supply.[110]

The main challenges for large scale application of methanol fuel cells now are methanol crossover, relatively low power density and slow reaction kinetics of methanol electrochemical oxidation.[106, 111-113] For the methanol crossover, high concentration of methanol can result in high energy density of methanol fuel cell. However, some of

methanol will diffuse through the separate membrane to the cathode. Then the methanol will be directly oxidized with oxygen on catalyst surface of cathode. This will reduce the performance of fuel cell with lower the efficiency, output current density and voltage.[111] The current relative low power density of direct methanol fuel cells prevents their application in directly driving the large vehicle.[112] The last challenge, which is also critical challenge for commercializing the fuel cell, is the low reaction kinetics of methanol electrochemical oxidation. The precious metal platinum is required on the both electrodes as catalyst for methanol fuel cell, which significant increases the total cost of methanol fuel cell.[106, 113]

For the indirect methanol fuel cell, the methanol was first converted into H_2 and CO_2, which was reacted at above 250 ℃.[114] Then H_2 was fed into fuel cell as methanol for direct methanol fuel for electricity generation. The schematic process of the indirect methanol fuel cell was shown in figure 1.10 (b). Here the methanol is used as the dense hydrogen carrier. It can solve the methanol cross over problem in direct methanol fuel cell. However, it adds fuel reforming process, which requests the higher temperature than the operating temperature of fuel cell. This will make the whole system more complicated and more requirements on heat management. Both direct fuel cell and indirect fuel cell demand the load platinum catalyst on electrodes. Therefore, cost of catalyst for both types of methanol fuel is still a big issue.

1.3.2 The catalyst Pt for fuel cell

The thermodynamic potential for methanol oxidation is low, just 0.02 V vs NHE which is close to hydrogen oxidation, but the reaction rate is very poor, about several

magnitude orders lower than that of hydrogen oxidation.[99] To construct the methanol fuel cell, people need to load catalyst Pt on the electrodes to enhance methanol oxidation. The mechanism for methanol oxidation on Pt catalyst surface, which is anode electrode, is as shown below:[94]

$$Pt\text{-}CH_3OH \rightarrow Pt\text{-}CO + 4H^+ + 4e^-$$

$$H_2O + Pt \rightarrow Pt\text{-}OH + H^+ + e^-$$

$$Pt\text{-}CO + Pt\text{-}OH \rightarrow CO_2 + H^+ + e^-$$

Although Pt is a key catalyst for methanol fuel cell, it is a limited and expensive noble metal. Therefore scientists have tried to increase the catalyst activity of Pt applied in fuel cell by reducing the size of Pt nanoparticles to 1 nm,[95] by adjusting facets of Pt nanoparticles,[96] by improving the dispersion of Pt nanoparticles,[100] by adding additives to Pt [101] or by improving the morphology of catalyst supports to increase their reactive area.[115, 116] The reasons behind these respective methods are first, because the area of Pt particle per unit mass is S (m^2/g) =6000/ρd; here d is the average diameter of Pt particles in nm; ρ is Pt density 21.4 g/cm^3.[117] Thus the smaller size of Pt nanoparticle results in the higher ratio of active area/mass. Secondly, catalyst activities of Pt's different facets vary due to different surface energy and surface densities of Pt atoms. Thirdly, scientists also modify the surface of the catalyst support to increase the dispersion of Pt particles, which makes full use of the surface of Pt particles. Fourthly, some additives to Pt, such as Ru or Ni can suspend the poisoning effect of carbon monoxide intermediate during methanol oxidation and prevent Pt from dissolving during the process. Finally, improving the morphology of catalyst support to increase their active area can increase the power density.

There are three major methods to load Pt nanostructure on the electrodes. The first procedure is to prepare the Pt nanostructure by reduction method. The reductant for this method can be $NaBH_4$,[118] ethylene glycol [119] or formic acid [120]with the Pt precursor hexachloroplatinic acid H_2PtCl_6. This method provides an easy way to deposit Pt and possibly load its nanostructure on many kinds of support. The disadvantage to this method is that it is difficult to control the mass, dispersion, and morphology of Pt deposited on support. Additionally, this method may pollute the surface of Pt nanoparticles with organic compounds during the reduction process. The second method for fabricating Pt nanostructure, especially nanoparticles, is to magnetron sputter Pt onto the catalyst support.[115, 116] For this method, it is easy to fabricate uniform Pt nanoparticles and load them on many kinds catalyst of supports. However, it is difficult to control particle size by manipulating conditions for sputtering Pt. The critical problems for this method are that it is hard to load Pt particles to specific sizes on catalyst support and the sputtering process wastes the most mass of Pt. Only surface Pt atoms are catalytically active and Pt within the volume of the particles is not utilized. Ideally one can coat a conductive high area support with a monolayer or very thin film of Pt to increase the mass activity.

The third method for fabricating Pt nanostructrure is electrochemical deposition.[115, 121-126] The reaction for this electrochemical method follows below:

$$PtCl_6^{2-}+2e \rightarrow PtCl_4^{2-}+2Cl^-$$

$$PtCl_4^{2-}+2e \rightarrow Pt+4Cl^-$$

There are several advantages to the electrochemical method for fabricating Pt nanostructure. First, it is possible to control the Pt mass which is loaded on the substrate in this process by adjusting time and potentials. Meanwhile, uniform Pt nanostructure is also likely during electrochemical deposition. An additional advantage is that when we load Pt catalyst directly on the composite electrode of a fuel cell, part of which may be nonconductive, the electrochemical method will ensure that all Pt nanostructures are electrochemically deposited onto only the conductive part of the electrode improving Pt utilization. There are three kinds of methods for electrochemical deposition of Pt on support. In the first type, people often electrochemically deposit Pt by cyclic voltammetry.[115, 121, 127, 128] The second type of electrochemical method is to deposit Pt by the potential-step method.[122] The third type of electrochemical method is to deposit Pt at constant potentials.[123-126]

To promote catalyst activity of Pt by improving the dispersion of Pt nanoparticles on the catalyst support, scientists tried to modify the surface of the carbon support. For example, Guha *et al.* treated the carbon support, such as activated carbon, carbon black, carbon nanofibers and nanotubes with a strong acid mix of HNO_3+H_2SO_4, which will introduce oxygen atoms on the carbon surface to form the surface oxygen complex or functional groups such as carboxyl, carbonyl and phenol groups. They found this kind treatment can be helpful for the dispersion of Pt.[129] Hull *et al.* proved that –C=O, –C–O–C–, –COO–, and –C–OH groups grafted on CNT surface are helpful in depositing highly dispersed Pt nanoparticles. The schematic picture about these functional groups on CNTs for improving the dispersion of Pt nanoparticles was demonstrated in figure 1.11. They found the Pt nanoparticles binding to CNTs by functional groups.[100] Meanwhile, Kim *et*

al. succeeded on loading the high dispersion of Pt nanoparticles on CNTs, the surface of which are modified by thiol groups. They found the thiol groups on the CNT surface are helpful for the dispersion of Pt nanoparticles.[118] There are also some other methods to modify the surface of carbon, such as by plasma or ozone treatment [130] or by a solution of hydrogen peroxide. [131]

Recently a general class of CNT surface chemistry based on diazonium salt decomposition has been developed[132]. In this chemistry the diazonium group decomposes to form stable N_2 and a highly reactive carbon cation radical that reacts with graphite. The schematic picture about the reaction for surface modification of CNTs is shown in Figure 1.12. This reaction can be controllably activated by electrochemistry at an electrode surface [133] for precise thickness and uniform control. The chemistry of the diazonium group can also be tailored [64, 133] to favor uniform metal ion coordination. We hypothesize that this will allow uniform nm-thick Pt electrodeposition on CNTs.

During the methanol oxidation process with Pt catalyst in fuel cell, the Pt catalyst is easily poisoned by intermediate products, such as CO, or corroded into solution. Thus extensive research work focused on suspending the CO poison effect by adding Ru to Pt nanoparticles.[132, 134, 135] The reasons Ru can suspend the CO poison effect are still under debate. One of reason was proposed to be the ligand effect, which claimed that the addition of Ru to Pt nanoparticles would weaken the Pt-CO bond and thus enhance CO oxidation.[136, 137] Another reason for this could be the negative shift of oxidation potentials for CO during the reaction at the presence of Ru, which was demonstrated by Yang *et al.*. The CO stripping voltammogram process in methanol solution was performed on the Pt and Pt/Ru thin film with in situ surface enhanced Raman

spectroscopy. During the CO stripping voltammogram process on Pt and Pt/Ru film, the oxidation potentials of CO shifted to more negative with increasing the amount of Ru in Pt film.[101]

Besides using Ru as an additive, Park *et al.* also tried to use Au as an additive to improve Pt catalyst activity in methanol oxidation. The mass activity of Pt in Pt/Au nanoparticles is better than that of the Pt nanoparticle due to the Pt's higher ratio of reaction surface/mass in Pt/Au nanoparticles. However, accounting for the total metal mass, Pt/Au nanoparticles had less mass activity than that of the pure Pt nanoparticles because Au strengthened Pt-CO bonding.[138] Furthermore, Radoslav Adzic reported that the gold additive can prevented Pt from dissolving in cathode for fuel cell.[139] The Pt modified with Au could maintain the same activity and surface area after 30,000 cycles of potential cycling between 0.6 and 1.1 volts under the conditions of O_2 reduction reaction. Comparing with this, there were sizable losses of the pure Pt catalyst under the same conditions.

However, both Au and Ru are expensive metals. Thus it is not prudent to reduce the cost of methanol fuel cell by using the Au and Ru as additive for the Pt catalyst. Furthermore, the Ru additive always switched the methanol oxidation potentials to more negative value, which would reduce the output energy efficiency of fuel cell. Technologists prefer inexpensive metals as the additives to Pt catalyst in fuel cell. In polymer electrolyte membrane fuel cell, Stamenkovic *et al.* discovered that nickel could be used as an additive to Pt catalyst to significantly improve its catalyst activity for splitting oxygen in fuel cells. The improvement was up to 90 times higher than that of the pure Pt catalysts. The mechanism for this is that the additive nickel can help Pt to release

the hydroxides, which prevent oxygen from reaching the catalyst.[140] Meanwhile the nickel can also be used as additive to Pt/Ru/Carbon system to improve its catalyst activity for methanol oxidation. However, there is a critical problem for nickel to be used as additive for the Pt catalyst in fuel cell applications, as it is not stable and easily dissolves during the process of methanol oxidation.[141] Therefore, scientists are still working on improving the Pt catalyst activity by searching new additive, improving its surface morphology etc.

The last strategy for promoting the Pt mass activity for fuel cell is to improve the surface morphology and conductivity of catalyst support.[142, 143] For example, the graphitic carbon has been used as catalyst support for Pt nanoparticles to improve its catalyst activity by H. Tang *et al.*.[127] The extensive research works has focused on the CNTs as the Pt catalyst support for fuel cell due to the advantages of high surface area, relative stability and high conductivity comparing with other carbon support.[127, 142-146] Scientists have worked on improving the CNTs support further for the Pt catalyst. The Pt/Ru nanoparticles were sputtered on CNTs grown directly on carbon cloth of methanol oxidation by Wang *et al.*.[134] Recently, aligned CNTs array has been used as catalyst support, which has a higher active area than the random CNTs in polymer composite. [116, 142]

1.3.3 The monolayer deposition by underpotential method

Because of their unique electronic, chemical and catalytic properties, which are quite different from bulk materials, metal monolayers have attracted intensive research attention.[147-151] The most of metal monolayers were deposited by underpotential method

or replacement method. For the underpontential deposition, the metal monolayers were electrochemical deposited on foreign metal substrate at the potential which is much less negative than equilibrium potential for depositing the bulk metal under same conditions. The mechanism is that the strong binding between the metal ion adsorbate and the metal substrate favor the deposition of the metal monolayers rather than metal particles.[152-154] Therefore the adsorption and electrochemical deposition of metal atoms adsorbate on the foreign metal substrate, which are polycrystalline and single-crystal electrodes, have been extensively investigated. Most of the metal substrate for the under potential deposition are Au/Ag/Pt/Cu.[155-157] The potential difference for depositing monolayer versus bulk films the substrate is related to difference of the work functions of the deposit and substrate, which would result in partial charge of the monolayer deposited on substrate.[155]

The metal monolayers deposited by underpotentials have various applications. One of the most attractive application is the development of monolayer catalyst, which are precious metal like Pt,[158-161] on foreign metal substrates like Au or Ru. When the morphology of the precious catalyst is monolayer, the geometry ideally renders all catalyst atoms active. This offers a promising strategy to improve mass activity of precious catalyst to maximum in theory and thus reduce the cost of renewable energy. For example, the mass activity of Pt monolayer coated on porous gold can reach the record high 2600 A/g, which is much higher than the mass activity of Pt nanoparticles 170 A/g.[142] The schematic process of Pt monolayer deposited by porous Au is shown in figure 1.13. The Cu monolayer was first electrodeposited on porous Au by under potential method. Then the Pt monolayer was deposited on Au by redox reaction

replacement of the Cu monolayer.[162] However, most of metal substrates for the catalyst like Au/Ru are still expensive. Therefore, coating the precious catalyst monolayer like Pt on cheap, conductive and stable catalyst support is a promising direction for reduce the catalyst cost for the renewable energy like fuel cell.

1.4 Catalytic conversion for water splitting

Solar energy is the very promising alternative and renewable energy, which is clean to environment and abundant on the Earth. The solar energy from one hour of sunshine on the Earth is enough to support demand of human society for whole year.[4] It seems the perfect solution for the conflict between energy demand and environmental protection of human society, which can also assist human to overcome the challenge on the limit of fossil fuel reserve. However, solar radiation varies with season, latitude, orientation and intermittency of day/night cycles. Industry and consumers request a constant and stable power supply. Thus storage of solar energy with a convenient and low cost system is critical for large scale application of solar energy. For storing solar energy, water electrolysis can split water directly into hydrogen and oxygen fuels but requires the proper catalyst system. The schematic process about storage of solar energy by converting the solar energy to fuel of hydrogen and oxygen is shown in figure 1.14. When electrical energy is required, the hydrogen and oxygen are consumed in a fuel cell to generate electricity. During the storage process of solar energy, not only hydrogen can be produced by water splitting ($H_2O \rightarrow ½O_2 + H_2$, G °=237.1 kJ) but also hydrocarbons can be generated by CO_2 reduction with water ($H_2O + ½CO_2 \rightarrow O_2 + ½CH_4$, G °=409.0 kJ). In both processes, catalytic water oxidation constitutes a key half reaction. This is

also the basic and fundamental step for the nature photosynthesis in plant, which store the solar energy by converting water and carbon dioxide to oxygen and carbohydrates. For the water oxidization, it requires to remove four electrons and four protons from two water molecules with concomitant formation of an O-O bond in this half reaction ($2H_2O \rightarrow O_2 + 4H^+ + 4e^-$), which cause a major challenge of artificial water oxidization for several decades.[163-165] If only one electron has been removed during the process, the reaction will only generate the hydroxyl radical, which is slow process ($H_2O \rightarrow \bullet OH + H^+ + e^-$).

To overcome this challenge, the natural water oxidation happens in green plants with assistance of oxygen evolving enhancer protein. The protein assists the strong oxidants which are generated by light to steal the electrons from water and assist the water splitting.[166] Scientists are always like to learn from the nature and imitate its behavior. Therefore, the synthetic catalysts, which are activated by electrochemical energy or strong oxidants, have been developed for artificial water splitting. The first well known synthetic catalyst for water splitting was the Ru complex blue dimer. It was assist homogeneous water oxidization by proton-coupled-electron transfer, which can avoid the charge buildup and the high energy intermediates.[167, 168] However same as oxygen evolving enhancer protein in plant, the blue dimer would be damaged and lost the catalyst activity during the process of water oxidization.[164, 167-170] Then the other catalysts like Ir complexes,[97, 98] Fe complexes[171] and polyoxometalates have been developed for the homogeneous water oxidization reaction.[172, 173] However, as shown in figure 1.14, the heterogeneous water oxidation catalysts are required for artificial photosynthesis to store the solar energy, where the catalyst can be loaded on matrix and

thus integrated into electrochemical or photoelectrochemical cells.[174-181] In this dissertation, the Ir complex has been electrochemically grafted on buckypaper with direct binding and indirect binding for heterogeneous water oxidization which is driven by electrochemical power. The catalyst activity like TOF of Ir complex grafted on CNTs was evaluated under different binding conditions for the catalyst loaded on the buckypaper. The stability of Ir complex catalyst during the process of catalytic water oxidization was tested in this dissertation.

1.5 Goals of the Ph.D. work

In summary, the Ph.D. dissertation is composed of two parts 1) membranes for electrochemical energy storage and 2) efficient catalysts support coupling for energy conversion. The first part is focused on the application of novel CNT/polymer membrane for electrochemical energy storage. The nanoscale bubbles generated by sine potential have been used as the valve of the pretreated CNT membrane for the electrochemical energy storage. The second part includes the catalyst Pt, Ir complex catalyst loaded on CNTs for methanol oxidization in fuel cell and for catalytic water oxidization in solar energy storage. The thickness of Pt film on CNTs was tuned from 10 nm to monolayer to improve the mass activity of Pt from 205 A/g to 2711 A/g for the methanol oxidization. Methods to more efficiently couple molecular catalyst to CNT supports were also examined. The catalyst activities of the Ir complex coupled to the CNTs by direct pi-bond linkage was proven to be one magnitude higher than that by carbonimide coupling.

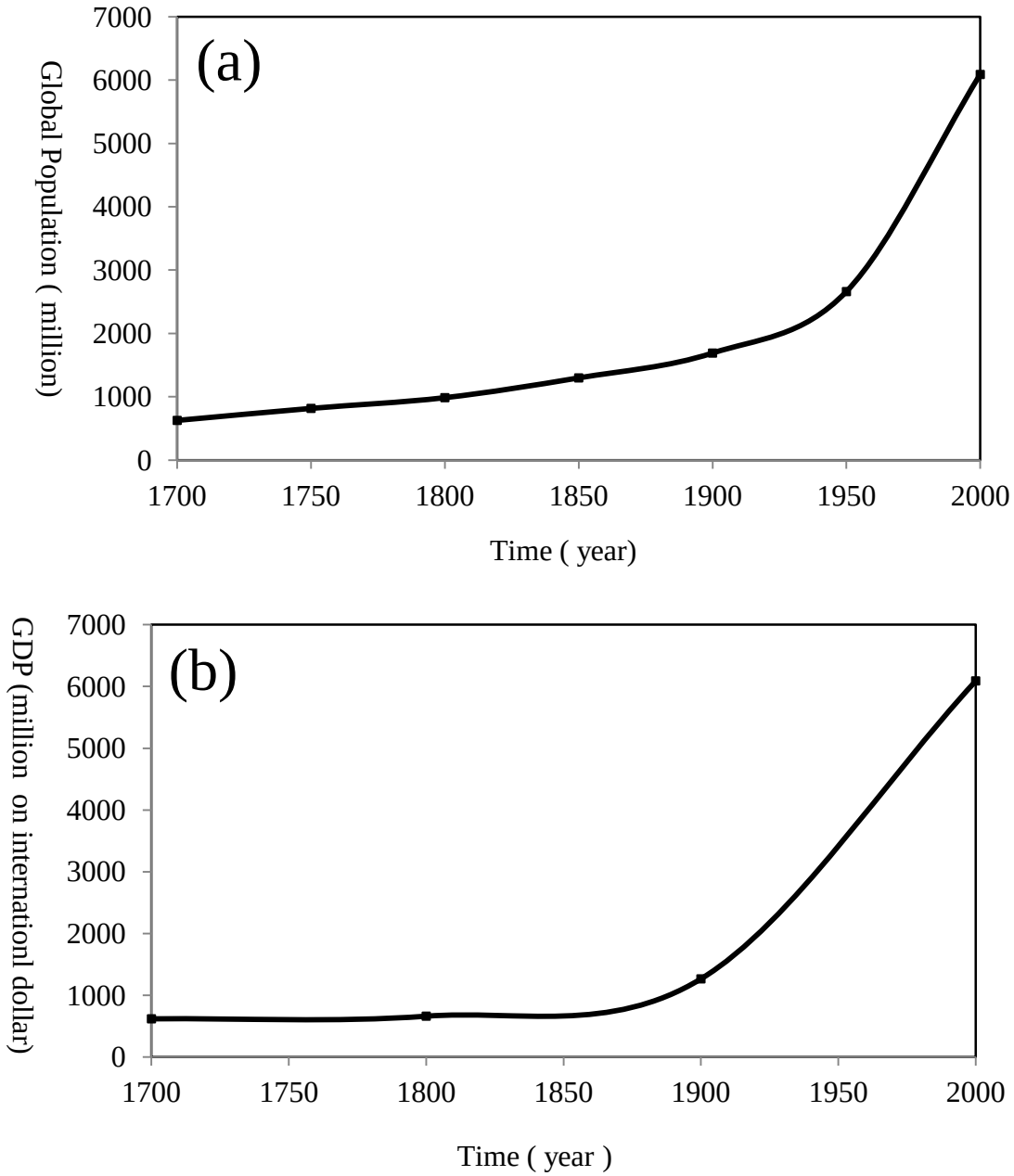

Figure 1.1 The global population (a) and GDP (b) in last three centuries from 1700 to 2000 (The data adapted from the reference [5])

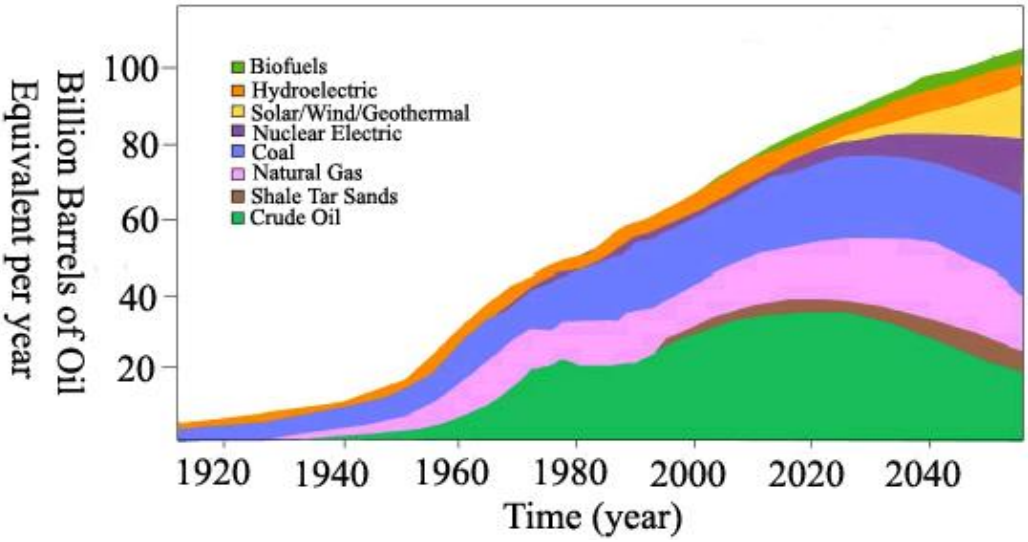

Figure 1.2 The history and tendency of global energy demand from 1920 to 2050 (The figure adapted from reference [10])

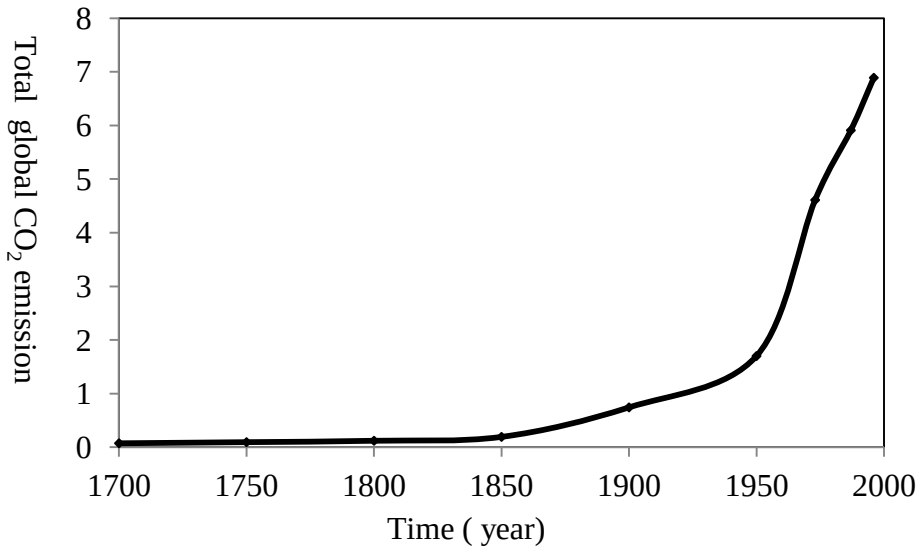

Figure 1.3 The total global CO_2 emissions in the last three centuries from 1700 to 2000 (The data adapted from [21])

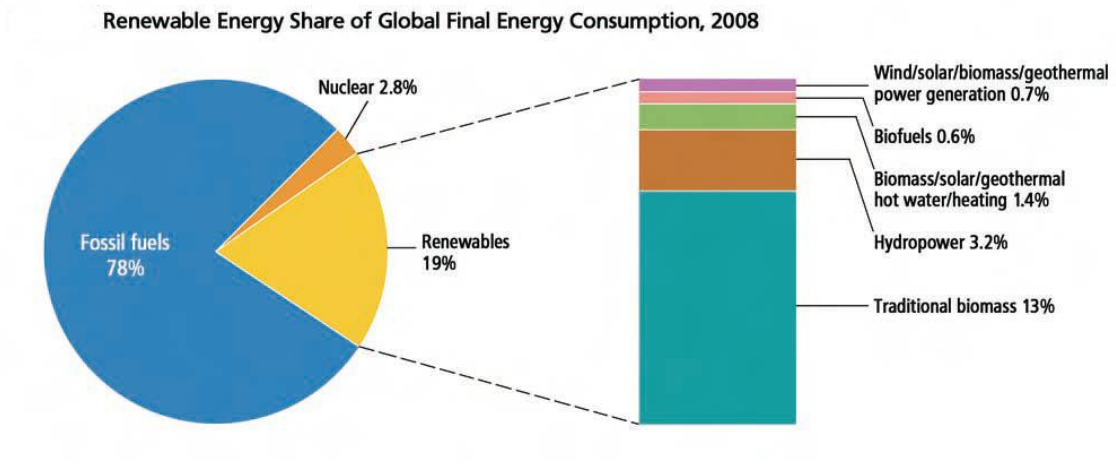

Figure 1.4 The percentage of renewable energy in total global energy consumption (The permission from reference of [27])

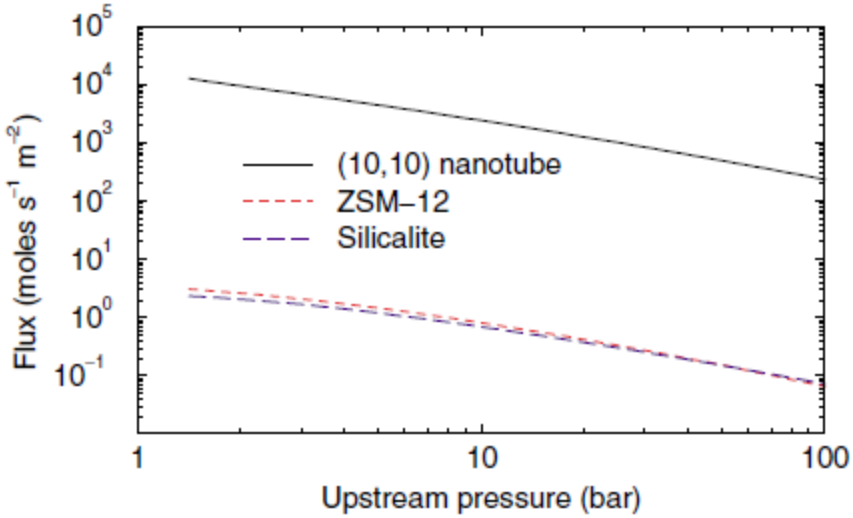

Figure 1.5 Simulated flux of methane across a10 μm thick membrane as a function of the upstream pressure. The pressure difference maintains at 1.38 bars. (Adapted from the reference [45])

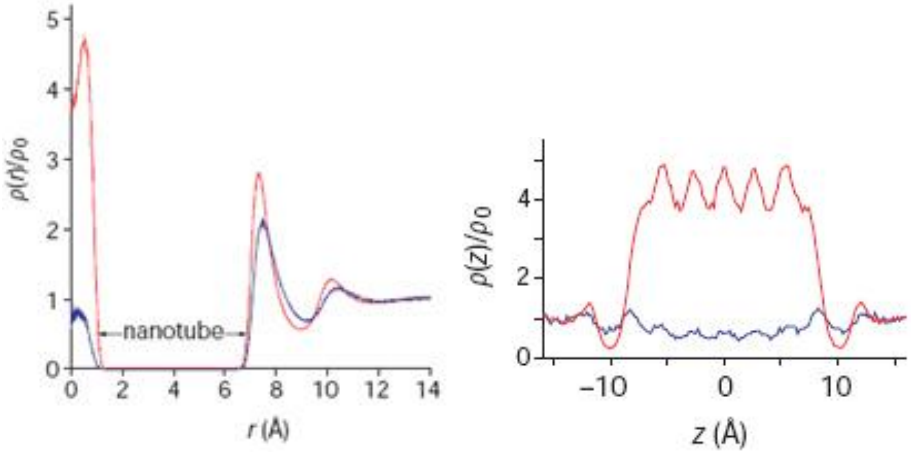

Figure 1.6 The simulation results of water density distribution in carbon nanotube (red, sp^2 carbon parameters; blue, modified carbon-water interactions). (The permission from reference [39])

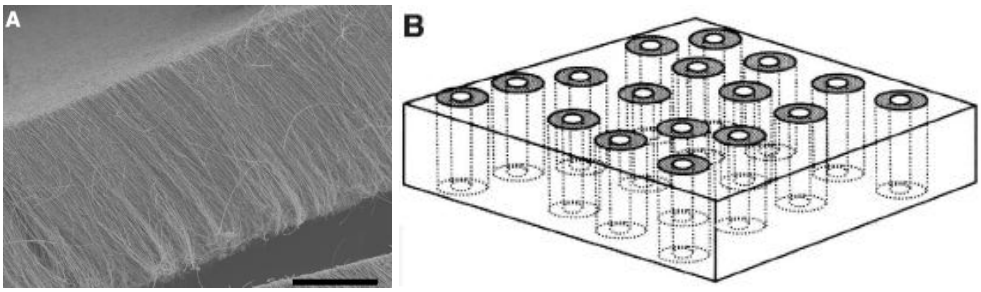

Figure 1.7 SEM of aligned CNTs and schematic picture of CNT membrane (The figures adapted from reference [55])

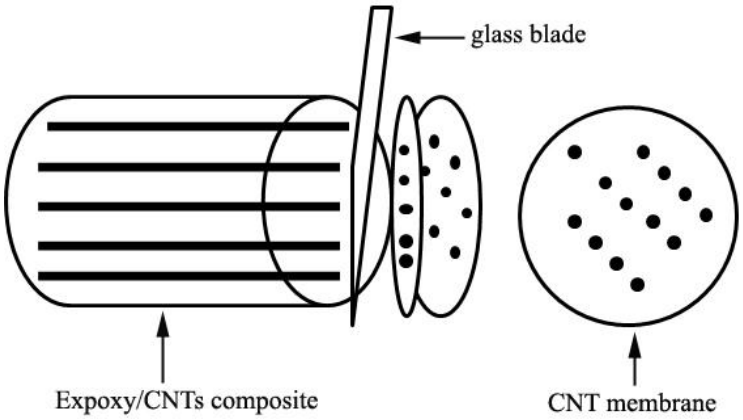

Figure 1.8 The schematic process of micro cutting for the CNT membrane fabrication

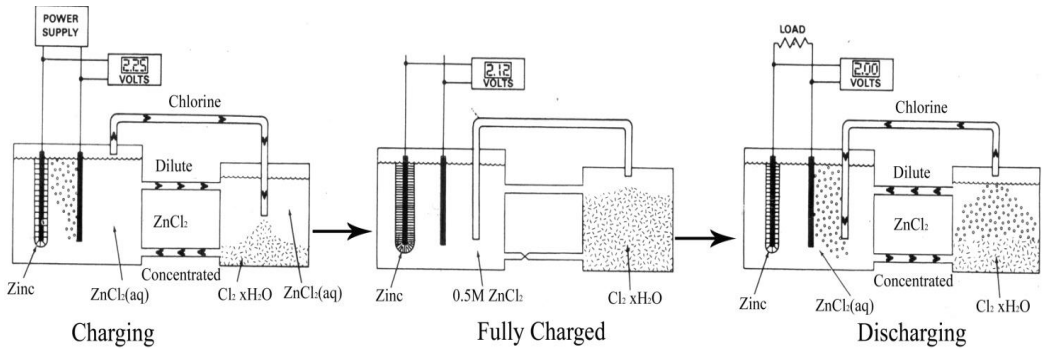

Figure 1.9 The schematic pictures for charging and discharging process of electrochemical flow battery (Adapted from reference of [92])

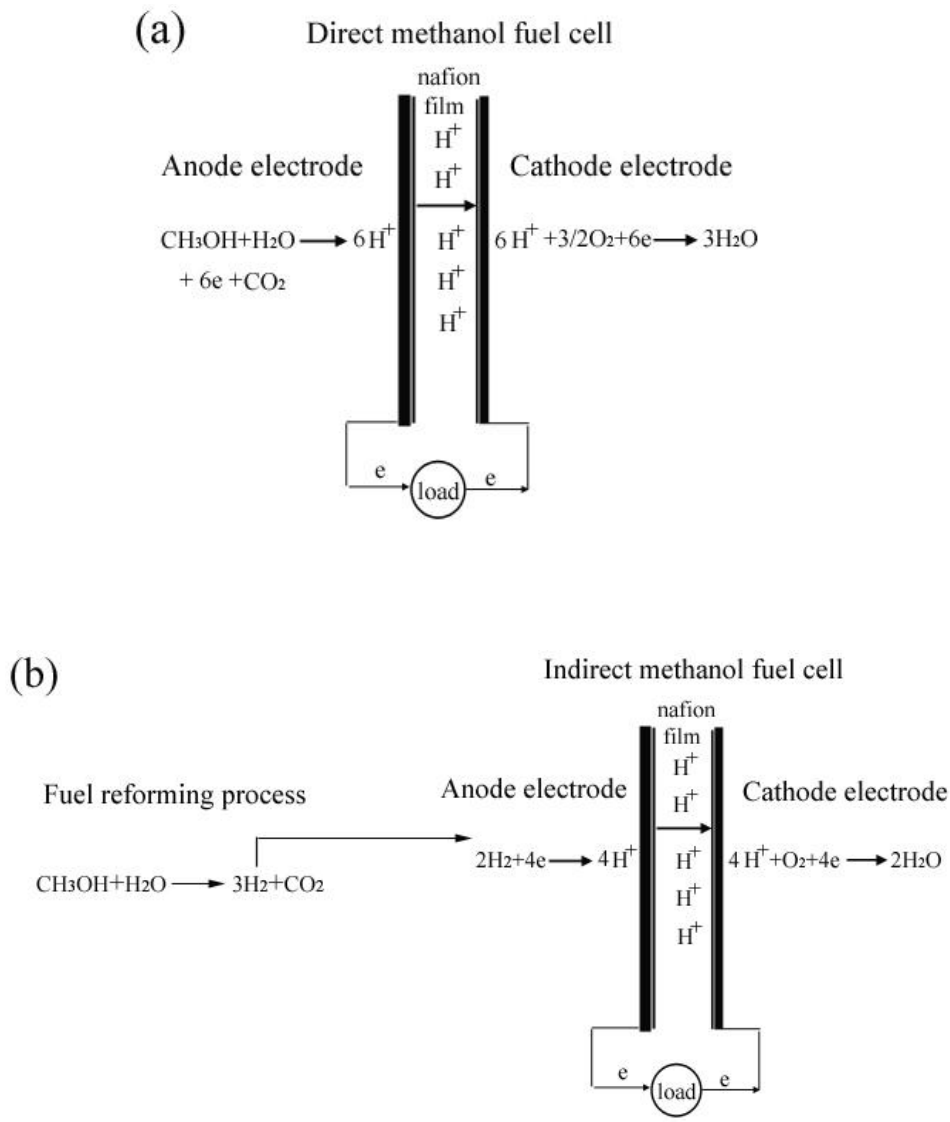

Figure 1.10 Schematic picture and related reactions of direct methanol fuel cell (a) and indirect methanol fuel cell (b)

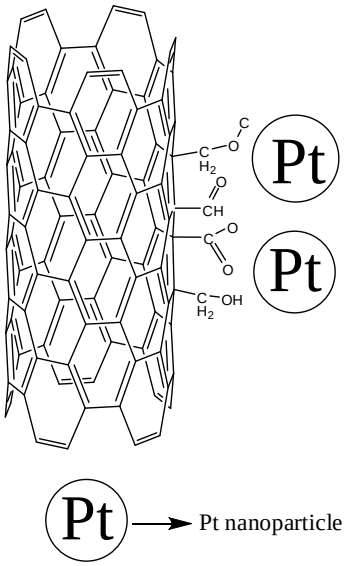

Figure 1.11 The surface modification of CNTs for the improvement on dispersion of Pt nanoparticles

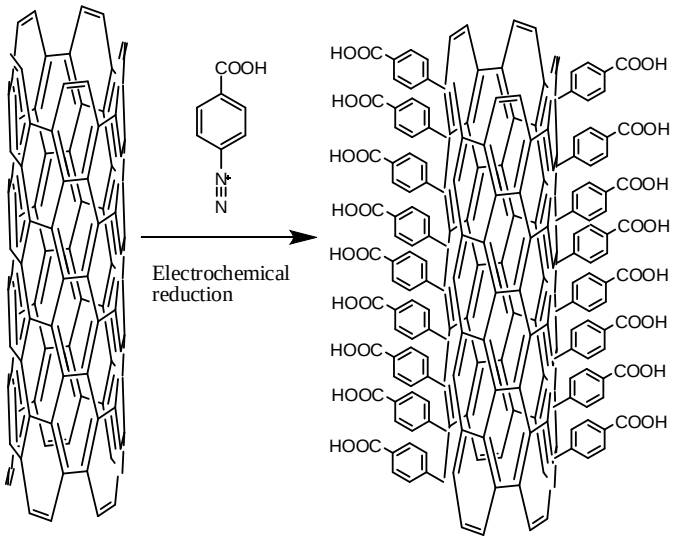

Figure 1.12 The schematic pictures for the surface modification of CNTs by electrochemical diazonium grafting

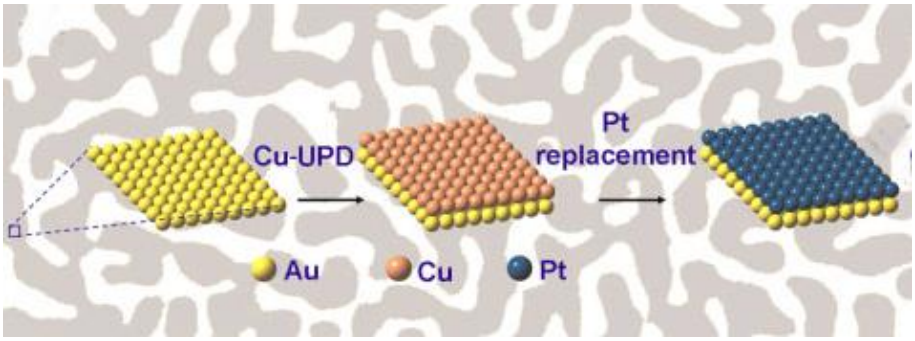

Figure 1.13 The schematic picture of Pt monolayer coated on porous Au(Reprinted with the permission from reference [159])

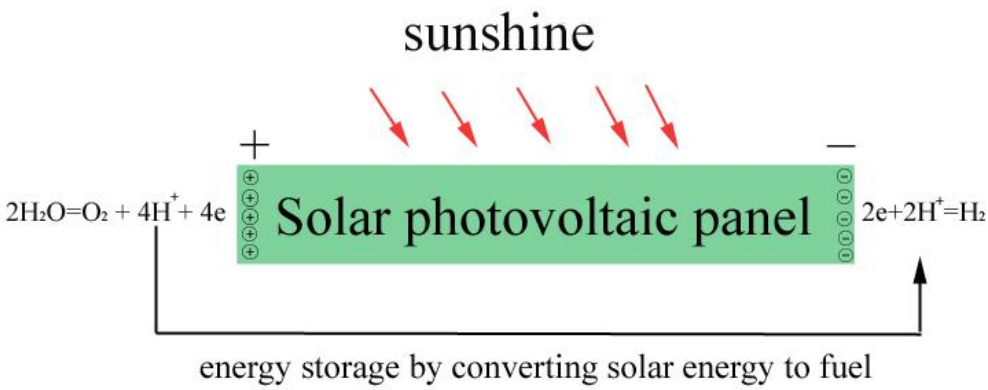

Figure 1.14 The schematic process about the storage of solar energy by converting the solar energy to oxygen and hydrogen fuel

Chapter 2 Nanoscale bubble valves on CNT membranes for chemical energy storage

This chapter is mainly based on the manuscript on writing to Advanced Materials:

Xin Su, Ji Wu and Bruce J Hinds, 'Nanoscale bubble valves on CNT membranes for chemical energy storage' on writing to Advanced Materials

2.1 Introduction

Shifting to renewable energy resources such as solar and wind will require dramatic new approaches in energy storage.[182-184] Chemical energy storage is appealing due to a very large energy density.[185, 186] However this requires stable electrodes with low overpotential, fast mass transport, and a valve system to stop diffusion while in the storage mode. Carbon nanotube membranes[55] are an exciting platform for energy storage since the mass transport through CNT cores is a thousand fold faster than pores of conventional materials, graphite is highly conductive and stable, and CNT surfaces can be functionalized with catalyst metals or complexes for a low overpotential[40, 42] Therefore, an effective valve to turn off the membrane during storage time needs to be developed. The molecular gate keeper, which has been developed for CNTs membrane, can not completely turn on/off CNTs membrane.[58, 64] But the bubble can be used as a near idea valve to reach complete on/off. Microscale bubbles have been used as the valves for micropump in microchannels.[68] Even according to the Laplace equation, the nanoscale bubbles are hard to maintain stable due to the high pressure inside them (140 atm for nanoscale bubbles in diameter of 20 nm).[187] The nanoscale bubbles have been observed with unexpected stability on hydrophobic surface due to small contact angle.[73-

[75, 188, 189] It was found that the average pressure in the flat nanoscale bubbles (large radius of curvature) is only about 1 atm,[73, 75, 189] which is reason for long term stability of nanoscale bubbles. Furthermore they are prone to form inside of the nanochannels [76] and the formation and growth of hydrogen nanoscale bubble can be controlled by electrochemical method.[77] Meanwhile, the nanofluid can be tuned by the bubbles [78]. Thus nanoscale bubbles formed on tips of CNTs of the membrane can be used as the controllable valve for the membrane. These bubbles can be generated on CNTs membrane by electrochemical method due to the good conductivity of CNTs.[55, 58, 64] Therefore, we hypothesize that the CNTs membranes with nanoscale bubbles as valve are excellent candidates for energy storage. Presented here is a novel electrochemical method to generate nm-scale bubbles at the tips of CNTs that can temporarily block the membrane. A 92% blocking efficiency is achieved when the bubbles are stabilized in a 30-60 nm diameter 'wells' at the tips of CNTs. This well is formed by the electrochemical oxidation of the conductive CNTs partially into the polymer matrix of the membrane.[55] Meanwhile, the nanoscale bubbles can be removed with 0.004 atm pressure to recover the transport through the CNTs membrane.

2.2 Experimental details and characterization methods

Fabrication of aligned MWCNTs membranes: The fabrication of aligned MWCNTs membranes were developed from our group's former paper.[58] To describe it briefly, aligned multi-walled CNTs with an average core diameter of ~7 nm and length of 150 μm were prepared via a chemical vapor deposition (CVD) approach using ferrocene/xylene as the feeding gas.[57] Next, Epon 862 epoxy resin (Miller Stephenson Chem. Co.), and hardener methylhexahydrophthalic anhydride (MHHPA, Broadview

Tech. Inc.) were thoroughly mixed using a ThinkyTM Mixer, which was employed to fabricate epoxy/CNTs composite using a casting method. As-prepared CNTs-Epoxy composite was then appropriately cured before being cut into CNTs membranes using a microtome equipped with a glass blade. The typical thickness of as-cut CNTs membrane is about 5 microns. Finally, the residual epoxy on the tips of CNTs was removed by H_2O plasma oxidation.

Electrochemical pretreatment of MWCNTs membrane: The polymer wells on tips of MWCNTs were created by electrochemical pretreatment on the CNTs membrane. The set up for this is shown in Figure 2.1a. This was performed in three-electrode cell using a potentiostat (PAR Model 263A) with the reference electrode of Ag/AgCl from Bioanalytical. Pt wire was used as the counter electrode. The electrolyte solution for this is 0.1 M KCl. The bottom of MWCNTs membrane was coated with ~25 nm gold film by using sputtering machine (Cressington coating system 308R) to get a good conductivity between the working electrode and CNTs of the membrane. The plane resistance across membrane after sputtering gold on it is 5 Ω/sq. In the pretreatment, parts of MWCNTs in MWCNTs membrane were electrochemically oxidized for 5 h at a potential of 2.5 V vs Ag/AgCl, in a solution of 0.1 M KCl.

Characterizations of the MWCNTs membranes: The surface morphology of CNTs membrane with/without electrochemical oxidization was characterized by Scanning Electron Microscopy (SEM) (Hitachi S-4300) under the operating voltage of 20 kV. The CNTs membrane was mounted flat on double sided conductive tape for top view. The absorbance of light through CNTs membrane before/after electrochemical oxidization was measured by UV-vis spectrophotometer (USB400-ISS-UV-vis Ocean Opticas Inc) to

figure out the percentage change of CNTs in the membrane during electrochemical oxidization.

Constant potential for generating big bubbles on MWCNT membrane: The exeperiment was carried out in the three-electrode cell using a potentiostat (PAR Model 263A), the MWCNTs membrane as the working electrode, Ag/AgCl from Bioanalytical as the reference electrode, Pt wire as the counter electrode to demonstrate the hydrogen reduction. The setup is shown in Figure 2.1b. The contant potential of -1.4 V vs Ag/AgCl was applied on the MWCNTs membrane. The electrolyte solution is 5 mM $[Ru(bipy)_3]^{2+}$/0.05 M H_2SO_4.

Transport measurement of MWCNTs membrane: The mass transport through the MWCNTs membrane was evaluated by the probe molecular tris(bipyridine)ruthenium(II) $[Ru(bipy)_3]^{2+}$. The experiment was carried out as described in Figure 2.1b. The feed side was the solution of 5 mM $[Ru(bipy)_3]^{2+}$/0.05 M H_2SO_4. And the permeate side was deionized Water. The concentration of $[Ru(bipy)_3]^{2+}$ transported into permeate side was measured by UV-vis spectrophotometer. The calibrationtion curve for the linear relationship between the concerntration of $[Ru(bipy)_3]^{2+}$ and the adsorption intensity of UV was demonstrated in figure 2.6. The flux rate of $[Ru(bipy)_3]^{2+}$ transported through the membrane was calculated according to the eqaution $J=(C_t-C_0)*V/t$, here C_t the concentration of $[Ru(bipy)_3]^{2+}$ in the permeate side at screening time t, C_0=0 M the initial concentration of $[Ru(bipy)_3]^{2+}$ in permeate side, V the volume of deionized water in permeate side, t the time for screening the membrane.

Cyclic voltamograms and sine potentials for generating nanoscale bubbles: The CV measurement was carried out in the three-electrode cell using a potentiostat (PAR Model 263A), the MWCNTs membrane as the working electrode, Ag/AgCl from Bioanalytical as the reference electrode, Pt wire as the counter electrode to demonstrate the hydrogen reduction. The setup is shown in Figure 2.1b. The electrolyte solution is 5 mM $[Ru(bipy)_3]^{2+}$/0.05 M H_2SO_4. The sine potentials applied on the MWCNT membrane for generating nanoscale bubbles were output by EDAQ potentiostat from EDAQ. The setup, working electrode, reference electrode, counter electrode, and the electrolyte solution for this were the same as those during the CV measurement.

Control experiments for forming nanoscale bubbles in polymer wells by surface modification: the pretreated MWCNT membrane with the polymer wells was immersed in the solution of 0.2 g butyltrichlorosilane (Aldrich Sigma) in 10.9 g hexane (EM Science) with Ar gas protection for 24 h. After the innerface of polymer wells are converted to hydrophobicity, the membrane was screened in the set up of Figure 2.1 b to test the transport of $[Ru(bipy)_3]^{2+}$. Then the parts of MWCNTs in the membrane were electrochemically oxidized again under the same conditions as before to recover the flux rate. The schematic picture about the surface modification of the polymer wells is shown in Figure 2.9.

2.3 Results and discussion

The schematic for creating the polymer wells to stabilize the nanoscale bubbles by the electrochemical method is shown in Figure 2.2a. To form the polymer wells, parts of MWCNTs in the MWCNTs membrane were electrochemically oxidized for 5 h at a

potential of 2.5 V vs Ag/AgCl, in a solution of 0.1 M KCl. The set up is shown in Figure 2.1a. After the electrochemical oxidization, as shown in the optical image of Figure 2.3, the CNTs become more transparent by the observation. It is obviously that parts of CNTs are burned away. Meanwhile, according to Figure 2.4, the absorbance of light through the MWCNTs membrane during UV-vis measurement decreased after electrochemically oxidizing the parts of MWCNTs in the membrane. This was due to that the parts of MWCNTs were burned away during the electrochemical oxidization process. According to the spectrum in visible light part, there were about 27% lengths of CNTs burned away on average by this process. Furthermore the SEM images of the top view of CNTs membrane before and after electrochemical oxidization in Figure 2.2 b, c confirmed that the parts of MWCNTs were burned away. Furthermore there were polymer wells, which were bigger than MWCNTs inner channels, left in the membrane.

To explore the best potential for generating the nanscale bubbles on MWCNT membrane, the constant potentials of -1.2 V vs Ag/AgCl was applied on MWCNT membrane. As shown in Figure 2.5, there were visible big bubbles generated on both side of membrane after applying the potentials on membrane several minutes as set up of Figure 2.1 b. However, the flux rate of $[Ru(bipy)_3]^{2+}$ transport through the membrane under these conditions was enhanced in initial several, which was due to the electrophoresis of $[Ru(bipy)_3]^{2+}$. Only when the big bubbles on the membrane continued to grow up and finally completely cover the whole surface of the membrane, the flux rate of $[Ru(bipy)_3]^{2+}$ would be blocked. This was demonstrated in Figure 2.7. It is obviously that it takes too long time to turn off the transport through the membrane by applying the constant potential to generate the big bubbles on the MWCNT membrane. It would also

bring the trouble to get rid of the bubble to recover the transport through the MWCNT membrane. Therefore, cyclic voltamograms (CV) measurement was performed with the MWCNTs membrane as the working electrode to figure out the best potential model for the nanoscale bubbles generated on tips of MWCNTs membrane. The setup for the CV was the same for the constant potentials shown in Figure 2.1b, which was also the same as that for testing the blocking efficiencies of nanoscale bubbles generated under different potential model. The potentials range of CV is from -0.8 V to +0.8 V vs Ag/AgCl. From the CV curve in Figure 2.8, there is hydrogen reduction happened during the range from -0.8 V to -0.2 V. This indicated that the hydrogen bubbles were generated at similar negative range of the potential when it was applied on the membrane using same set up. In order to prevent the bubbles from growing up, the sine potential with similar potential range from -0.8 V to +0.8 V vs Ag/AgCl has been used to generate nanoscale bubbles on membrane. This could turn on/off the membrane in quick response time.

Firstly, the blocking efficiencies of nanoscale bubbles, which were generated by applying the sine potentials on the CNTs membrane with/without electrochemical pretreatment, were measured with set up shown in Figure 2.1b. From Table 2.1, nanoscale bubbles generated by sine potentials on MWCNTs membrane without any pretreatment cannot effectively block the transport through the membrane. The blocking efficiency is only 21%. However, after electrochemically oxidizing the parts of the MWCNTs in the membrane to form polymer wells, the nanoscale bubbles generated by sine potential can block the 92% of mass transport through the membrane. It is obvious that the polymer wells, which are formed at CNTs tips by electrochemical pretreatment, can help to stabilize the nanoscale bubbles. Thus it can enhance the blocking efficiency

greatly. Meanwhile, the base line of sine potentials applied on pretreated CNTs membranes were switched from 0 V to +0.4 V and -0.4 V to investigate which part of sine potentials is responsible for the blocking efficiency. From Table 2.1, when base line of sine potential is at +0.4 V and thus the whole sine potential in the range from 0 V to +0.8 V are positive, blocking efficiency is 0%. However, when the base line of sine potentials is at 0 V or -0.4 V, the blocking efficiencies under both conditions are similar and about 90%. Therefore, only the negative part of the sine potential is responsible for generating nanoscale hydrogen bubbles to block the transport through the membrane. This is consistent with the CV curve obtained under the same set up that the part of negative potential during CV can generate the hydrogen bubbles. Meanwhile, from the control experiments, after converting the inner face polymer wells in pretreated membrane to be very hydrophobic with surface modification of butyltrichlorosilane, the flux rate through the membrane was also completely block. By converting the inner face of polymer wells to be hydrophilic with electrochemical oxidization of the parts of MWCNTs again, the flux rate through the MWCNT membrane can be recovered.

In order to figure out the best time for generating enough gas to block the transport through the CNTs membrane, the relationships between blocking efficiencies of nanoscale bubbles and the times for generating the bubbles were tested and shown in Figure 2.10. The blocking efficiency would increase with the time and reach the saturation after 10 minutes. Meanwhile according to the calculation, the total volume of polymer wells in the membrane is 4.6 E-06 cm^3. The total volume of gas generated by 78.8 uA, which is average current of sine potentials applied on the CNTs membrane, is 9.120 E-06 cm^3 per second. Saturated solubility of H_2 in water is 0.017 cm^3 per cm^3. The

diffusion coefficient of H_2 at room temperature is 5.0 E-5 cm^2/s. Flux rate of hydrogen when hydrogen is saturated in polymer wells, $J_{H2}=A*D*\Delta C/l$= 9.115 E-06 cm^3/s (here A the porosity area of the membrane, D the diffusion coefficient, l the depth of polymer wells, assuming 1.3 μm in average). Therefore, the time used to make hydrogen saturated in water will be less than 1s. But the time need to generate the enough gas to fill the whole polymer wells with diffusion of hydrogen is 919 s. The exact polymer wells depth would determine the time for completely block the transport through CNTs membrane.

Furthermore, in order to test the on/off properties of nanoscale bubbles valve, after the transport of MWCNTs membrane was blocked by nanoscale bubbles generated by the sine potential, the pressure difference of 0.004 atm was applied on the feed side of set up. The results are shown in Table 2.2. The most of nanoscale bubbles can be removed by the small pressure difference to almost completely recover original transport through the CNTs membrane.

2.4 Conclusion

In conclusion, nanoscale bubbles can be formed on CNTs to block flow through CNTs membrane to act as valves. The polymer wells formed by electrochemical pretreatment in CTNs membrane are helpful to stabilize the nanoscale bubble generated on CNTs' tips of the membrane and thus greatly enhance the blocking efficiency of transport through the membrane. Sine potentials were needed to generate stable nanoscale bubble for blocking the transport through CNTs membrane and the negative parts of the sine potentials are responsible for generating nanoscale bubbles. The nanoscale bubbles

formed in the polymer wells, at tips of CNTs, can be removed using a 0.004 atom pressure. Therefore nanoscale bubbles can be used as valve for the CNTs membrane. The CNTs membrane with nanoscale bubbles as valves have great potentials for application in the energy storage of solar and wind power.

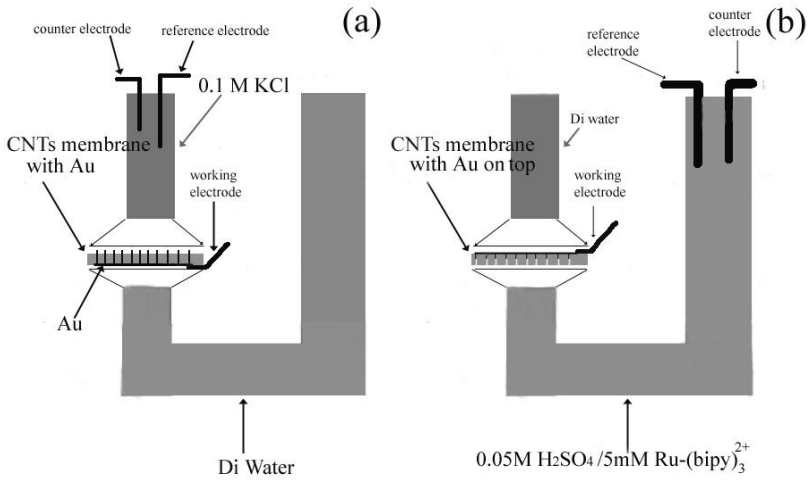

Figure 2.1 The schematic of the setup (a) for the electrochemical oxidation of MWCNTs to produce polymer wells and (b) testing approach for demonstrating nanoscale bubble blocking the diffusion through CNTs membrane

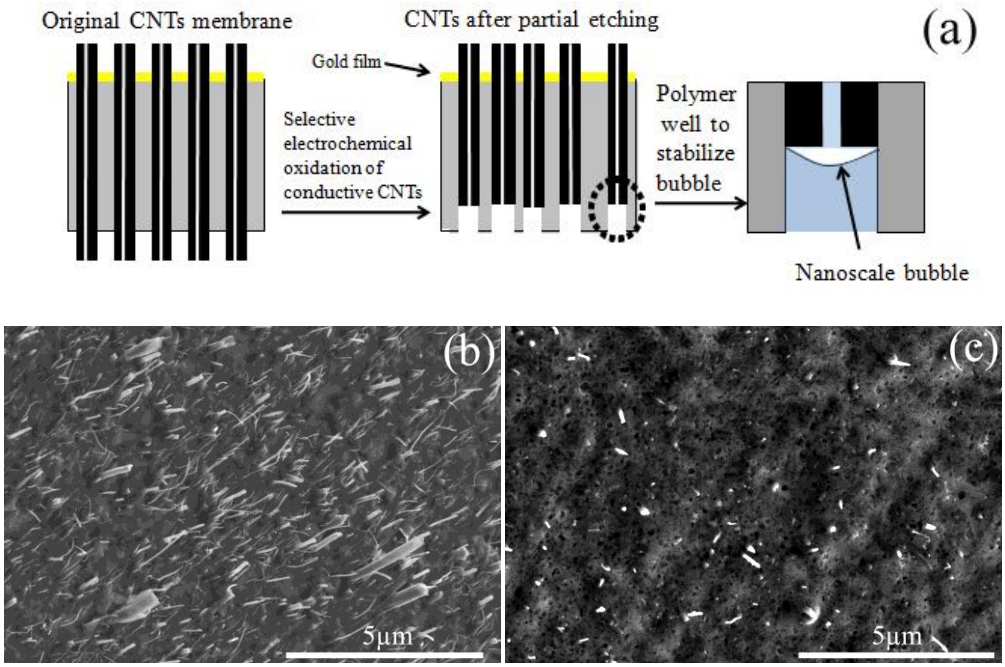

Figure 2.2 The mechanism about the nanoscale bubbles blocking the transport through MWCNTs membrane. (b), (c) the SEM top view images of the MWCNTs membrane before and after electrochemical oxidization

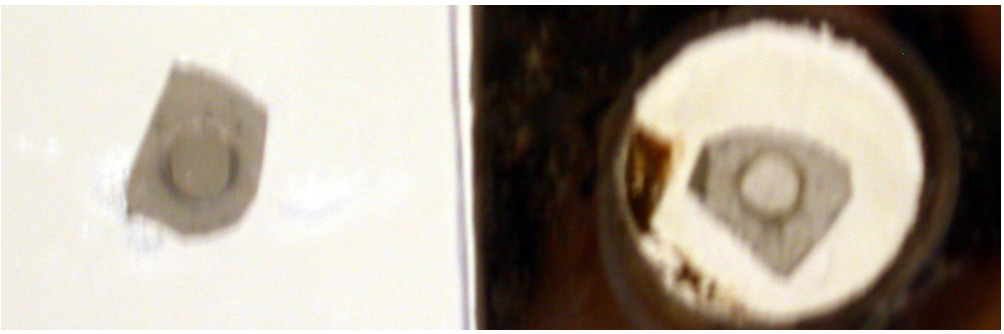

Figure 2.3 Optical images of MWCNTs membrane with and without electrochemical oxidization

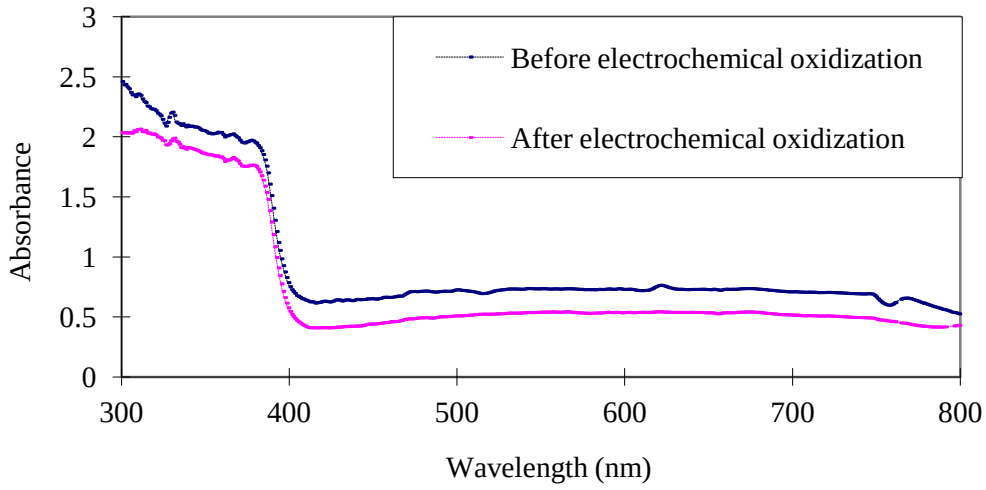

Figure 2.4 The UV-vis spectra of the MWCNTs membrane before and after electrochemical oxidization with the air as the reference

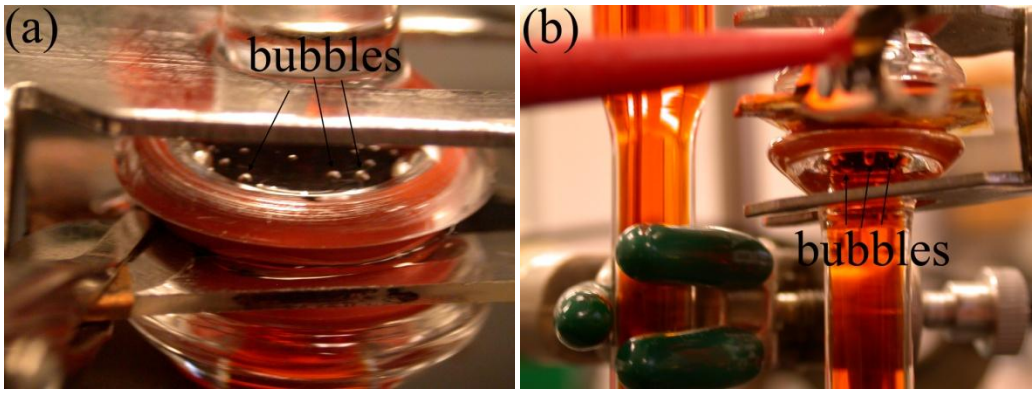

Figure 2.5 Optical images of the big bubbles generated on the MWCNT membrane at constant potential of -1.2 V vs Ag/AgCl

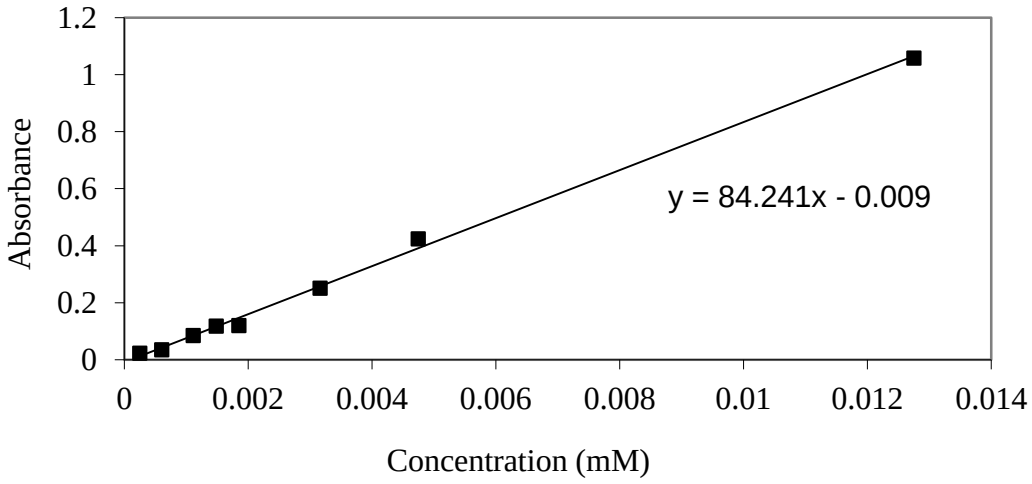

Figure 2.6 The calibration curve for the relationship between the concentration of $[Ru(bipy)_3]^{2+}$ and the absorbance of the UV

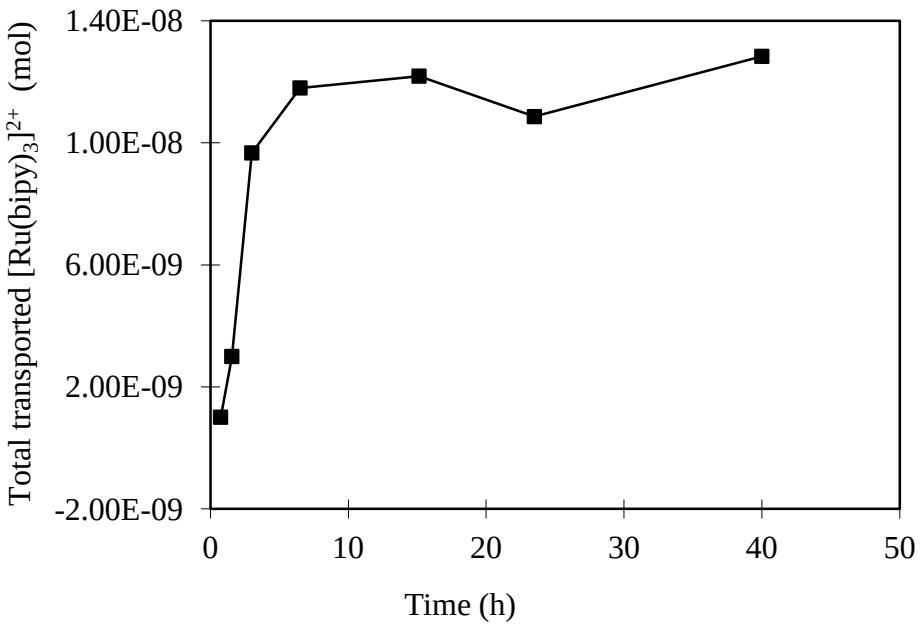

Figure 2.7 The relationship between the total amounts of $[Ru(bipy)_3]^{2+}$ transported through membrane and screening time, when the constant potential (-1.2 V vs Ag/AgCl) is applied on the membrane.

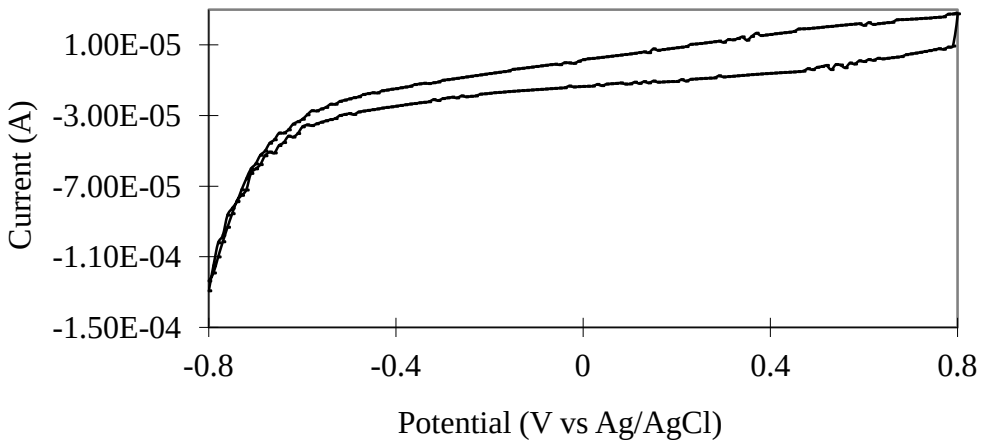

Figure 2.8 Cyclic voltammogram of the MWCNTs membrane in a solution of 0.05 M H_2SO_4/5 mM $[Ru(bipy)_3]^{2+}$, at a scan rate of 100 mv/s and with set up shown in figure 2.1b

Table 2.1 A series of blocking efficiencies of nanoscale bubbles generated by the different potentials on a MWCNTs membrane, which is pretreated by electrochemical oxidization (5 mM $[Ru(bipy)_3]^{2+}$/0.05 M H_2SO_4 in feed side; deionized water in permeate side).

Membrane conditions	Potentials applied on membrane	Blocking efficiency
Bare membrane	Sine potentials: potentials -0.8 v to +0.8 v; frequency: 200 Hz, 10 minutes	21%
1st Pretreated Membrane	0	0%
1st Pretreated Membrane	Sine potentials: potentials -0.8 v to +0.8 v; frequency: 200 Hz, 10 minutes	92%
2nd Pretreated Membrane	Sine potentials: potentials 0 v to +0.8 v; frequency: 200 Hz, 10 minutes	0%
2nd Pretreated Membrane	Sine potentials: potentials -0.8 v to +0.8 v; frequency: 200 Hz, 10 minutes	80%
2nd Pretreated Membrane	Sine potentials: potentials -0.8 v to 0 v; frequency: 200 Hz, 10 minutes	87%

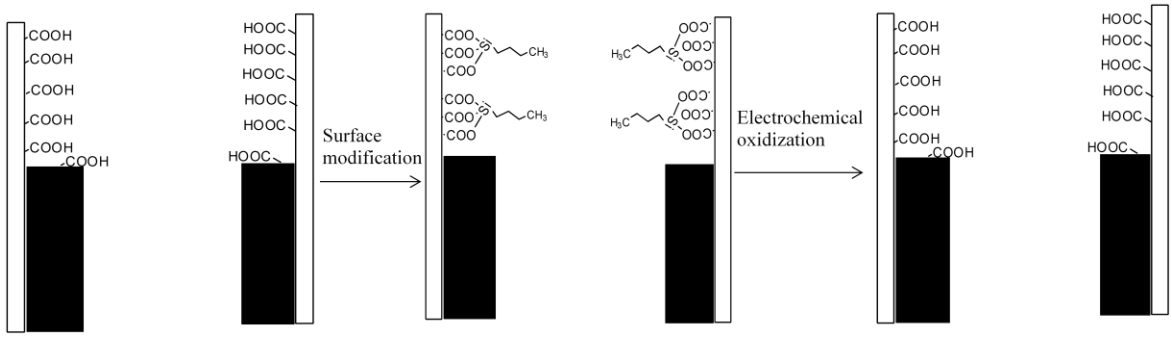

Figure 2.9 The schematic picture for the surface modification of polymer wells for the control experiment

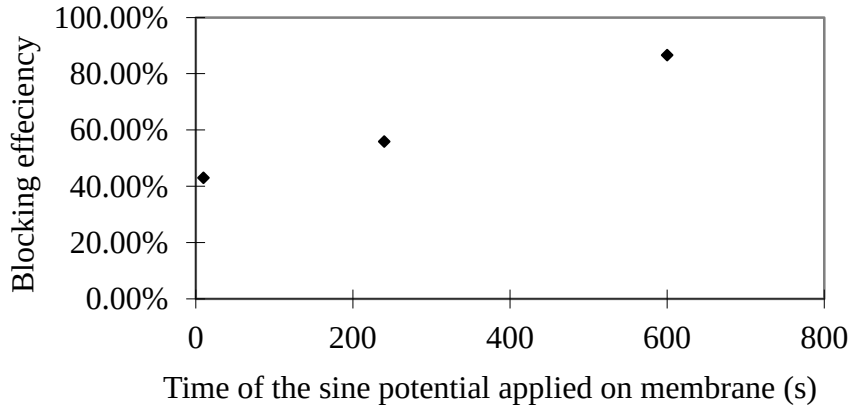

Figure 2.10 The blocking efficiencies of nanoscale bubbles depend on the time of sine potential applied on CNTs membrane

Table 2.2 A series of block efficiencies before/after that nanoscale bubbles on pretreated MWCNTs membrane, are removed by pressure gradient from bottom to top of membrane. (5 mM $[Ru(bipy)_3]^{2+}$/0.05 M H_2SO_4 in feed side; deionized water in permeate side)

Membrane conditions	Potentials applied on membrane	Blocking efficiencies
Pretreated membrane	0	0%
Pretreated membrane	Sine potentials: potentials -0.8v to +0.8v; frequency: 200Hz, 10 minutes	84%*
Pretreated membrane	Nanoscale bubbles removed by the 0.004 atm pressure gradient.	21%*

Chapter 3: The MWCNT membrane used for electrochemical energy storage

3.1 Introduction

To overcome the challenge on instability and poor reliability of renewable energy (wind power, solar energy) for large scale application, energy storage has attracted intensive research attention. Electrochemical energy storage offers a promising and convenient strategy for the smart grid of renewable energy with direct conversion between the electrical energy and chemical energy.[32-34] Many kinds of the electrochemical energy storage have been developed like lead-acid battery, nickel-cadmium battery, sodium-sulfur battery, redox flow battery, lithium ion battery, etc..[79, 80] They can be applied in the energy storage system for solar energy, emergence power supply and even the electric vehicles. The membranes/separators are the critical parts for batteries for converting the chemical energy to electrical energy. For example, for the redox flow battery, they should prevent the transport of active chemicals but allow the transport of charge carriers.[83] Extensive research works have focused on modification of the membrane by preventing the cross contamination/reaction of chemicals in two sides of the membrane for the battery.[84-87] The membrane for the redox flow battery to store energy should have the low permeability to the active chemicals, which can minimize the self discharge rate of the battery, and should have high conductivity for the selected ions, which can improve the efficiency of energy conversion. Meanwhile, the membrane should be inert to the active chemicals for longer life performance.[88, 89] For the rechargeable flow battery, the membranes/separators are usually requested to allow the reactive ions during the charge. After the charge process, the membrane should block the transport of reactive chemicals as redox flow battery.[90, 91] The schematic process of the

whole system for the rechargeable electrochemical flow battery is shown in figure 1.9. During the charging process, the active chemicals Cl^- was electrochemical oxidized to Cl_2, which was transported to reservoir. After the battery was fully charged, the active chemical was stored in the reservoir with the valve close. For discharging the battery, the valve was open and the active chemical was transported to the reactive side to generate the electrical power.[92]

It was reported that the CNT membrane could be an exciting platform for energy storage since the mass transport through CNT cores is a thousand fold faster than pores of conventional materials, which can enhance charge/discharge process for the energy storage.[58, 60] According to our former chapter, CNT membrane with nanoscale bubble as valve can be used as an smart membrane for controlling the transport on/off through the membrane. Meanwhile graphite is highly conductive and stable and CNT surfaces can be functionalized with catalyst metals or complexes for a low overpotential.[40, 42, 55, 93] Owing to all the properties mentioned above, the pretreated CNT membrane turns out to be the ideal membrane for the rechargeable electrochemical flow battery. Thus here it is reported that the novel pretreated CNT membrane with polymer wells, which have been coated with gold on the membrane as electrodes, have been applied as the membrane for the rechargeable electrochemical flow battery to store the electrochemical energy. The mechanism and phenomena of self discharge rate by storing electrochemical energy with the neutral molecular and charge ion are presented and discussed with the calculated and experimental results.

3.2 Experimental details and characterization methods

Fabrication of aligned MWCNTs membranes: The fabrication of aligned MWCNTs membranes was developed according to our group's former paper.[58] To describe it briefly, aligned multi-walled CNTs with an average core diameter of ~7 nm and length of 150 μm were prepared via a chemical vapor deposition (CVD) approach using ferrocene/xylene as the feeding gas.[57] Next, Epon 862 epoxy resin (Miller Stephenson Chem. Co.), and hardener methylhexahydrophthalic anhydride (MHHPA, Broadview Tech. Inc.) were thoroughly mixed using a ThinkyTM Mixer, which was employed to fabricate epoxy/CNTs composite using a casting method. As-prepared CNTs-Epoxy composite was then appropriately cured before being cut into CNTs membranes using a microtome equipped with a glass blade. The typical thickness of as-cut CNTs membrane is about 5 microns. Finally, the residual epoxy on the tips of CNTs was removed by H_2O plasma oxidation.

Electrochemical pretreatment and gold electrodes on MWCNTs membrane: The polymer wells on tips of MWCNTs were created by electrochemical pretreatment on the CNTs membrane as we did before. This was performed in three-electrode cell using a potentiostat (PAR Model 263A) with the reference electrode of Ag/AgCl from Bioanalytical. Pt wire was used as the counter electrode. The electrolyte solution for this is 0.1 M KCl. The bottom of MWCNTs membrane was coated with ~25 nm gold film by using sputtering machine (Cressington coating system 308R) to get a good conductivity between the working electrode and CNTs of the membrane. In the pretreatment, parts of MWCNTs in MWCNTs membrane were electrochemically oxidized for 5 h at a potential of 2.5 V vs Ag/AgCl, in a solution of 0.1 M KCl. After the pretreatment, the gold was

sputtered on both sides of membrane to form 50 nm gold electrodes, which covered on the surface of membrane. The schematic structure of the membrane with a series of pretreatment was shown in figure 3.1.

Characterizations of the MWCNTs membranes: The surface morphology of CNTs membrane with a series pretreatment was characterized by Scanning Electron Microscopy (SEM) (Hitachi S-4300) under the operating voltage of 20 kV. The parts of CNTs membrane were mounted flat on double sided conductive tape for top view of both sides and the cross-section image of the membrane. The gold particles were electrolessly deposited into the polymer wells of the membrane after electrochemical pretreatment. The membrane before/after this was cut into pieces to get the cross section image of the membrane to demonstrate the structure of the pretreated CNTs membrane. The porosity of the MWCNTs membrane was evaluated by the probe molecular ruthenium bipyridine hexahydrate $[Ru(bipy)_3]^{2+}$ as before.

Charge and discharge process of the membrane: The set up for the charge and discharge was shown in figure 1. The charge process was carried out in the two electrodes using EDAQ potentiostat. The feed solution was 5 mM $FeCl_2$, $FeCl_3$ or $K_4[Fe(CN)_6]$ and permeat side was 15 μl deionized Water. The gold electrodes coated on the top of the polymer wells was used as working electrode. The Fe wire was seviced as the counter electrode. The the output voltage of the membrane after charge was monitored by multiple voltage meter GDT 292A for the self discharge of the membrane. The sine potentials was applied on bottom electrodes of the membrane after charge to generated hydrogen in feed solution to improve the self discharge rate. The setup and the electrolyte solution for this were the same as two electrodes system as mentioned above.

3.3 Results and discussion

The schematic mechanisms and processes about the charge and electrochemical energy storage of the CNT membrane were show in figure 3.1. During the charging process of the MWCNT membrane, the voltage of +1.2 V was applied on working electrode coated on top side of membrane. The set up was shown in figure 3.1. When the feed solution was 5 mM $FeCl_2$, the Cl^- ions transported through MWCNT membrane, which were driven by the electrical field and concentration gradient. Then ions were electrochemically oxidized to Cl_2 at working electrode in the reservoir, where the high energy chemicals were stored. The volume of deionized water was ~15 μl in permeate side. According to the equation $Cl_2+H_2O=HCl+HClO$, the chlorine Cl_2 in reservoir would react with water. Assuming that the concentration of Cl^- is 10 mM in the reservoir, the Ka and concentrations of the reaction products are shown in table 3.1. It is obvious that more than 80% Cl_2 would react with water and generate HClO. Meanwhile, according to the Ka for the equation $H_2O + HClO = H_3O^+ + ClO^-$ in table 3.1, all of HClO would stay as neutral molecules [190-194]. Therefore, all chemicals stored in reservoir were neutral HClO and Cl_2 under the experimental conditions.

The flux rate can be calculated according to the Fick's law of diffusion

$$J = -D * \Delta C / l * A \qquad (3.1)$$

where D is diffusion coefficient, ΔC is the concentration difference of molecules between the reservoir and the feed side, L is the thickness of the membrane and A is porous area of the membrane. As shown in table 3.2, the initial flux rate of HClO is 2.1 nanomol/h.[195, 196]. Therefore, if the flux rate of HClO could be maintained at initial

value, the concentration of HClO in permeate side C^{ox} at time t could be calculated by the following equation 2

$$C^{ox} = (C^0V - Jt)/V \tag{3.2}$$

where C^0 is the initial concentration of HClO, V is the volume in permeate side, t is the time, and J is initial flux rate of HClO through the membrane. The full battery reaction equation is $HClO+H^++Fe=Fe^{2+}+Cl^-+H_2O$. Thus the output voltage can be calculated from Nernst equation

$$E = E^0 - \alpha - \frac{0.05916\text{V}}{\text{z}} * \log\,(C^{red}/\text{C}^{ox}) \tag{3.3}$$

where E^0-α is the initial potential of the reaction in the battery, z is charge transfer during the reaction, C^{red} is the concentration of reducing agents in the reaction, C^{ox} is the concentration of oxidizing agents in the reaction. When the membrane is full charged, the time t is equal to 0 and E is equal to 1.2 V. With assumption that the flux rate of HClO maintained at initial values during the storage process, the relationship between output voltage E and time t can be obtained by combining equation 2 and 3 for equation 4

$$E = E^0 - \alpha - \frac{0.05916\text{V}}{\text{z}} * \log\,(C^{red} * V/(C^0V - Jt)) \tag{3.4}$$

The related values for the parameters of the equation 4 were shown in Table 3.3. The curve of E vs t was shown in figure 3.4 with the corresponding experimental datum.

When the feed solution was 5 mM $K_4[Fe(CN)_6]$, the $Fe(CN)_6^{4-}$ ions flowed through MWCNT membrane during the charging process and under the same conditions. Then ions were electrochemically oxidized to $Fe(CN)_6^{3-}$ at working electrode in reservoir,

which was also stored there. The volume of deionized water was same as before. The diffusion coefficient and the electrophoretic mobility of $Fe(CN)_6^{3-}$ was shown in Table 3.2. [197] The total diffusion flux rate of $Fe(CN)_6^{3-}$ can be calculated by following equation

$$J = -D * \Delta C/l * A - \mu EC/l * A \quad (3.5)$$

where μ is electrophoretic mobility, E is electrical field, C is the concentration of the ion in feed side, L is the thickness of the membrane and A is porous area of the membrane. The initial total flux rate J was 112 nanomole/h at the inner electrical voltage of 1.2 V. It would only take 0.67 h to completely deplete the $Fe(CN)_6^{3-}$ in reservoir, if the flux rate could maintain at initial value during the process. The full battery reaction equation here is $Fe(CN)_6^{3-}+e= Fe(CN)_6^{4-}$. With same assumption mentioned above, the output voltage E vs time t can also be calculated with equation 4. The related parameters were shown in table 3.3. The curve of E vs t was shown in figure 3.4 with corresponding experimental datum.

For the corresponding experimental part, first the surface morphology of the CNT membrane was demonstrated by the SEM images for the bottom and top sides of the pretreated CNT membrane (figure 3.2 a,b). The gold film coated on the bottom side of CNT membrane with CNTs sticking out. And the porous polymer wells in the top side of CNT membrane with gold coated on it. The structure of the CNT membrane after pretreatment was furthermore confirmed by the SEM images of the cross section of the CNT membrane (figure 3.2 c, d). They showed that the parts of CNTs were electrochemically oxidized from top side of the membrane and left the polymer wells in it. Furthermore, the gold particles were electrolessly deposited into the polymer wells of the

pretreated CNT membrane. The cross section images of CNT membrane after that (figure 3.2 e, f) confirmed the structure mentioned above.

Then the membrane with a series pretreatment was used to store the electrochemical energy by charging as set up in figure 3.1. When the feed solution is 5 mM $FeCl_2$, after the membrane was charged by applying +1.2 V on it, the output voltage by storing $HClO/Cl_2$, which was shown in figure 3.3, can be maintained at initial value very well. This matched with the prediction from the calculation before. However, when the feed solution is 5 mM $FeCl_3$ and opposite voltage of -1.2 V was applied on the top electrodes on the membrane to charge the membrane by reducing Fe^{3+} to Fe^{2+} and storing Fe^{2+} ions in top of membrane, the self discharge rat by storing Fe^{2+} turned out to drop very quickly at initial. This was due to the quick diffusion of Fe^{2+} under the inner electrical field across the membrane. After the depletion of Fe^{2+} in reservoir, $HClO/Cl_2$ generated at counter electrode in feed solution during the charging process let the output voltage maintain at -0.6 V.

Meanwhile, it was shown in figure 3.4 that the self discharge rate of the membrane by storing $Fe(CN)_6^{3-}$ was poor, when charging conditions for storing $Fe(CN)_6^{3-}$ are the same as that for $HClO/Cl_2$. This matched the predication by calculation mentioned before. As we calculated before, this is because that $HClO/Cl_2$ is neutral gas and the $Fe(CN)_6^{3-}$ are the ions with charge. During the process of self discharge, due to the inner electrical field across the membrane, the diffusion rate of the charge ions should be much faster than that of neutral molecular $HClO/Cl_2$. From figure 3.4, the self discharge rate by storing $Fe(CN)_6^{3-}$ is much more poor than that by storing the $HClO/Cl_2$. These experimental results matched very well with the calculated results.

Meanwhile, during the charging process for storing the $HClO/Cl_2$, the total charge of during the process is $275*10^{-6}$ C, which was calculated based on the I-t curve in figure 3.5. Assuming that coulombic efficiency for the charging was 100%, the total amount of Cl_2 generated in reservoir could reach $8.6*10^{-8}$ mol. The total volume of the deionized water in reservoir was 15 μl. Finally, if there was no reaction between the Cl_2 and H_2O, the concentration of Cl_2 in reservoir after charge is about 6 mM. This value is close to 5 mM that we used for the calculation to predict the output voltage mentioned above.

To improve the self discharge rate of the flow battery with CNT membrane further, the sine potential from -0.8 V to +0.8 V was applied on bottom side of the CNT membrane and in feed solution of 5 mM $FeCl_2$ to generated bubble. The self discharge rate of the membrane under diffusion conditions with/without nanoscale bubbles as shown in figure 3.6. The self discharge rate can be slightly improved after nanoscale bubbles generated on the bottom of membrane.

3.4 Conclusion

The electrochemical pretreatment can create the asymmetrical CNT membrane with polymer wells in one side and CNTs protruding from the other side. The pretreated CNT membrane, with both sides having gold electrodes, can be used for the electrochemical energy storage. The electrochemical energy, which was stored with the neutral molecules $Cl_2/HClO$, can be maintained much more stable and longer time than that stored with charge ions $Fe(CN)_6^{3-}/Fe^{3+}$. This is due to the fact that the storage potential electric field will not accelerate neutral molecules and mass transport is limited by Fickian diffusion through a low porosity membrane. In the case of ions, the electric

field from stored potential, accelerates ions the electrophoresis based mass transport The nanoscale bubble can be used as valve to improve the ability of the novel membrane to store the electrochemical energy with neutral molecular.

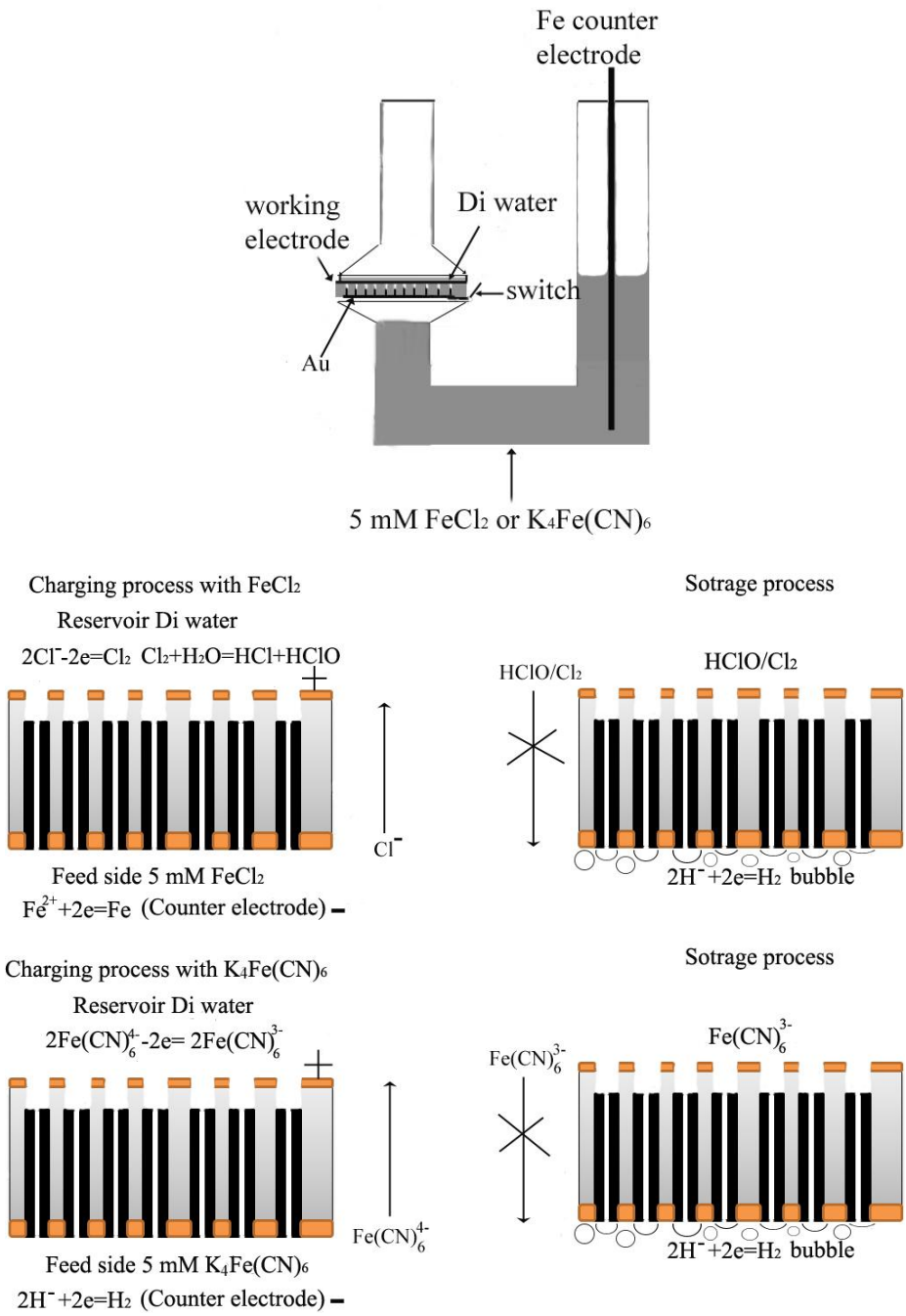

Figure 3.1 The schematic set up and mechanism of MWCNT membrane for the redox flow battery

Table 3.1 Ka for reaction equations: $Cl_2+H_2O=HCl+HClO$ and $H_2O+HClO=H_3O^+ + ClO^-$ and the related concentrations of molecules and ions under the experimental conditions

Reaction equation	Ka	Cl_2	HCl	HClO
$Cl_2+H_2O=H^+ + Cl^+ + HClO$	$5*10^{-4}$ [190, 198]	2 mM	10 mM	10 mM
Reaction equation	Ka	HClO	H_3O^+	ClO^-
$H_2O+HClO=H_3O^+ + ClO^-$	$3*10^{-8}$ [199]	10 mM	10 mM	$3*10^{-5}$ mM

Table 3.2 The related diffusion coefficient and the flux rate of HClO and $[Fe(CN)_6]^{3-}$ transport through the MWCNT membrane

	Coefficient	Thickness of membrane	Concentration in reservoir	Porous area of membrane	Flux rate
HClO	$1.3*10^{-5}$ cm^2/s [195, 196]	5 µm	10 mM	$2.3*10^{-6}$ cm^2	$2.1*10^{-9}$ mol/h
$[Fe(CN)_6]^{3-}$	$6.7*10^{-6}$ cm^2/s* $9.3*10^{-4}$ cm^2/Vs**[197]	5 µm	5 mM	$2.3*10^{-6}$ cm^2	$112.1*10^{-9}$ mol/h

* Diffusion coefficient, ** Electrophoretic mobility

Table 3.3 The related parameters for the Nernst equations for the cell reactions: 1) $HClO+H^{+}+Fe=Fe^{2+}+Cl^{-}+H_2O$ and 2) $Fe(CN)_6^{3-}+e=Fe(CN)_6^{4-}$

	E^0-α	z	V	C^{red}	C^0	J
Reaction 1	1.13 V	2	15 µl	5 mM Fe^{2+} 10 mM Cl^-	10 mM HClO	$2.1*10^{-9}$ mol/h
Reaction 2	1.2 V	1	15 µl	5 mM $Fe(CN)_6^{4-}$	5 mM $Fe(CN)_6^{3-}$	$112.1*10^{-9}$ mol/h

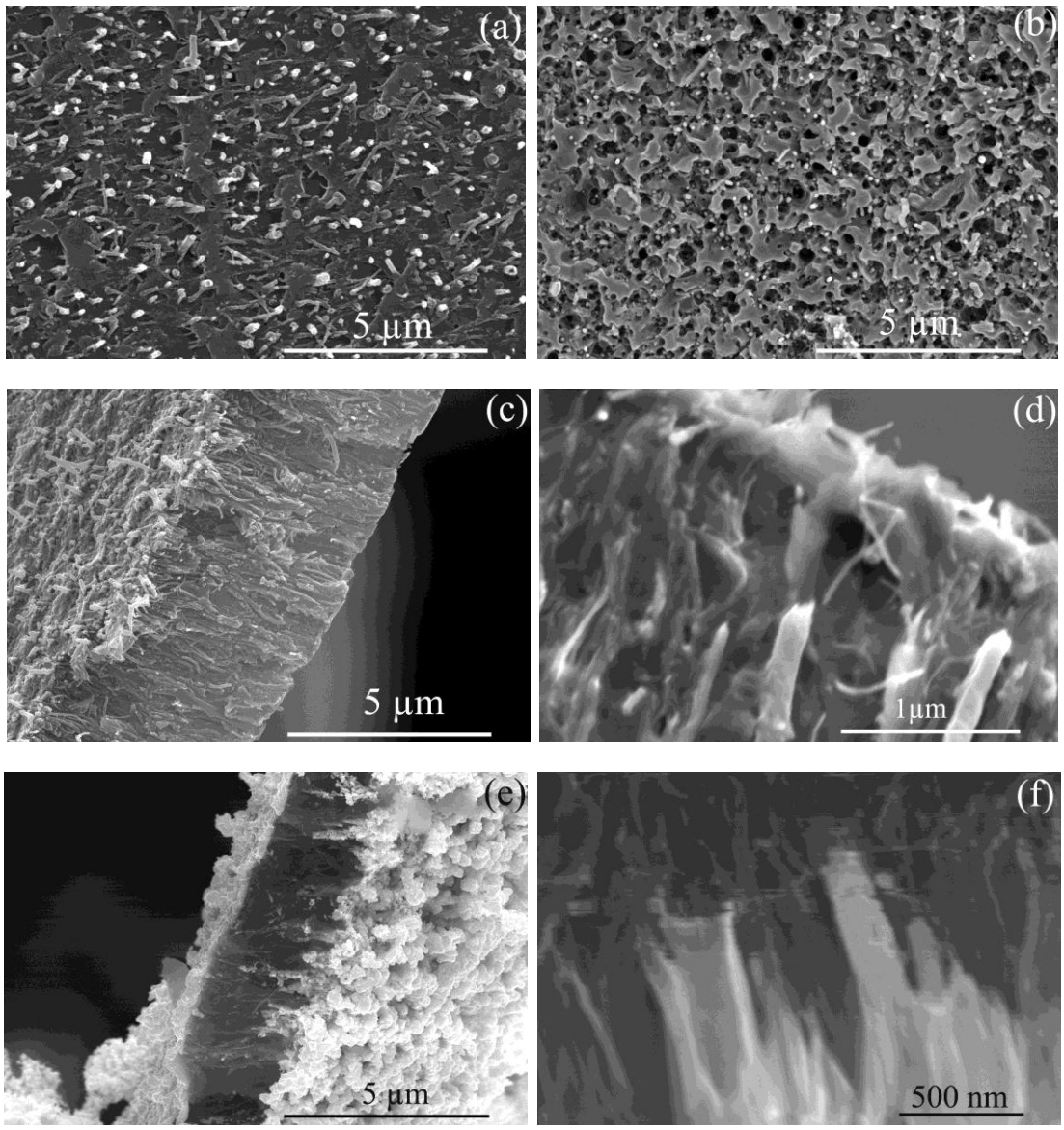

Figure 3.2 (a) (b) SEM image of membrane bottom (CNTs sputtered with Au) and top (porous polymer wells sputtered with Au). The cross section image of CNT membrane before/after electrolessly depositing Au into polymer wells.

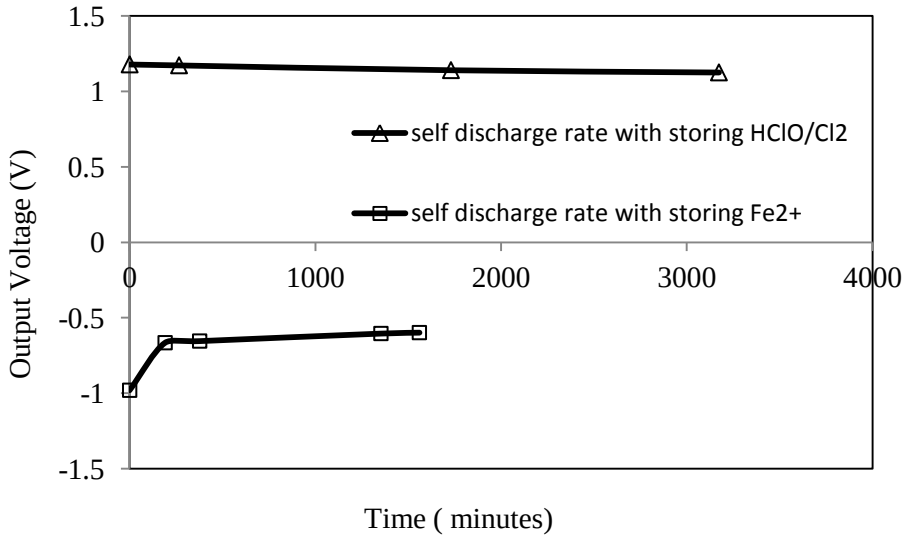

Figure 3.3 The self discharge rate of the battery by storing $HClO/Cl_2$ (Δ) in reservoir and by storing Fe^{2+} (□) in the reservoir

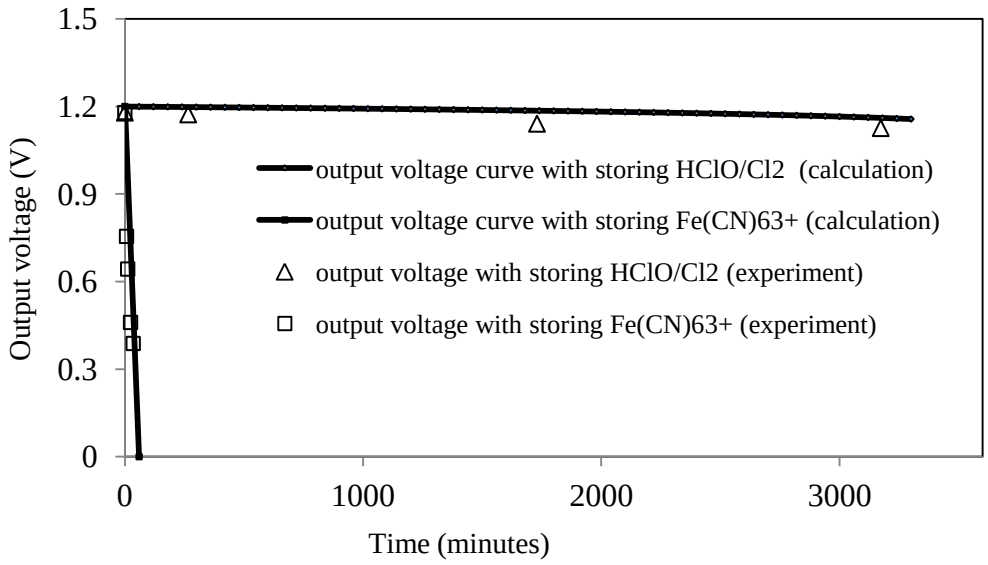

Figure 3.4 The self discharge rate of the battery by storing $HClO/Cl_2$ (Δ) in reservoir and by storing $Fe(CN)_6^{3-}$(□) in the reservoir from the calculations and the experiments.

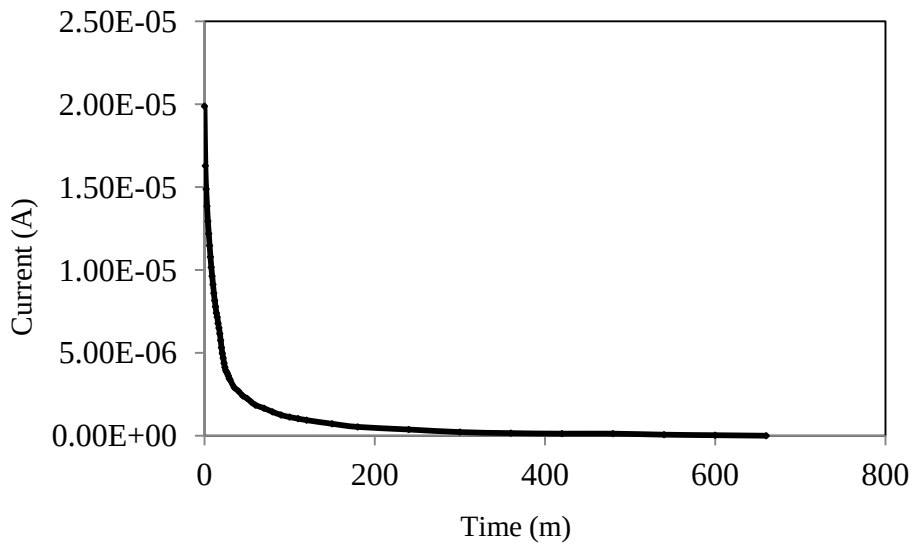

Figure 3.5 The current vs time during charging process of the CNT membrane at 1.2 V with the feed solution of 5 mM $FeCl_2$ and deionized water in permeate side.

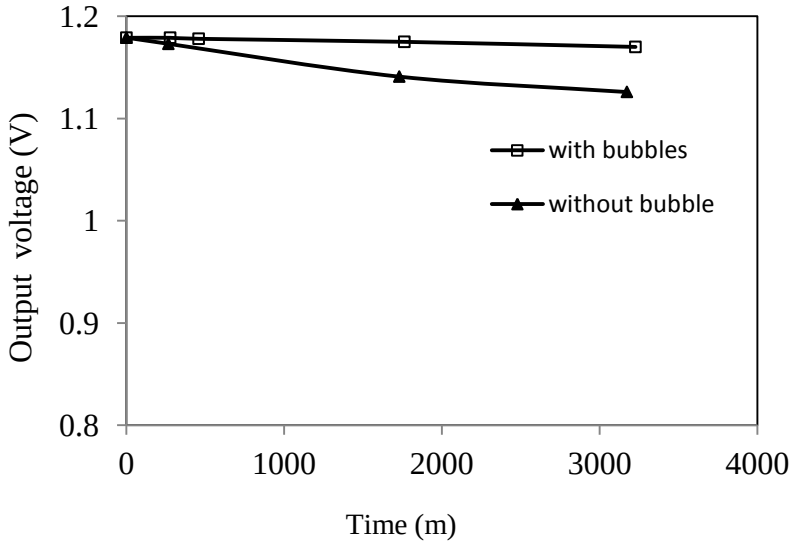

Figure 3.6 The self discharge of the flow battery with (□)/without (▲) nanoscale bubble as valve under the diffusion conditions

Chapter 4: Catalytic activity of ultrathin Pt films on aligned carbon nanotube arrays

This chapter is based on the manuscript:

Xin Su, Ji Wu and Bruce J Hinds, 'Catalytic Activity of Ultrathin Pt Films on Aligned Carbon Nanotube Arrays', Carbon, 2011, 49, 1145.

4.1 Introduction

Due to increasing energy demands and the possibility of significant methanol production via biomass conversion, there is active research focused on direct methanol fuel cells for electricity generation. The theoretical potential for the standard methanol cell is 1.25 V, which is close that for hydrogen cell. Furthermore the theoretical energy density of methanol fuel cell can reach 6.1 kWh/kg,[200] which is 10 times higher than that of Li battery[201] which is a critical factor in the transportation sector. However the methanol reaction rate is several orders of magnitude lower than that of hydrogen oxidation on metal electrodes.[99] Methanol fuel cell fabrication thus requires catalytic Pt loading onto the surfaces of electrodes to have useful methanol oxidation rates. Although Pt is an efficient catalyst for methanol fuel cells, it can be the most expensive component. Therefore scientists have been trying to increase the catalytic activity of Pt in fuel cell by reducing the diameters of Pt nanoparticles to as small as 1 nm [119] for the highest surface to volume ratio, by adjusting facet orientations of Pt nanocrystals [96] to be the most reactive faces, or by monolayer growth on nanoporous Au.[159] The ideal system is to have a stable and uniform nm-scale coating of Pt directly on the surface of a high area conductive electrode that is open to the fast mass transport of flowing liquids.

Carbon nanofiber and nanotube mats are the strong candidates for catalyst supports, due to their high surface area, conductivity, and chemical stability.[115, 116, 127] Carbon nanotube (CNT) arrays in particular, have high specific surface areas due to the small diameter (10-40 nm) of CNTs and high areal density (~10^9 /cm^2). The chemical inertness of carbon fibers makes the uniform coatings a challenge since Pt will continue to deposit onto an initial Pt nucleation site instead of the high energy graphite surface. In electro-plating, microns to submicron Pt particles thus result with very poor surface to volume ratios reducing the catalytic mass activity. A variety of treatments have been explored on carbon supports to improve Pt catalytic activity by controlling the Pt nanoparticle dispersion onto carbon fibers/tubes.[100, 129-131] These techniques rely on strong oxidation of fibers/tubes by plasma and ozone,[130] or hydrogen peroxide[131] and strong oxidizing acids[100, 129] with limited success.[100, 129-131, 202, 203] Recently a general class of CNT surface chemistry based on diazonium salt decomposition has been developed.[132] This surface modification can be controllably activated by electrochemistry at an electrode surface [133] for precise thickness control. The chemistry of the diazonium group can also be tailored [64, 133] to favor uniform metal ion coordination and, we hypothesize, allow uniform nm-thick Pt electrodeposition on CNTs.

Another difficulty with Pt electrodes in MeOH fuel cells is poisoning of the Pt surface by CO byproducts. Additives such as Ru,[135, 204] Ni,[140, 141] Au [139] have been used to enhance the activity and stability of catalyst by reduction of CO poisoning. However the surface additives can be etched over time reducing the electrode stability and performance. Needed are alternate methods to eliminate CO poisoning that are stable for indefinite periods of time.

Here we describe an electrochemical method to produce uniform nm-scale thick Pt films on a high area array of CNTs. The mass-activity of Pt catalyst is dramatically improved due to its large surface to volume ratio on CNT supports. A new voltage pulse method, between the operational voltage 0.7 V and a recovery voltage 0 V (vs. Ag/AgCl), was found to eliminate the effects of CO poisoning of Pt electrode without the requirement of potentially unstable additives.

4.2 Experimental details and characterization methods

Materials: Aligned CNTs were grown on quartz slides for 2 h by chemical vapor deposition method which ferrocene / xylene were used as precursors at 700 ℃ as previously reported [57]. The epoxicure resin and hardener were purchased from Buehler. The chloroplatinic acid hydrate was from Aldrich. The aryl diazonium salt was synthesized in the lab according to the references reported by Belanger et al..[205] 5 g of p-aminobenzoic acid was dissolved in 20 ml of deionized water at 60 ℃ with magnetic stir. Then 7 ml of concentrated HCl solution was added into it dropwise. The mixture was then cooled down to -3 ℃ and 15 ml of a cold solution of 3 M sodium nitrite were added slowly to it. The whole solution was kept at -3 ℃ one hour for complete reaction. Then the mixture was then filtered. To this, 10 ml of a cold solution of 4.5 M $NaBF_4$ was added to stabilize the diazonium salt. About 30% of the water was evaporated under low vacuum. The concentrated solution was cooled down to -3 ℃ for diazonium salt crystallization. The salt was finally vacuum filtered and rinsed by cold water and ether.

Preparation of the Pt Deposited on Aligned CNTs: The schematic of the process to prepare aligned CNT substrates is shown in Figure 4.1. The goal was to stabilize an

aligned array of CNTs with only the tip region embedded into an epoxy support. At first, an epoxy film was spun coat on a glass substrate at 5000 rpm. The film thickness of the epoxy was about 10 μm. Aligned CNTs (40~120 μm in length) grown on quartz slides were pressed on epoxy film at a weight loading of 25 g/cm^2. The sample was then kept in a vacuum oven at 60 ℃ for 16 hours to cure the epoxy. After the epoxy was completely cured, the quartz substrate could be easily separated from the CNTs by mechanical pealing. The aligned CNTs, which were partly embedded in epoxy film coated on glass slide, were used as the working electrode. The electrochemical deposition of Pt on aligned CNTs was performed in three-electrode cell using a potentiostat (PAR Model 263A) with the reference electrode of Ag/AgCl from Bioanalytical. Pt wire was used as the counter electrode. The electrolyte solution for electrochemical depositions were 4.8 mM H_2PtCl_6/0.1 M HCl/0.3 M NaCl. The solution was purged by Ar gas for 10 minutes before use.

Surface Modification of CNTs: The surface of CNTs was modified via an approach of aryl diazonium grafting, which had been known to react covalently with CNTs and graphite [64, 132, 133]. This was carried out for 40 s, at a potential of -0.6 V (vs Ag/AgCl) and in the solution of 5 mM aryl diazonium salt ($H_5C_7O_2N_2BF_4$)/0.1 M HCl/0.1 M KCl. Before diazonium grafting, the electrolyte solution was purged by Ar gas for 20 minutes to remove the oxygen adsorbed on the aligned CNT substrates and in solution. The theoretical monolayer thickness of this functional group grafted on the carbon surface was approximately 0.7 nm.

Cyclic Voltammogram (CV) and Programmed Pulse Potentials: The CV measurements were carried out in the three-electrode cell using a potentiostat (PAR Model 263A) with a reference electrode of Ag/AgCl. The Pt deposited on aligned CNTs was used as the working electrode and the Pt wire as the counter electrode. The electrolyte solutions were 0.5 M H_2SO_4 and 1 M methanol/ 0.5 M H_2SO_4. All the solutions were purged by Ar gas for 20 minutes before running CV to remove the adsorbed gas in solution and the surface of sample.

ICP-OES Analysis: After CV measurement, the sample was rinsed by deionized water 6 times and then immersed in aqua-regia (concentrated HCl and concentrated HNO_3 with a volume ratio of 3:1) for 24 h to completely dissolve Pt. The concentration of Pt in the solution was detected by ICP-OES (Varian Vista Pro). For Pt film, the calibration curve for ICP consisted of five datum points and was linear in the range 0.02 mg/l to 1 mg/l. The detection limit was 0.02 mg/l and the sample concentration was near 0.14 mg/l. Meanwhile, for Pt nanoparticles, the calibration curve for ICP also consisted of five datum points and was linear in the range 0.1 mg/l to 10 mg/l. The sample concentration was near 7.05 mg/l.

SEM, EDS and HRTEM: The morphology and composite of the sample were characterized by Scanning Electron Microscopy (SEM), Energy Dispersive Spectroscopy (EDS) (Hitachi S-4300) under the operating voltage of 20 kV and High Resolution Transmission Electron Microscopy (HRTEM), EDS (Jeol-2010f) under the operating voltage of 200 kV. For SEM, portions of the sample were cut and mounted on double sided conductive tape. The electrodes were conductive and no charging effects were seen. For HRTEM, the CNT arrays were ultrasonically dispersed by Branson 1510 in deionized

water for 15 minutes. Several drops of solution were placed on the copper TEM grids from Electron Microscopy Science and solvent evaporated.

4.3 Results and discussion

The aligned CNT arrays offer significant advantages for fuel cell electrodes since they are highly conductive and have a high active surface area (785 cm^2 over a nominal 1 cm^2 substrate area). Though conductive, the graphitic CNTs are chemically stable and highly inert to corrosion. The CNTs used range from lengths of 40 μm to 120 μm and have outer diameters of ~50 nm. The as grown aligned CNT arrays are transferred to an epoxy polymer film that binds to only the top 10um of CNT tips. The advantages of transferring CNTs to an adhesive layer[55, 206] is to recycle the relatively expensive quartz substrates used in the CVD growth and have a flexible and chemically inert polymer act as the final electrode support. The top view and cross-sectional SEM images of the aligned CNTs substrates are shown in Figure 4.2 (a) and (b). The conductive CNTs composing the array cross each other within the epoxy and the open electrode volume giving a measured in sheet resistance of 100 ohm/ sq. The sheet resistance of aligned CNTs array decreased to 21 ohm/ sq after uniformly coating with Pt. The sheet resistance can be reduced further by increasing thickness and approach that required for fuel cell applications.[207, 208]

The primary hypothesis here is that electrochemical grafting of ligands that can coordinate metal ions onto CNTs will aid in the uniform electrodeposition of Pt, thereby increasing Pt mass activity. Graphitic surfaces, such as CNTs, are well known to be chemically inert and uniform coatings are unfavorable compared to island growth onto

defects or other nucleation sites. As a control experiment, Pt was first electrodeposited on the unmodified CNTs [125] at a potential of -0.15 V (vs Ag/AgCl) and in a solution of 4.8 mM H_2PtCl_6/0.1 M HCl/0.3 M NaCl for 1.5 h. As shown in Figure 3 (a), the morphology of Pt particles deposited on bare aligned CNT substrates is highly nonuniform with large crystallites and poor surface to volume ratios. The high surface energies of bare CNTs favor the Pt growth onto existing crystals instead of forming a uniform Pt coating on CNTs. The HRTEM image of the unmodified CNT, in a region away from large Pt particles, after electrodeposition, is shown in Figure 4.3 (b). No uniform coating of Pt is observed on the unmodified CNTs and the deposited Pt is exclusively within the large particles. To have a thin (1-2 nm thick) uniform Pt deposition onto CNTs, the surface of CNTs was modified with functional carboxyl groups via a diazonium grafting method.[64, 132, 133] After the surface modification of CNTs with carboxyl groups, Pt was electrodeposited under the same condition as described above. The SEM image in Figure 4.3 (c) shows that the surface modification of the CNTs with the carboxyl groups can prevent the formation of large Pt particles during the electrochemical deposition. From the corresponding HRTEM and EDS data in Figure 4.3 (d) a uniform Pt coating of ~2 nm is seen on top of a polybenzoic acid film (~2 nm). EDS spectra in the inset confirms the presence of Pt in the image. ICP analysis of a solution of Pt dissolved from the CNT array quantifies 6.9 μg Pt that had been deposited on the aligned CNT array (0.3 cm^2 planar sample surface area). Cyclic Voltammogram (CV) was used to evaluate the catalytic activity of the Pt nano-coatings on CNTs which were modified with carboxyl groups. The CV was first performed for hydrogen reduction in a solution of 0.5 M H_2SO_4 and at a scan rate of 100 mV/s. The CV curve is

similar to classic curve of Pt nanostructure reported by Wallace *et al.*.[96] Methanol oxidation by the Pt coated CNTs was then studied by CV with a solution of 1 M CH_3OH/0.5 M H_2SO_4 at a scan rate of 20 mV/s. From the current level in Figure 4 (b) and the mass of Pt measured by ICP, we observe a mass activity for methanol oxidation above 400 A/g (blue line), which is much higher than that of Pt nanoparticles on bare CNTs ~20 A/g (red line), due to the ultra-thin and uniform coating on the CNTs having a much larger surface to volume ratio. This is also a significant improvement compared to the reports by Liu *et al.* of 181 A/g.[115] Furthermore, from the insert in Figure 4.4 (b), the experimental curve of peak currents ratios vs different scan rates from 20 mV/s to 100mv/s matched the calculated curve from Randles–Sevcik equation: $I_p=2.69\times10^5 AD^{1/2}n^{3/2}v^{1/2}C$. This demonstrates that there is no apparent mass-transport limitation of methanol through the CNTs arrays.

The CV of Figure 4.4 (b) shows a CO oxidation peak at 0.55 V (vs Ag/AgCl) and a methanol oxidation peak at 0.75 V (vs Ag/AgCl). It is well known that CO generated during methanol oxidation can poison the Pt catalyst surface [204]. As shown in Figure 4.5 (a), the current density for methanol oxidation on Pt/CNT electrode at 0.7 V (vs Ag/AgCl) dropped quickly due to the CO poisoning. During the course of control experiments, we found that we can recover the current almost entirely by applying a short voltage pulse at 0 V (vs Ag/AgCl). These pulse potentials at 0V eliminated the effect of CO poisoning and hence dramatically improved catalyst activity at the operating voltage of 0.7 V. This new recovery pulse method has significant application in fuel cell operations since additives such as Ru, which can corrode with time, are not needed. From Figure 4.5 (a), the current density of the Pt nanostructure under the pulse potentials can be maintained at

300 A/g for more than 3000 s, which is about 19 times of that under a constant potential of 0.7 V (vs Ag/AgCl). The sequence of operational (0.7 V, 10 s) and recovery (0 V, 1-10 s) pulses is shown in Figure 4.5 (b). As shown in Figure 4.5 (c), the optimal recovery time was found to be between 5 and 7 seconds. This would give an overall efficiency of 62% of operating current accounting for lost current production during the recovery time. The pulse potential method can be used with two or more cells in tandem with programmed switching. This would result in continual energy output while retaining the high mass activity of catalyst. Here, the pulse potential appears to remove absorbed CO very efficiently from the surface of the catalyst during the recovery time and the mechanism is currently under investigation.

4.4 Conclusion

Development of a high area, conductive and chemically stable catalyst support is important for fuel cell development. The surface modification of CNTs via diazonium grafting of a metal coordinating functional groups significantly improved the morphology of Pt, achieving uniform 2 nm-thick coatings. The thin organic layer does not impede electrical conductivity and the mass activity of Pt reached 400 A/g, which is a significance enhancement over other reports of high area carbon electrode supports.[100, 115, 129] It was also demonstrated that by applying a simple recovery pulse potentials, the current density of methanol oxidation can be maintained at a value as high as 300 A/g for 3000 s, which is about 19 times of that using a constant potential of 0.7 V (vs Ag/AgCl). This recovery method can eliminate the need for chemically unstable additives to prevent catalyst poisoning.

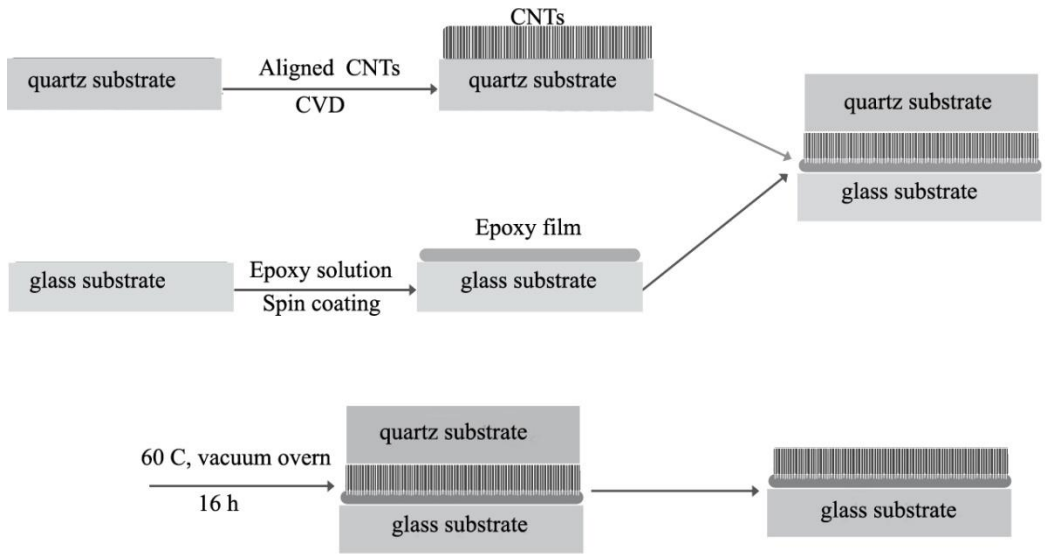

Figure 4.1 Schematic of the process for preparing the aligned CNT array electrodes

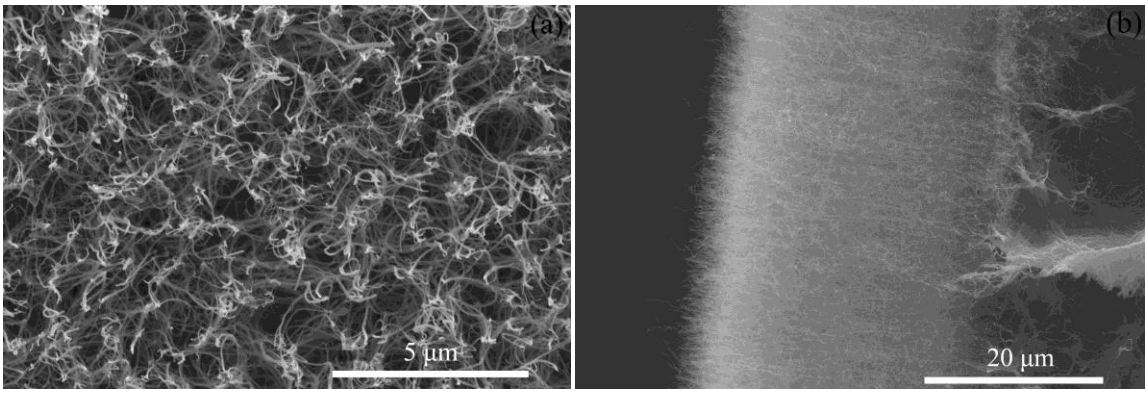

Figure 4. 2 SEM images of aligned CNT electrodes after epoxy transfer (a) top view; (b) cross sectional view.

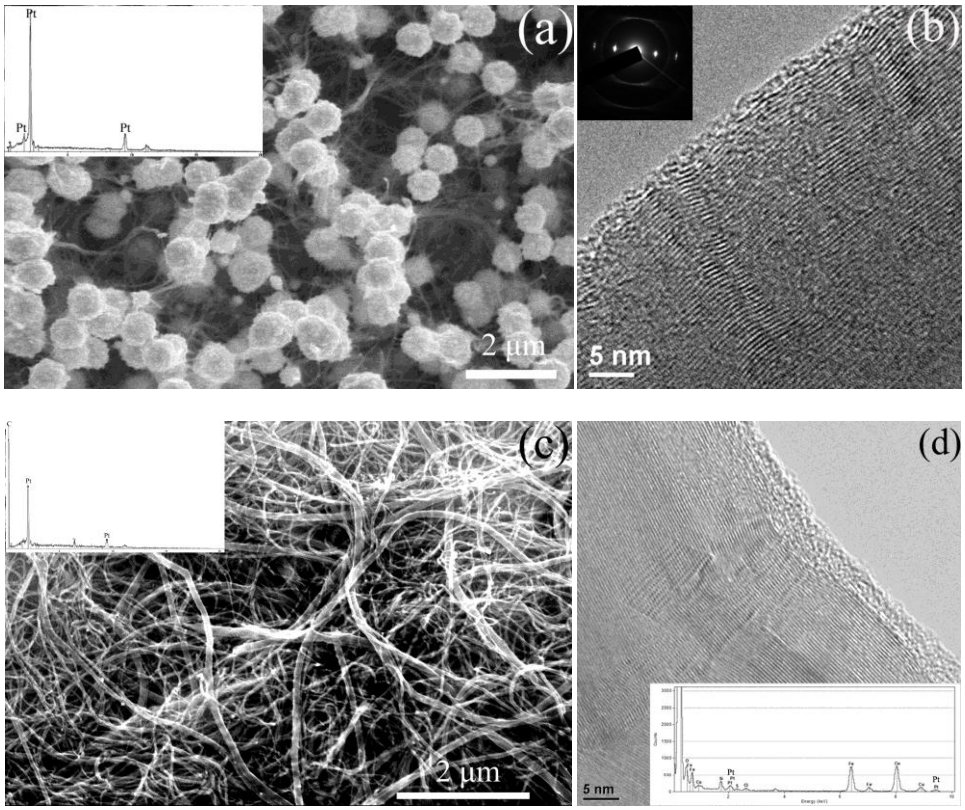

Figure 4. 3 (a) SEM image of Pt particles electrodeposited on the untreated CNTs; (b) HRTEM image of CNT away from large Pt particles showing absence of thin Pt layer; (c) SEM image of Pt electrodeposited onto the CNTs with surface treatment of carboxyl groups from electrochemical diazonium grafting; (d) HRTEM image of uniform ~2 nm thick Pt coating on treated CNTs.

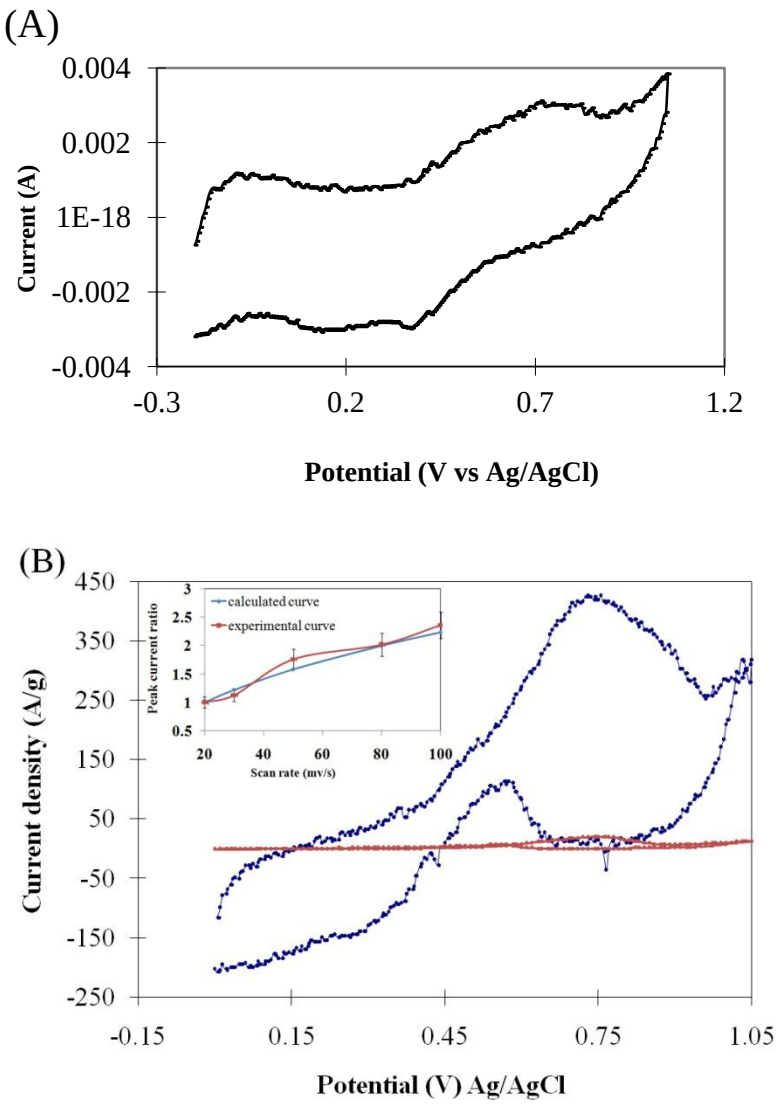

Figure 4.4 (A) Cyclic Voltammogram of Pt nanofilm deposited on CNTs grafted with carboxyl groups in a solution of 0.5 M H_2SO_4 and at a scan rate of 100 mV/s; (B) Cyclic Voltammogram of Pt nanofilm (blue) and Pt nanoparticles (red) on untreated CNTs in a solution of 1 M CH_3OH/0.5 M H_2SO_4 and at a scan rate of 20 mV/s. Insert figure is the experiment (red) and calculation (blue) showing Randles–Sevcik behavior of peak currents ratios vs scan rates from 20 mv/s to 100 mv/s.

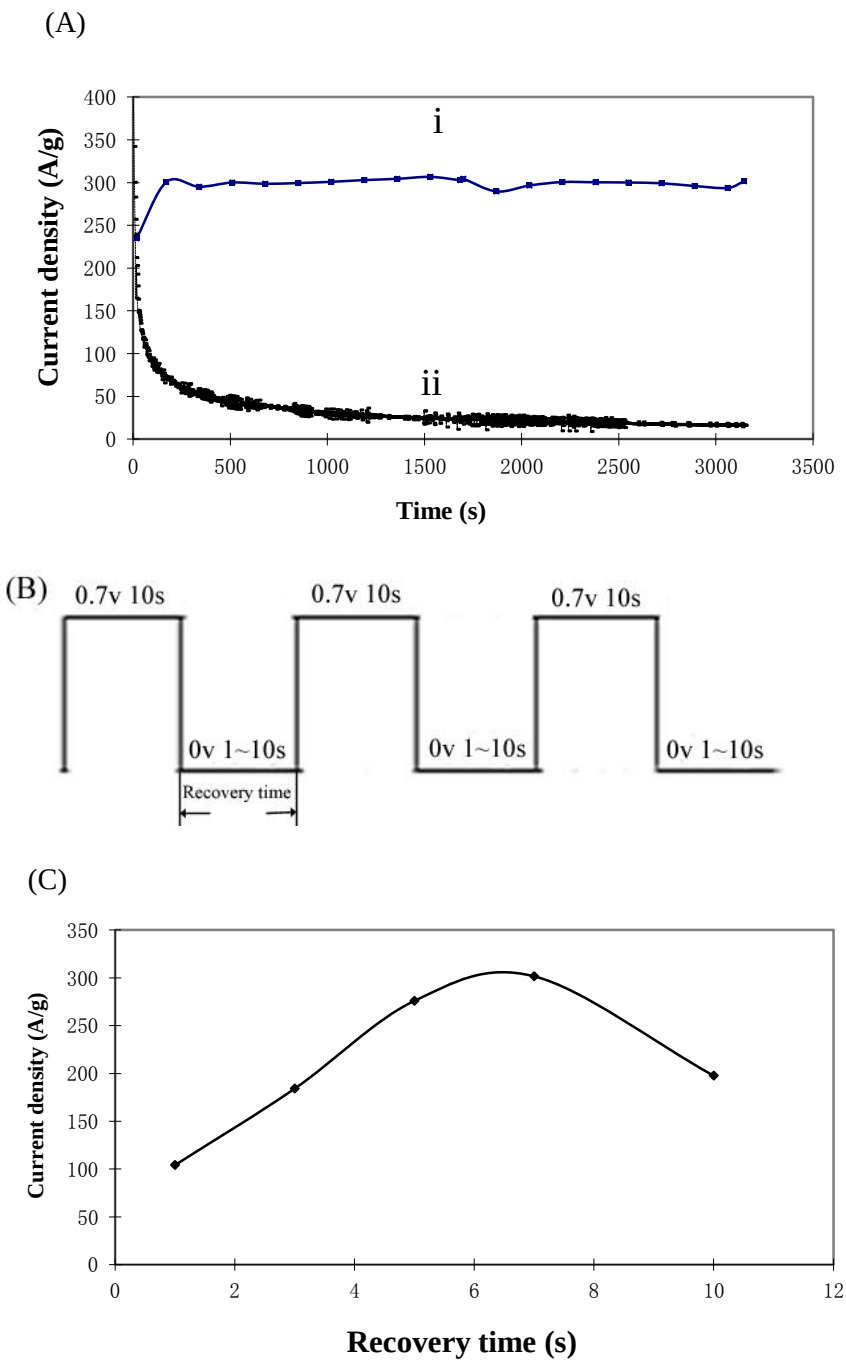

Figure4. 5 (A) The steady state current densities of methanol oxidation vs time (i) applying programmed pulse potential， with a recovery time of t=7 s, (ii) applying constant potential of 0.7 V (vs Ag/AgCl) on the sample; (B) Diagram of programmed pulse potentials with recovery pulses for Pt catalyst activity; (C) Steady state current densities of methanol oxidation vs. the recovery time of programmed pulse potentials.

Chapter 5: Pt monolayer deposition onto carbon nanotube mats with high electrochemical activity

This chapter is based on the manuscript submitted to Journal of Materials Chemistry:

Xin Su, Xin Zhan and Bruce J Hinds, 'Pt monolayer deposition onto carbon nanotube mats with high electrochemical activity' accepted by Journal of Materials Chemistry

5.1 Introduction

There is intensive research focused on methanol fuel cells to meet increasing renewable energy demands of human society [209-211] through biomass conversion. To have a usable methanol oxidation rate in a fuel cell, catalytic Pt is required as an electrode material and is the most expensive component.[212, 213] Since only the surface of the metal is catalytically active, scientists have been trying to increase the mass activity of Pt in fuel cells by reducing the diameters of Pt nanoparticles to as small as 1nm for the highest surface to volume ratio [214] or by adjusting facet orientations of Pt nanocrystals to be the most reactive faces.[96] The goal of this work is to produce the geometry that ideally renders all Pt atoms catalytically active: a monolayer of Pt over a stable and conductive high-area electrode. The underpotential deposition of metal monolayer on the metal substrates such as Au, Pt, Ag have been widely investigated. [152, 215, 216] The highest reported mass activity of Pt for methanol oxidation was 2600 A/g, which used a Pt monolayer growth over the surface of nanoporous Au.[159, 162] Though chemically stable, the catalyst support of porous gold is mechanically brittle and nearly as expensive as the Pt. Thereby it negated the economic advantages of the monolayer technique. The ideal

catalyst support system is relatively inexpensive support that is chemically inert, conductive and has extremely high surface area.[93, 217]

Carbon nanotube mats, often referred to as buckypaper, are the strong candidates for catalyst supports, due to their high surface area, conductivity, and chemical stability. [93, 127, 142] However, the Pt's mass activity in the system of Pt/CNTs was relative low due to the poor dispersion of Pt on CNTs.[100, 129, 142] The chemical inertness and hydrophobicity of carbon nanotubes make the Pt coatings a challenge since large particles grow on the nucleation sites instead of forming a homogenous coating. By electrochemical surface modification of MWCNTs with carboxylate groups to coordinate with metal ions, uniform ultrathin Pt films have been grown.[93] Here surface modification of MWCNTs has been used to coat Pt to the monolayer limit resulting in unprecedented mass activity. It is known that monolayers of Cu can be deposited by underpotential method, where the electroplating potential of the surface monolayer is significantly different than bulk Cu electrodeposition. However the Cu monolayer precursor requires strong binding between Cu ions and surface of the substrate.[115, 152, 159, 218, 219] Electrochemical grafting methods can render MWCNTs to be hydrophilic and offer the strong binding between metal ions and the surface of MWCNTs.[93, 100, 220, 221] Presented here is a facile way to coat Pt monolayer on MWCNTs with surface modification by replacing the Cu monolayer precursor. The mass activity of Pt monolayer coated on MWCNTs can reach 2711 A/g, which is more than 10 times of that of nm-scale thick Pt films.

5.2 Experimental details and characterization methods

Materials: MWCNTs were grown on quartz slides for 2 h by chemical vapor deposition method which ferrocene / xylene were used as precursors at 700 ℃ as previously reported.[57] The MWCNTs were pretreated by concentrated HCl to remove accessible Fe before use. The potassium tetrachloroplatinate (II) was from Alfa Aesar and 4-amino-2,3,5,6-tetrafluorobenzoic acid was purchased from SynQuest.

Preparation of Buckypaper: The 10 mg of MWCNTs were dispersed with a Branson 1510 ultrasonic horn in 15 ml of ethanol. Then the solution was vacuum filtered over 1 μm pore (4.7 cm diameter) Teflon filter paper from Sterlitech.

Surface Modification of MWCNTs: The surface of MWCNTs was modified via electrochemical oxidization of 4-amino-2,3,5,6-tetrafluorobenzoic acid, which had been known to react covalently with MWCNTs. This was carried out by Cyclic Voltammetry (CV) from 0.4 V to 1.7 V (vs Ag/AgCl), in an ethanol solution of 0.1 M $LiClO_4$ / 3 mM 4-amino-2,3,5,6-tetrafluorobenzoic acid and at a scan rate of 20 mV/s. The buckypaper was used as working electrodes with a reference electrode of Ag/AgCl and the Pt wire was serviced as the counter electrode. Before CV, the electrolyte solution was purged by Ar gas for 20 minutes to remove the oxygen adsorbed in the solution. The solution and counter electrodes were in 1cm diameter glass tubing with an o-ring seal (1.2 cm diameter) at the bottom of glass fitting on top of the CNT mat. Hence the active area for electrochemical experiments is 1.13 cm^2

Process of coating Pt monolayer/film on MWCNTs: The schematic of the process to coat Pt monolayer on MWCNTs was shown in Figure 1. After the MWCNTs' surface

was modified with carboxylic groups, the buckypaper was immersed in the solution of 0.5 mM $CuSO_4$ for 3 h. The electrode deposition was carried out in the three-electrode cell using a potentiostat (PAR Model 263A) with a reference electrode of Ag/AgCl. The buckypaper was used as the working electrode and Pt wire was used as the counter electrode. The electrolyte solution of $CuSO_4$ was purged with Ar gas for 20 minutes before the deposition to remove the absorbed O_2 gas in the solution and the surface of sample. After Cu monolayer deposition, the buckypaper was immersed immediately into a solution of 0.01 M $HClO_4$/0.1 mM K_2PtCl_4 for 5 minutes with Ar gas protection. The thick Pt film on MWCNTs for comparison was obtained by repeating the Cu monolayer and Pt replacement cycle 5 times.

Cyclic Voltamograms (CV): The CV measurements were carried out in the three-electrode cell using a potentiostat (PAR Model 263A) with a reference electrode of Ag/AgCl. The Pt monolayer/film coated on buckypaper was used as the working electrode and the Pt wire was serviced as the counter electrode. The electrolyte solutions were 0.5 M H_2SO_4 and 1 M methanol/0.5 M H_2SO_4. All the solutions were purged by Ar gas for 20 minutes before running CV to remove adsorbed O_2 in the solutions and the surface of the samples.

ICP-AES Analysis: The sample was rinsed by deionized water 6 times and then immersed in aqua-regia (concentrated HCl and concentrated HNO_3 with a volume ratio of 3:1) for 24 h to completely dissolve Pt. The concentration of Pt in the solution was detected by a Varian Vista Pro Inductively Coupled Plasma Atomic Emission Spectroscopy (ICP-AES). The calibration curve for ICP consisted of five datum points and was linear in the range 0.02 mg/l to 1 mg/l .The detection limit was 0.02 mg/l and the

samples' concentrationof Pt monolayer / Pt film were near 0.027 mg/l and 0.044 mg/l respectively. The volumes of samples for the Pt monolayer and Pt film are 15 ml and 50 ml respectively.

SEM, XPS, TEM, EDS and STEM: The morphology and composite of the samples were characterized by Scanning Electron Microscopy (SEM) (Hitachi S-4300) under the operating voltage of 20 kV, X-ray Photoelectron Spectroscopy (XPS) (Kratos 800) under the operating voltage of 15 kV, Transmission Electron Microscopy (TEM), Energy Dispersive Spectroscopy (EDS) and Scanning Transmission Electron Microscopy (STEM) (Jeol-2010f) under the operating voltage of 200 kV. For SEM, portions of the sample were cut and mounted on double sided conductive tape. The samples were conductive and no charging effects were seen. For XPS, portions of the sample were cut and mounted on sample stage with double sided tape. For TEM and STEM, the samples were ultrasonically dispersed by Branson 1510 in deionized water for 15 minutes. Several drops of aqueous solution were placed on the copper TEM grids from Electron Microscopy Science and solvent evaporated.

5.3 Results and discussion

The schematic coating process of Pt monolayer on MWCNTs was illustrated on figure 5.1. First the MWCNTs of buckypaper were modified with carboxylic groups in electrochemical grafting process of 4-amino-2,3,5,6-tetrafluorobenzoic acid in ethanol solution of 0.1 M $LiClO_4$/3 mM 4-amino-2,3,5,6-tetrafluorobenzoic acid [221, 222]. The carboxylate functionality is critical to forming uniform films by coordinating Cu ions for monolayer formation. The fluorinated benzoic acid is another important feature since the

strong C-F bonds are resistant to further electrochemical grafting and gives a self-limiting reaction near one monolayer. Thicker polymer deposition using non-fluorinated benzoic acid adds an undesired insulating layer between MWCNT and Pt monolayer thereby reducing current density. The functionalized buckypaper was then immersed in 0.5 mM $CuSO_4$ solution to allow Cu^{2+} ions to absorb on the MWCNT's surface coordinating with the carboxylate groups. After the absorbed Cu ions were reduced to metallic state to form Cu monolayer using underpotential method. Finally, the Pt monolayer was coated on MWCNTs by replacing the Cu monolayer with Pt ions due to the much larger reduction potential of the Pt.

Shown in figure 5.2 is the CV curve for the electrochemical grafting of 4-amino-2,3,5,6-tetrafluorobenzoic acid onto MWCNT buckypaper. The oxidation peak current for the amine gradually reduced from 3.8 mA to 2.8 mA during 1st to 14th scans and then from 2.8 mA to 2.5 mA during 14th to17th scans. It was finally stable at 2.5 mA from 17th to 20th scans. Reduction of current to a stable level indicates a self-limiting surface reaction with a thin layer of grafted carboxylic functionality.[221, 223] It is inferred that the relatively inert fluoro benzene prevents further polymerization during the surface modification.

After the surface modification, metallic Cu was electrochemically plated onto the MWCNT buckypaper. Linear sweep voltammetry is used to prove that a Cu monolayer is present due to the large difference in oxidation potential between bulk Cu (~0.02 V vs Ag/AgCl) and monolayer (0.2 V vs Ag/AgCl). Figure 5.3 shows the linear sweep voltammetry (LSV) curve for Cu stripping for samples with various Cu plating conditions. A Cu monolayer was successfully deposited onto the surface modified buckypaper at a

potential of 0 V vs Ag/AgCl, for 480 s and in a solution of 0.5 mM $CuSO_4$. By increasing the deposition time at 0 V vs Ag/AgCl from 480 s to 2400 s, both oxidation peaks for Cu monolayer and bulk Cu indicate that the plating is not completely self-limiting and it is possible to have more than a monolayer if too long a deposition time is used. If the deposition potential is reduced from 0 V vs Ag/AgCl to -0.1 V vs Ag/AgCl at 480 s bulk Cu is deposited. As a control experiment, the optimal electroplating conditions were applied to buckypaper without surface modification. There was no obvious peak during the LSV curve for Cu oxidation, thus the carboxylic surface modification of CNTs enables coordinate of Cu ions to MWCNTs' surface, which is critical for the Cu monolayer deposition.

Electron microscopy characterization was employed to demonstrate monolayer coverage and the exclusion of nanoparticle or thick film growth. First thick (~10 nm) coating samples were made by repeating the coating process 5 times to demonstrate uniform coverage and that the microscopy could detect such structures. The coating was readily seen by both SEM and TEM as seen in figure 5.4a and 5.4b and the EDS spectra in figure 5.4f confirmed that the film coated on MWCNTs was Pt. In the case of optimal monolayer coating conditions, the SEM image of figure 5.4c show that there was neither a thick Pt coating nor isolated Pt nanoparticles. The XPS spectra in figure 5.4g demonstrated that there was Pt on the MWCNTs after monolayer processing, but not of sufficient amount to see with the less sensitive EDS method. The circle areas of Hi-res TEM images figure 5.4d indicates the likely presence of monolayer of Pt with visible of graphite plane under it, but an inherently non-periodic monolayer is beyond the resolution of the TEM instrument of about 3 monolayers. The corresponding circle areas

of STEM image figure 5.4e of the MWCNTs in dark field also is consistent with the results in bright field TEM. Though below the detection limit, the microscopy is consistent with a monolayer of Pt since the presence of Pt was easily measured in the sample by XPS, ICP-AES, and electrochemical activity.

The electrochemical performance of the Pt monolayer was characterized by Cyclic Voltammogram (CV) peak current levels and then quantifying the amount Pt present in the sample by ICP-AES to get the mass activity. The CV curve (figure 5.5a) of a Pt monolayer on MWCNT buckypaper in an acidic solution (0.5 M H_2SO_4) demonstrated strong H_2 reduction peaks compared to the bare buckypaper thereby demonstrating the presence of Pt catalyst. Pt is also catalytically active for MeOH fuel cells. Cyclic Voltammogram (figure 5.5b) of the Pt monolayer coated MWCNT buckypaper sample was performed in a solution of 1 M CH_3OH/0.5 M H_2SO_4 and at a scan rate of 20 mV/s and shows strong catalytic activity compared to the control sample with Pt thick film. From the peak current and measure amount of Pt by ICP-AES, the mass activity of Pt monolayer was able to reach 2711 A/g. This was about 13 times of that for the ~10 nm Pt film coated on MWCNTs of buckypaper and is slightly higher than that of Pt monolayer coated on porous gold.[115] It is important to note that from the CV curve of figure 5.5b, the CO oxidation peak had been significantly reduced. CO poisoning of pure Pt is a common problem of MeOH fuel cells and is not seen in our case. This could be due to the unique sample structure with carboxyl functional groups on MWCNTs surface and Pt monolayer structure. It has been reported that the surface functional groups and additives can reduce the poison effect of CO during the methanol oxidations, due to weakening Pt-CO binding.[204, 224]

Although still considered as an exotic material, CNTs are an extremely high surface area material that is conductive and chemically inert to corrosion. Even at relatively high prices that are associated with new materials before scaled up process development, there is a strong economic argument for their use in fuel cell/catalytic applications where rare metals are the most expensive part and their price will only increase with increased demand. In the case of CNTs the raw materials of hydrocarbons and Fe/Co catalyst are abundant. Pt monolayer activity has been demonstrated on expensive porous Au electrodes where the surface area of porous gold is in the range from 8.7 m^2/g to 14.2 m^2/g.[225] As shown in table 5.1, the surface area of the buckypaper is 51.9 m^2/g from BET test and 54 m^2/g from geometric estimation with CNTs' diameter (60 nm) and graphite's density (2.1 g/cm^3). Thus the surface area density of buckypaper is about 3 to 6 times higher than that of porous gold. Meanwhile, the MWCNTs in diameter above 20 nm are presently $5 per gram from commercial company (i.e.Cheap Tubes Inc), which is similar to what we use in our work. In our case the material cost for CNTs is 0.38 cents and the Pt cost is 0.002 cents. For the porous Au case, the price of gold list on market reached was $57.9 per gram at 09/14/2011, which is similar to that of Pt. Accounting for the same surface area, the buckypaper is only 1/61 price of the porous gold as catalyst support. Furthermore the buckypaper is highly flexible, mechanically robust [226, 227] and can offer enhanced pressure flow rates through it.[40, 42, 228] These superior properties and this new ability to deposit Pt monolayers make it a promising catalyst support for fuel cells in future.

5.4 Conclusion

In this report, highly efficient Pt monolayers can be coated on MWCNT mats for fuel cell and catalytic electrodes. This is achieved by using CV oxidization of fluorbenzoic acid to CNT surfaces to have favorable Cu ion coordination that can be reduced to a Cu monolayer by a under-potential deposition method. This Cu monolayer is then stoichiometrically exchanged with Pt. The Pt monolayer coated MWCNTs shows high electrochemical activity. The mass activity of Pt monolayer is 2711 A/g about 13 times higher than that of the ~10 nm thick Pt film coated on MWCNTs. To the best of our knowledge, Pt monolayer is first time deposited on CNTs, which is much cheaper than the metal substrate porous Au. Meanwhile the mass activity of Pt monolayer/CNT electrode has reached the record high value, which is at least 6 times higher than that of other reported Pt/carbon electrodes [93, 100, 115]. In addition to high mass activity and low cost, the Pt monolayer coated on buckypaper has several advantages such as high surface area, flexibility, mechanical robust and enhanced pressure flow.

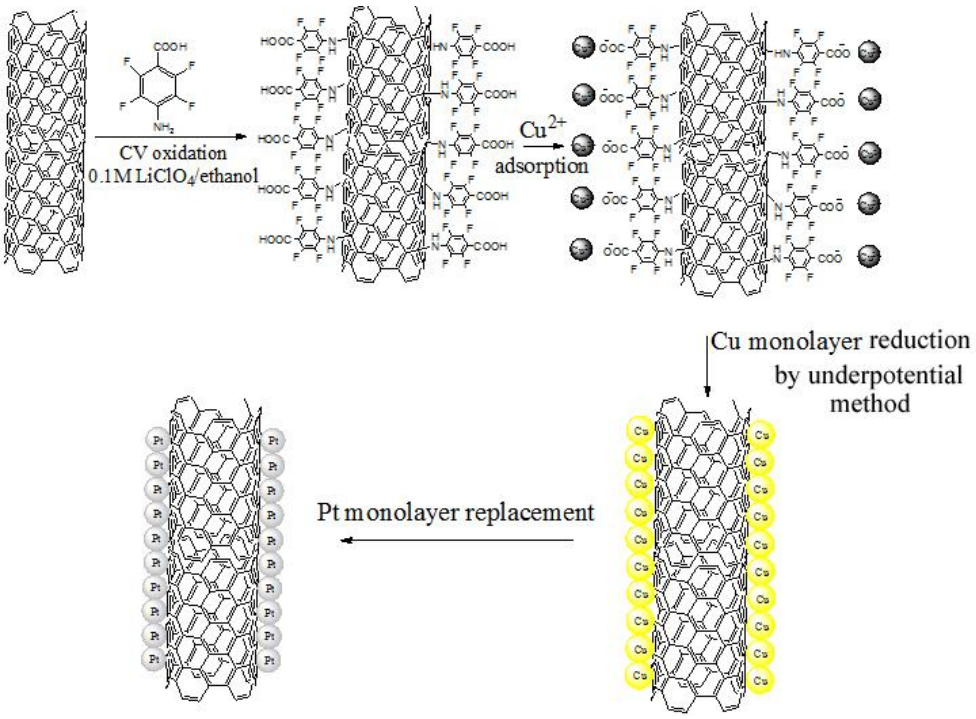

Figure 5.1 Schematic illustration of the fabrication procedure for Pt monolayer coating onto MWCNT mats.

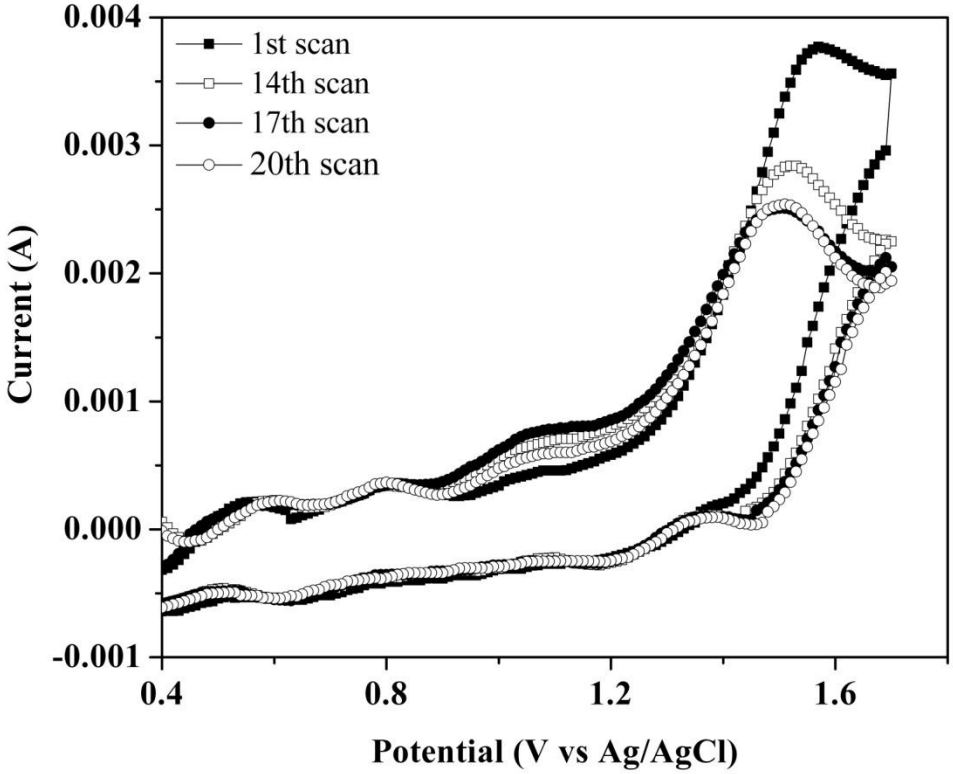

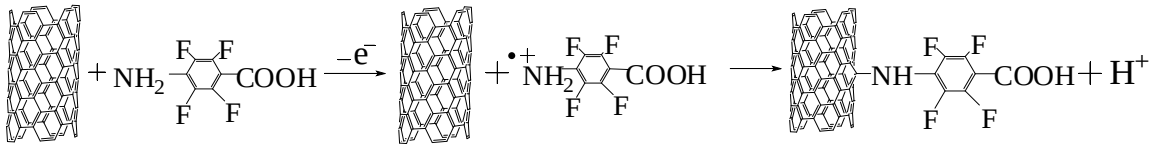

Figure 5.2 Cyclic Voltammograms on buckypaper in the ethanol solution of 0.1 M $LiClO_4$/ 3 mM 4-amino-2,3,5,6-tetrafluorobenzoic acid, the 1st (■), 14th (□),17th (●) and 20th scans (○) cycles at the scan rate of 20 mV/s. The reaction equation for surface modification.

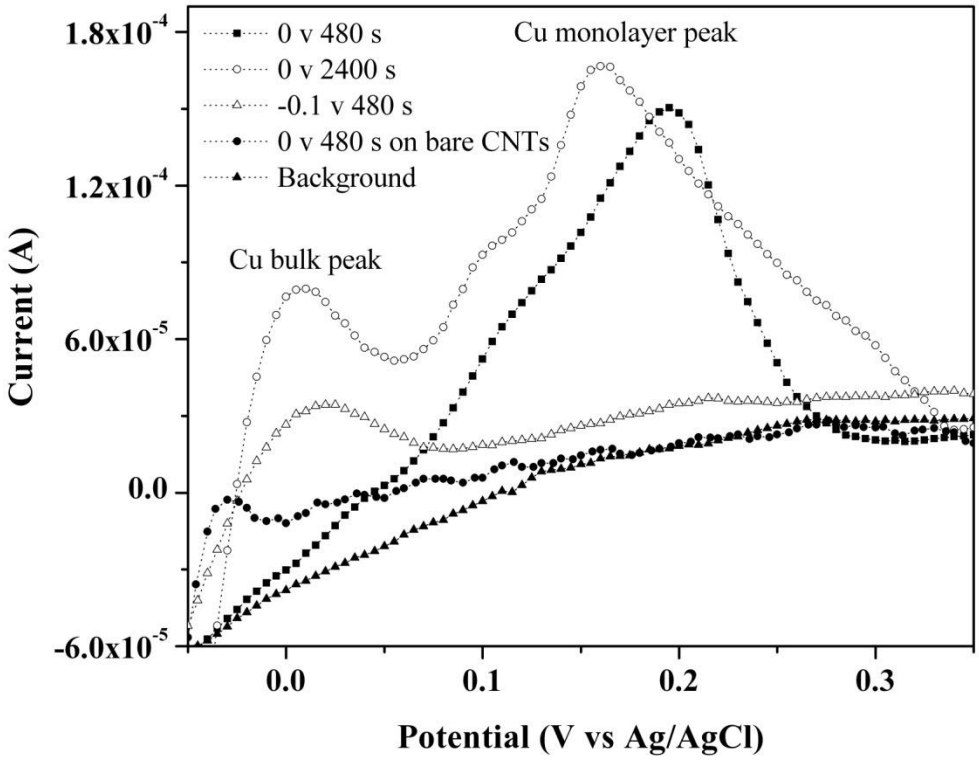

Figure 5.3 Cu stripping current vs applied potentials. The samples are Cu deposited MWCNTs with/without surface modification under different conditions(at 0 V 480 s (■), at 0 V 2400 s (○), at -0.1 V 480 s (Δ), background (▲) on MWCNTs with surface modification, 0 V 480 s on bare MWCNTs (●))

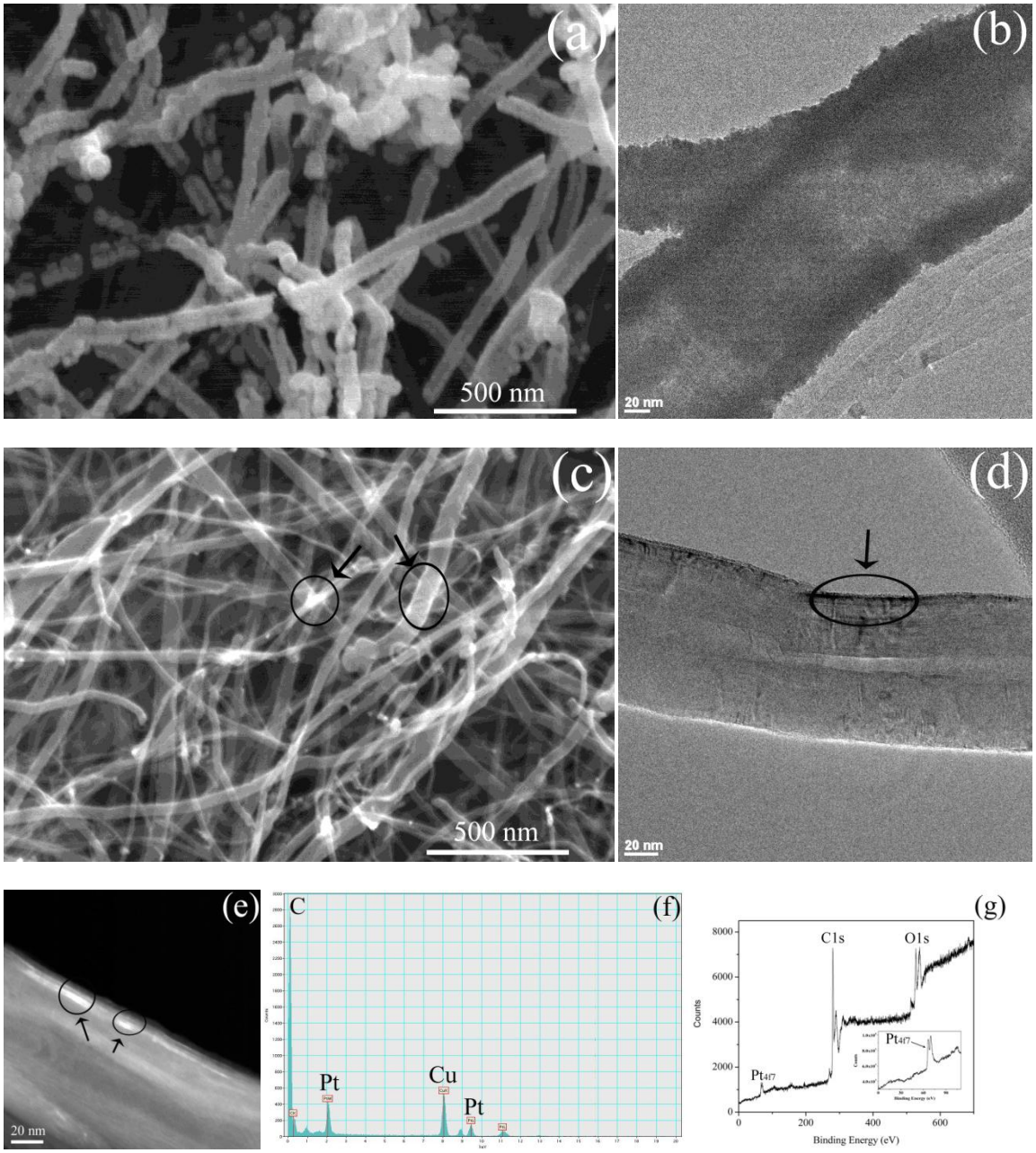

Figure 5.4 (a) SEM image and (b) TEM image of Pt film coated on MWCNTs by repeating coating, (c) SEM image,(d) TEM image in bright field and (e) STEM image in dark field of the Pt monolayer coated on MWCNTs, (f) EDS of Pt thick film coated on MWCNT, (g) XPS of Pt monolayer coated on MWCNTs.

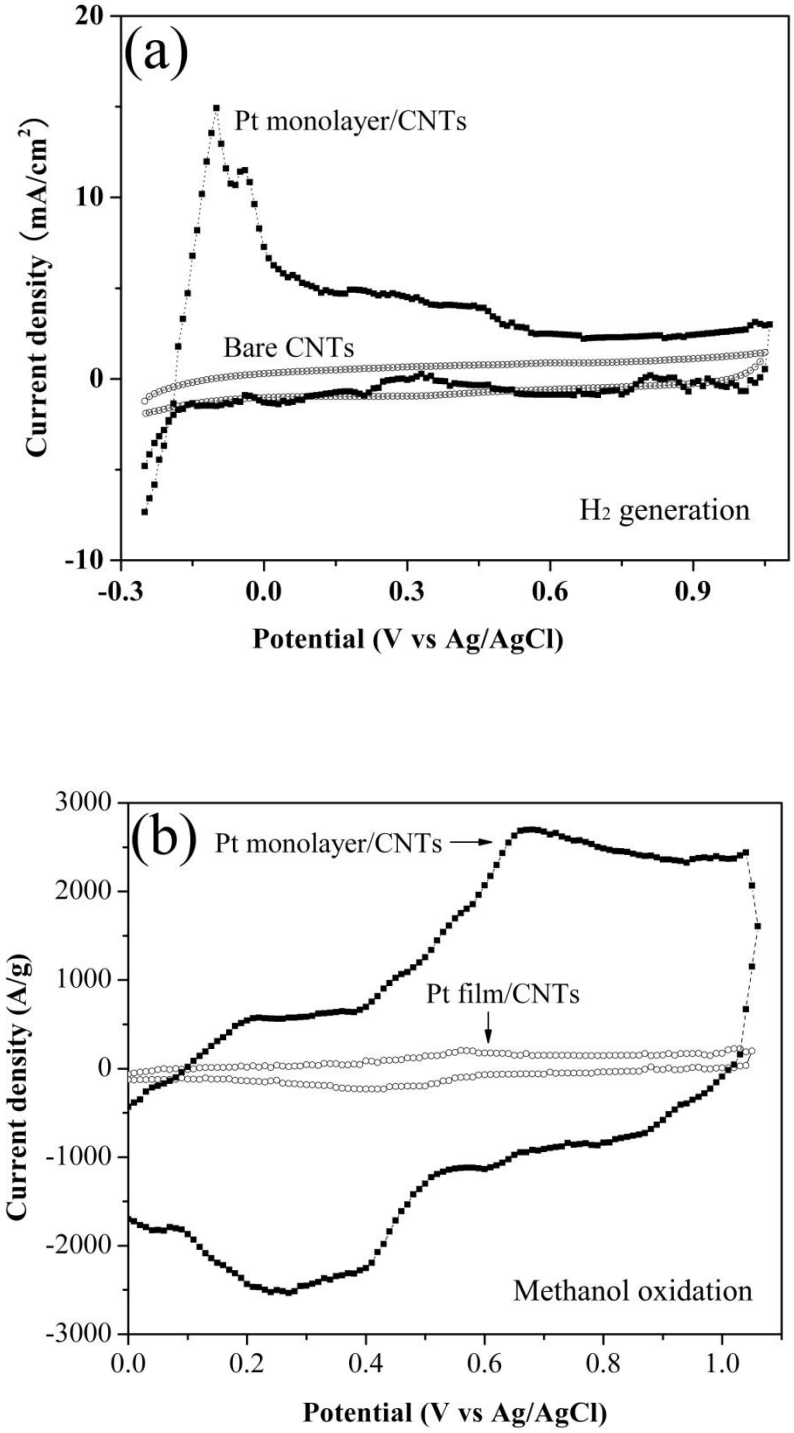

Figure 5.5 (a) Cyclic Voltammogram of Pt monolayer (■) coated on MWCNTs of buckypaper/ bare MWCNTs (○) in a solution of 0.5 M H_2SO_4 and at a scan rate of 100 mV/s; (b) Cyclic Voltammogram of Pt monolayer (■) and film (○) coated on MWCNTs of buckypaper in a solution of 1 M CH_3OH/0.5 M H_2SO_4 and at a scan rate of 20 mV/s

Table 5.1 The relative parameters between the Pt monolayer coated on MWCNTs and porous Au

Samples/reference	Surface area density of the support (m^2/g)	Cost of the support	Mass activity (A/g)
Monolayer Pt/MWCNTs	51.9 (BET test) and 54 (calculation)	$5 per gram	2711
Film Pt/MWCNTs	51.9 (BET test) and 54 (calculation)	$5 per gram	205
Monolayer Pt/porous Au[115]	From 8.7 to 14.2 [225]	$58 per gram	2600

Chapter 6: Electrochemical catalytic water oxidation by buckypaper grafted Ir complexes

6.1 Introduction

The growing global energy demand, limited fossil fuels reserve and global warming problem request large-scale production of clean energy from renewable sources [229]. The solar energy is an important renewable energy for the demand. Due to the diurnal and non uniform distribution of solar radiation on the surface of Earth, it is critical to develop convenient storage of solar energy for its large-scale utilization. The storage should have relative high efficiency and low cost. The strategy to store solar energy by converting the harvested solar energy into the form of chemical fuels such as hydrogen or hydrocarbons has great potential in application. [230]

The hydrogen or hydrocarbons, which are generated to store the solar energy, can be produced by water splitting ($H_2O \rightarrow ½O_2 + H_2$, G°=237.1 kJ) or by CO_2 reduction with water ($H_2O + ½CO_2 \rightarrow O_2 + ½CH_4$, G°=409.0 kJ). For these two processes, catalytic water oxidation is a key step. Therefore, a large number of catalysts for homogeneous water oxidation have been developed based on Ru complexes,[164, 167, 169, 170] Ir complexes,[97, 98] Fe complexes,[171] and polyoxometalates.[172, 173] Several catalysts for heterogeneous water oxidation such as cobalt oxide [174-176] and iridium oxide nanoparticles [177, 178] were also discovered and integrated into electrochemical or photoelectrochemical cells.[179-181] However, activities and stabilities of all of these known water oxidation catalysts are still relatively poor for the practical application. The Scientists have tried to develop new catalyst and the loading method for improving the

catalyst activities. [231, 232] Here we reported an Ir complex catalyst, which can be grafted on buckypaper by direct binding and indirect binding for water splitting by electrochemical method. The catalyst activity of the Ir catalyst was greatly improved by the direct binding method.

6.2 Experimental details and characterization methods

Materials: Synthesis Ir catalyst of chloro(η-pentamethylcyclopentadienyl)((4'-amino-2,2'-bipyridine- N,N')iridium(III). A mixture of $[Cp^*IrCl_2]_2$ (60 mg, 0.075 mmol) and 4-amino-2,2'-bipyridine (26 mg, 0.15 mmol) in 5 mL of dimethylformamide (DMF) was stirred at room temperature under argon for 15 h. Half of the solvent was then removed by distillation under vacuum. Addition of diethyl ether (20 mL) resulted in the precipitation of the complex as the chloride salt. The solid was washed with diethyl ether and hexane to give the product. Yield: 50 mg (64 %). H NMR ($CDCl_3$): 8.92 (d, 1H), 8.32 (d, 1H), 8.25 (d, 1H), 8.17 (t, 1H), 7.75 (m, 1H), 7.51 (s, 1H), 6.86 (m, 1H), 1.68 (s, 15H). MS (ESI): 534.09 m/Z, expected 534.13 m/Z for $[M]^+$. This was done by the cooperator Dr Xie in University of North Carolina at Chapel Hill (UNC).

Synthesis of the catalyst diazonium salt: this was done according to our former work.[93] 5 mg catalyst was dissolved in 1 ml of deionized water. Then 5 mg of concentrated HCl solution was added into it drop wise. The mixture was then cooled down to -3℃ and 0.5 ml of a cold solution of 1 mg sodium nitrite were added slowly to it. The whole solution was kept at -3℃ one hour for complete reaction. Then the mixture was then filtered. To this, 0.5 ml of a cold solution of 1 mg $NaBF_4$ was added to stabilize

the diazonium salt. After getting the solution above, the whole solution was used as solution for diazonium grafting on buckypaper.

Methods for loading the catalyst: 1. The catalyst loaded by directly binding: This was carried out were carried out in the three-electrode cell using a potentiostat (PAR Model 263A) with a reference electrode of Ag/AgCl. The buckpaper was used as the working electrode and the Pt wire as the counter electrode. It was performed for 4 minutes, at a potential of -0.6 V (vs Ag/AgCl) and in the solution of diazonium salt of Ir catalyst as prepared above. Before diazonium grafting, the solution was purged by Ar gas for 20 minutes to remove the oxygen adsorbed on the buckypaper and in solution. 2. The catalyst loaded by indirectly binding: The surface of catalyst support was first modified via an approach of aryl diazonium grafting, which had been known to react covalently with CNTs and graphite.[64, 132, 133] This was carried out in the solution of 5 mM aryl diazonium salt ($H_5C_7O_2N_2BF_4$)/0.1 M HCl/0.1 M KCl under same conditions above. Before diazonium grafting, the electrolyte solution was purged by Ar gas for 20 minutes to remove the oxygen adsorbed on the aligned CNT substrates and in solution. After this surface modification the Ir catalyst was loaded on catalyst support by EDC (1-Ethyl-3-(3-dimethylaminopropyl) carbodiimide) coupling. For the EDC coupling, 10 mg EDC was dissolved in 1 ml 0.1 M MES buffer solution and then the whole solution was loaded on the catalyst support for 0.5 h to active the carboxyl functional groups of the support's surface. Then the 5 mg original Ir catalyst was dissolved in the solution, which was further kept on the catalyst support for overnight to indirectly bind the Ir catalyst on the support.

Cyclic Voltammogram (CV) and time test: The CV measurements were carried out in the three-electrode cell using a potentiostat (PAR Model 263A) with a reference electrode of Ag/AgCl. The Ir catalyst grafted buckypaper was used as the working electrode and the Pt wire as the counter electrode. The electrolyte solutions were pH=5, I=0.1 M, CH_3COOH/CH_3COONa. The time test of the sample was carried out in the same solution and set up with constant potential of 1.4 V vs Ag/AgCl.

Oxygen detection: the oxygen was generated when the constant potential of 1.4 V vs Ag/AgCl was applied on the buckypaper in the buffer solution pH=5, I=0.1 M CH3COOH/CH3COONa. Before the oxygen generation in solution, the Ar gas purged the solution 20 minutes to get rid of the oxygen adsorbed on the buckypaper and in solution. The volume of the solution is 4.3 ml. The concentration of O_2 generated in solution from water splitting was detected by the e-corder oxygen sensor, which was calibrated by degas and air saturate buffer solutions.

ICP-MS/XPS analysis: Quantity and evidence of catalyst loaded on buckpaper were determined the ICP-MS and confirmed by XPS. These tests were performed by cooperator Kathryn E. deKrafft in University of North Carolina at Chapel Hill.

6.3 Results and discussion

The Ir catalyst was loaded on glassy carbon by direct and indirect binding respectively. The schematic processes of direct binding and indirect binding for loading the Ir catalyst on glassy carbon were shown in figure 6.1. For the direct binding, the Ir catalyst was firstly converted to diazonium salt form according to our former work.[93] Then the Ir catalyst was loaded on glassy carbon by electrochemical diazonium grafting

of Ir catalyst diazonium salt. For the indirect binding, the surface of glassy carbon was modified with carboxyl groups under same conditions above by diazonium grafting of lab mad benzoic acid diazonium salt. Then the Ir catalyst was loaded on glassy carbon by EDC coupling the amino groups of catalyst and the carboxyl groups of glassy carbon. The CV of the glassy carbons, which were grafted Ir catalyst by the direct binding and the indirect binding, were carried out from 0~1.4 V vs Ag/AgCl in the buffer solution pH=5, I=0.1 M CH_3COOH/CH_3COONa to evaluate the catalyst activity under different binding methods. As shown in figure 6.2, the current peaks of CV for the catalyst loaded on glassy carbon by direct binding is one magnitude order higher than that for the catalyst loaded on glassy carbon by indirect binding. The ICP and XPS analysis in figure 6.3 performed by UNC collaborators, demonstrated that the Ir catalyst was loaded on glassy carbon by direct binding and indirect binding with similar amount (0.25 nanomole). Thus it is obvious that the electrocatalytic activity of Ir catalyst loaded on glassy carbon by direct binding is much better than that loaded by indirect binding. This could be due to more efficient electron transport.

Then the Ir catalyst was loaded on buckypaper by direct binding, which has much higher active surface area than that of glassy carbon. The current vs time during the diazonium grafting of Ir complex catalyst on buckypaper was shown in figure 6.4. The current decreased quickly due to the loading of catalyst on surface of MWCNTs. Before/after Ir complex was grafted on buckypaper, CV was carried out on the sample from 0~1.35 V vs Ag/AgCl to demonstrate the catalyst activity of Ir complex. As shown in figure 6.5, the peak current of CV of buckpaper in the buffer solution pH=5, I=0.1 M CH_3COOH/CH_3COONa was significantly increased after loading the catalyst on

buckypaper. It is obvious that Ir complex grafted onto buckypaper sample has dramatically improved electrochemical water splitting during the CV. The amount of Ir complex catalyst grafted on buckypaper with 12 mm in diameter was $2.36*10^{-9}$ mol. This measurement was obtained by ICP-MS, which is performed by UNC collaborator. With the knowledge of the amount of metal catalyst and the CV peak current at 1.35 V (vs Ag/AgCl) we could calculate a TOF of 12.1 s^{-1} under the CV which is over one magnitude order faster than similar catalytic systems, presumably due to more efficient electron coupling through the delocalized pi-bond system.

To estimate the current efficiency for generating the O_2 by electrochemically splitting water with Ir catalyst, the constant potential of 1.4 V vs Ag/AgCl was applied on the buckypaper grafted the Ir catalyst in the buffer solution pH=5, I=0.1 M CH_3COOH/CH_3COONa to generate the O_2. The concentration of O_2 generated in solution from water splitting was detected by the e-corder oxygen sensor. The efficiency of the current was calculated with the volume of the buffer solution, the concentration of O_2 and the total charge during the O_2 generation. The volume of the buffer solution is 4.33 ml. As show in figure 6.6 (b) , the concentration of O_2 increased very quickly due to the generation of O_2 and then reach stable after applying the constant potentials for 30 s. It takes more than 150 s to reach stable value due to the diffusion of O_2 from sample surface to the detecting sensor. The background of the buffer solution in the same set up without applying the potential on the sample was also measured by the sensor to rule out the leakage from air or other influence during the test. From curve in figure 6.6 (b), the concentration of O_2 generated by applying 30s constant potential is about 60% of the saturated value of O_2 in water. The whole charge during applying 1.4 V vs Ag/AgCl on

the buckypaper to generate O_2 is 0.22 C, which could be calculated from the curve in figure 6.6 (a). Thus the efficiency of current to generate O_2 is 129%, which is slightly above 1 due to systematic errors during the test. Furthermore, TOF of the catalyst was calculated under these conditions, which is 7.9 s^{-1}. This is similar to that of the IrO_2 colloid film.[233]

However, when the constant potential of 1.4 V vs Ag/AgCl was applied on buckypaper grafted Ir catalyst for 17 h in the buffer solution, large amount of oxygen bubbles were generated and MWCNTs were visibly etched away during the process. This process is confirmed in figure 6.7, where shown are the CV on bare buckypaper (□), buckypaper grafted Ir catalyst (●), and buckypaper grafted Ir catalyst after time test (Δ). The peak current of CV for the sample decreased greatly after 17 h time test, below that of the initial catalyst free sample. This is because the MWCNTs were etched away during the oxygen generation, which would reduce the active surface area of the sample.

6.4 Conclusion

The catalyst activity of the Ir catalyst loaded on to the carbon support by direct binding through delocalized pi-bond is significantly better than that of the catalyst loaded by indirect binding through carboimide linkage. The TOF of the Ir catalyst to split water at the constant potential of 1.4 V vs Ag/AgCl is 7.9 s^{-1}, which is loaded on buckypaper by direct binding. However, the most difficult aspect of O_2 formation at the anode is highly oxidative intermediates to oxidize organic ligands of catalyst and carbon support. carbon support. The oxidation of our support system is seen making application in water splitting

difficult. However, direct coupling of electro-catalyst through delocalized pi-bond will have important application in energy conversion in less oxidizing environments.

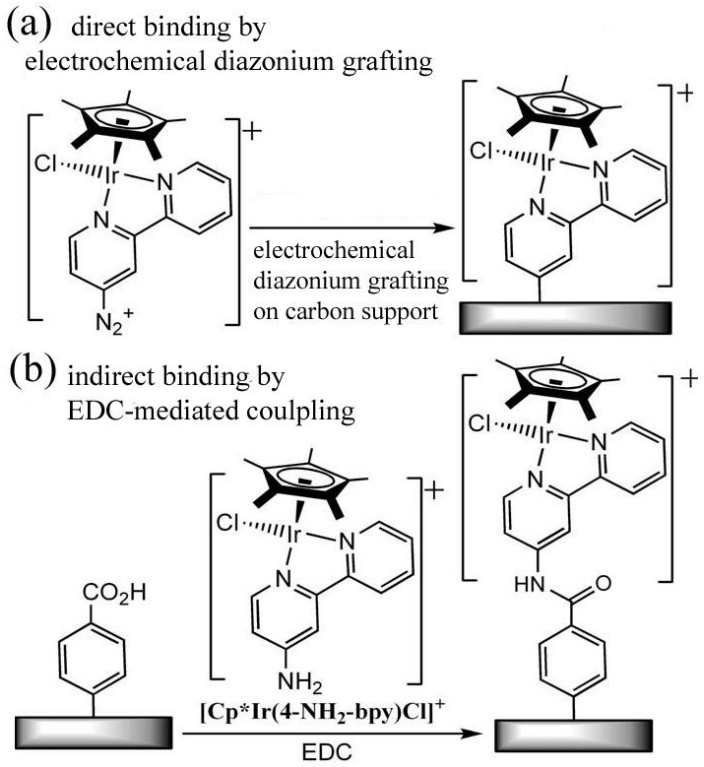

Figure 6.1 The schematic processes of direct binding and indirect binding for loading the Ir catalyst on glassy carbon

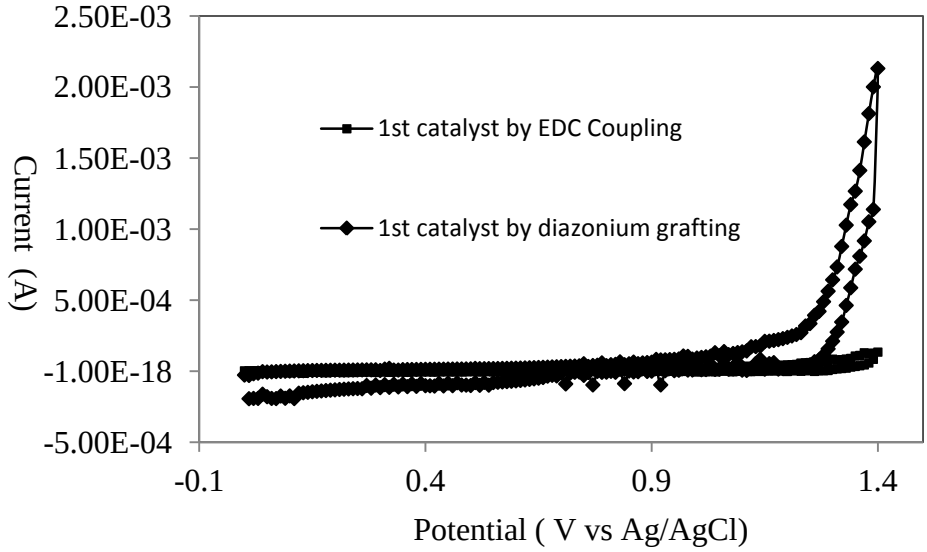

Figure 6.2 the CVs for catalyst activity of the Ir complex catalyst, which is directly diazonium grafting on buckypaper (▲) and CV of the Ir complex catalyst which is indirectly binding to buckypaper by EDC coupling (■) in buffer solution pH=5, I=0.1 M CH_3COOH/CH_3COONa

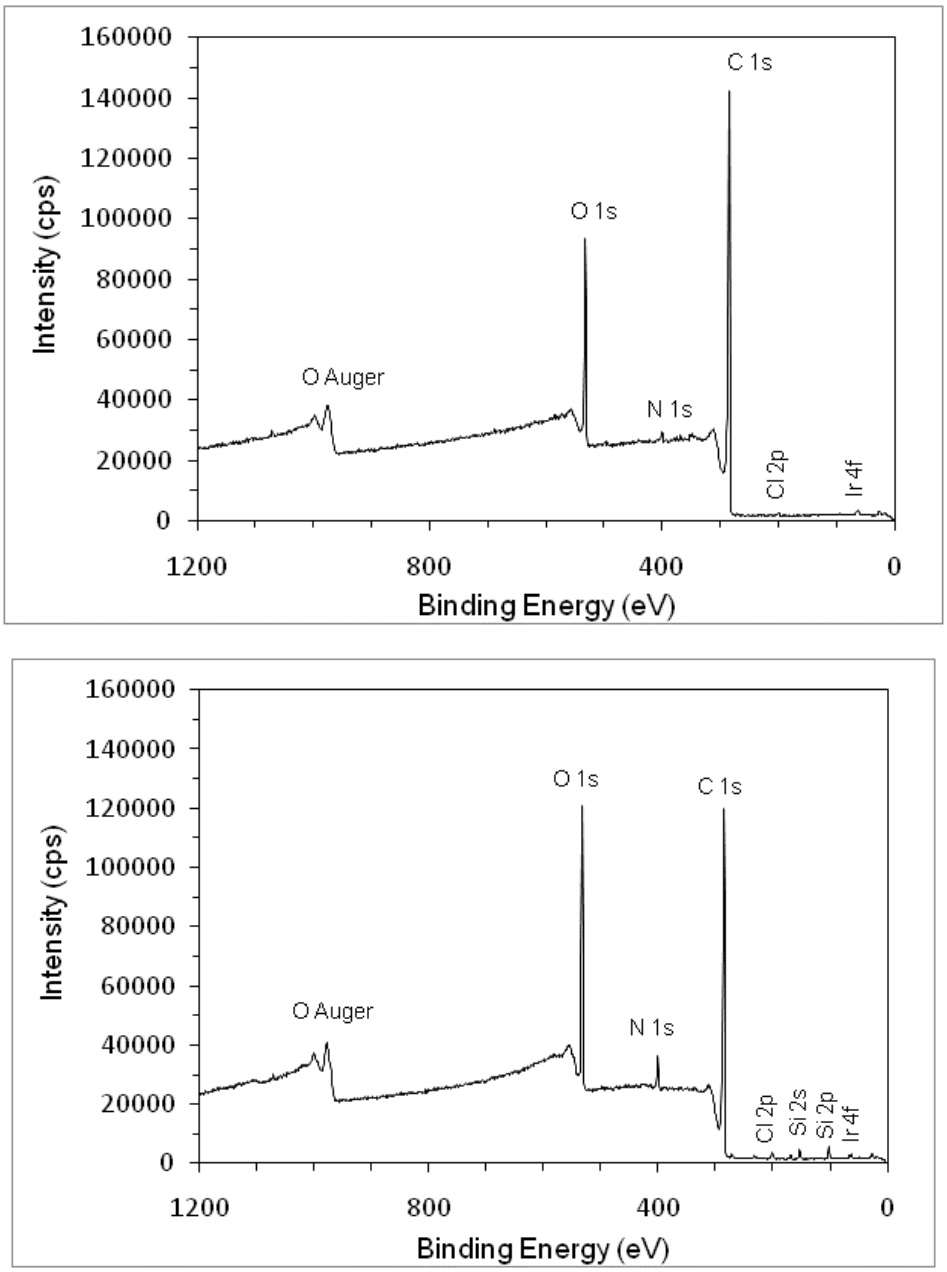

Figure 6.3 XPS full spectra of glassy carbon electrodes loaded with 1 by EDC coupling (a) and diazonium grafting (b). (This was done by UNC)

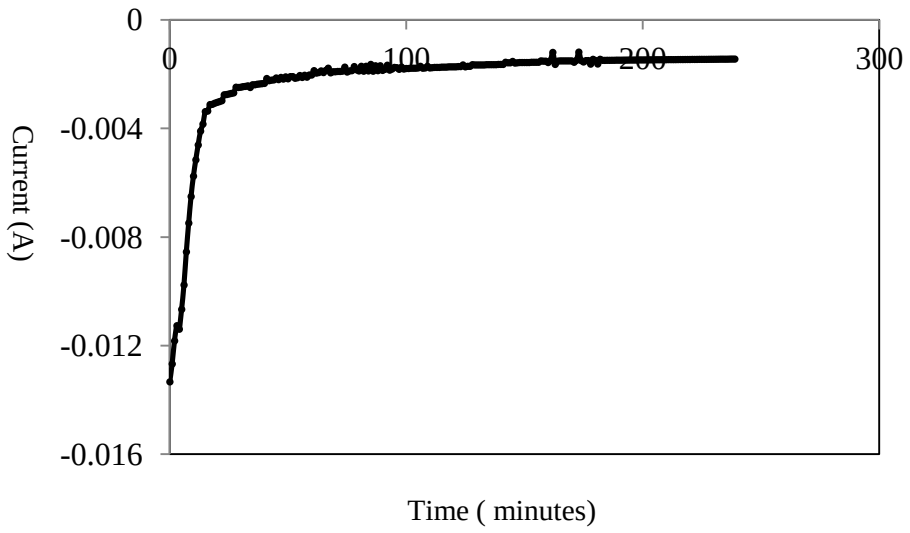

Figure 6.4 Current vs time during electrochemical diazonium grafting the 1st Ir complex catalyst on buckypaper

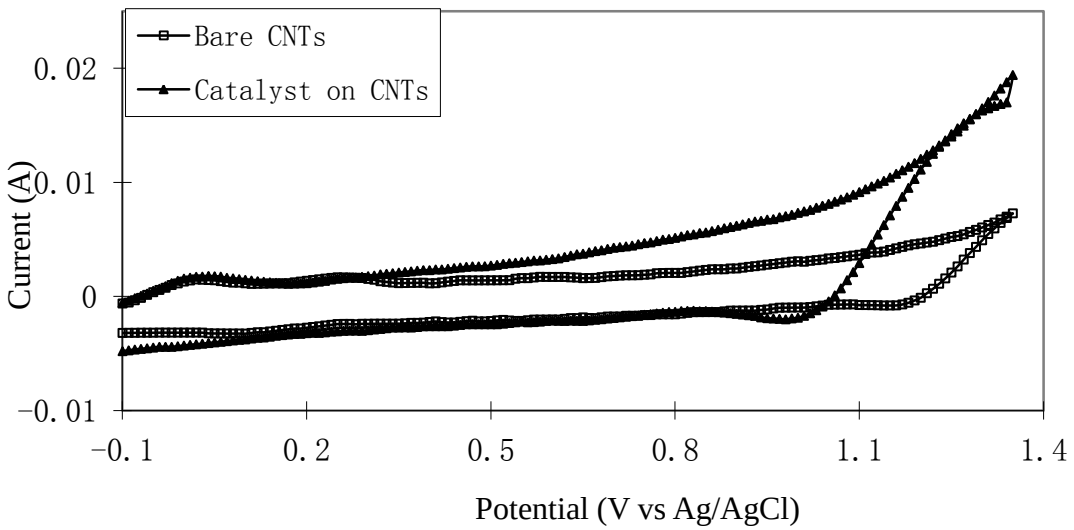

Figure 6.5 The CVs for catalyst activity of the Ir complex catalyst, which is directly diazonium grafted on buckypaper (▲) and CV of bare buckypaper (□) in buffer solution pH=5, I=0.1 M CH_3COOH/CH_3COONa

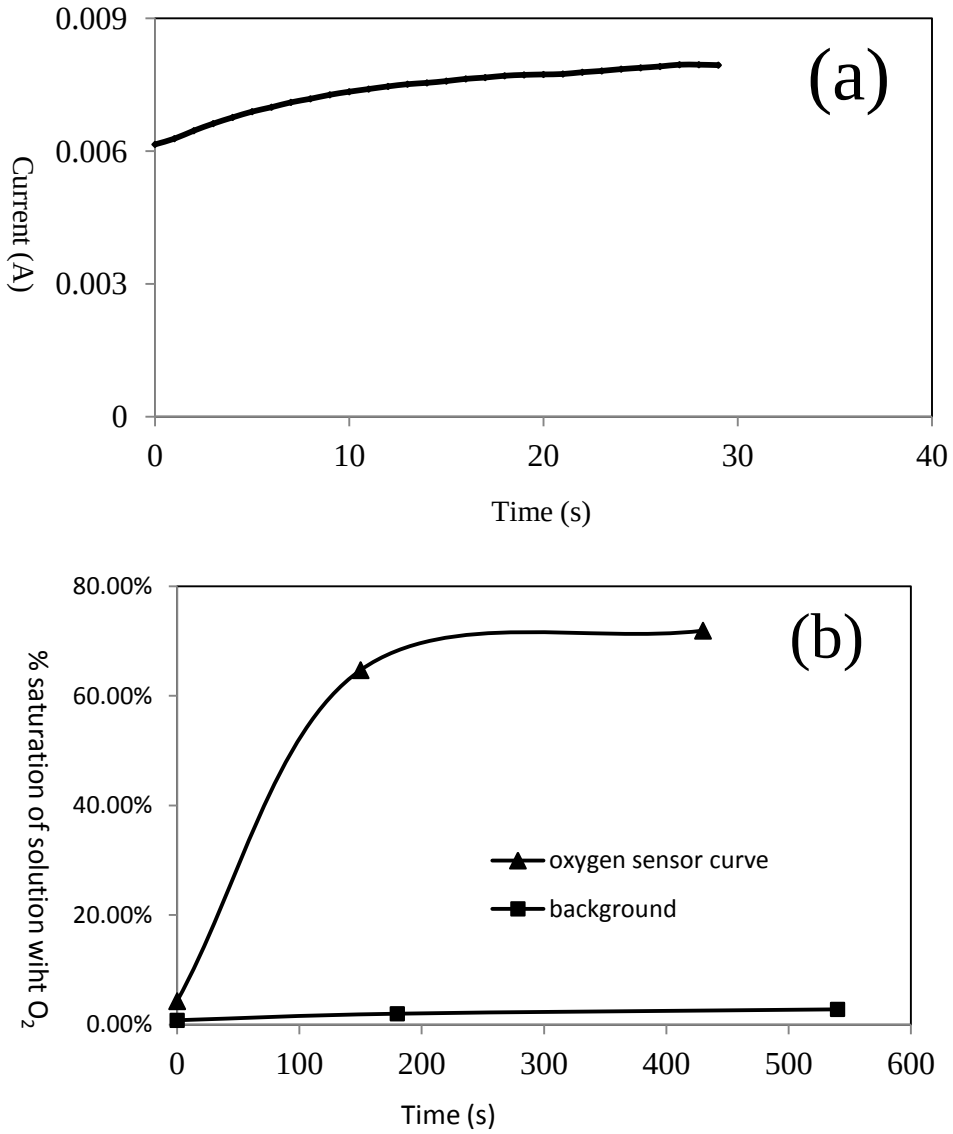

Figure 6.6 (a) Current during constant potential electrolysis at 1.4 V vs Ag/AgCl in buffer solution pH=5, I=0.1 M CH_3COOH/CH_3COONa and (b) the accompanying generation of O_2 detected in solution for 1 loaded onto CNTs by diazonium grafting. The amount of O_2 corresponding to 100% saturation is generated at 129% current efficiency, based on integration of the current up to this point.

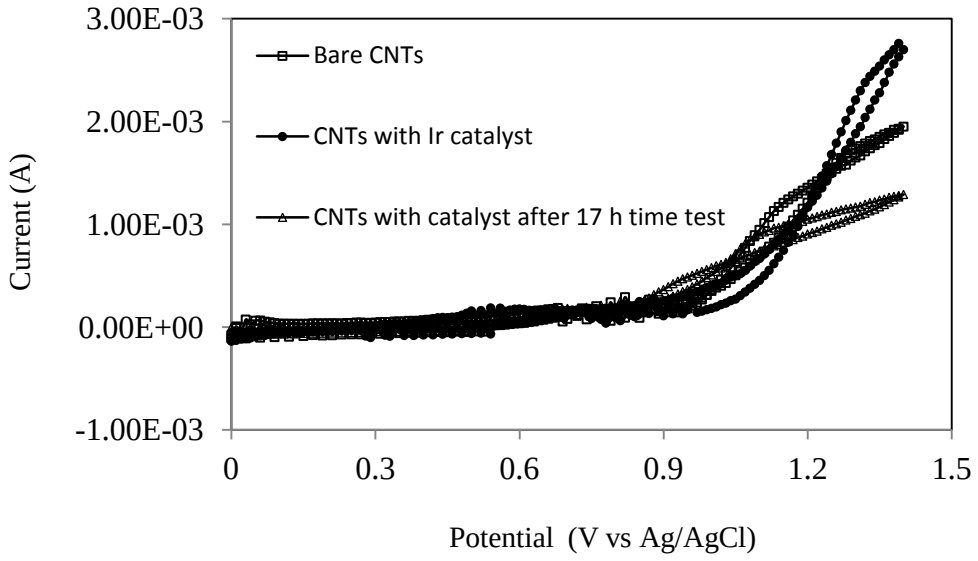

Figure 6.7 The CV of bare CNTs, initial CV of CNTs with grafted Ir complex and the CV the of CNTs with grafted Ir complex after 17 h time test at 1.4 V vs Ag/AgCl in buffer solution pH=5, I=0.1 M CH_3COOH/CH_3COONa.

Chapter 7: Conclusion and future research direction

The Ph.D. dissertation is mainly focused on the energy storage and conversion using carbon nanotube platforms. For the energy storage, the novel aligned CNT membrane has been applied in the electrochemical energy storage with nanoscale bubbles as valve in chapter 2, 3. The main conclusions in this part of the dissertation are points 1 through 3. For the energy conversion, the main conclusions of Pt catalysts for methanol fuel cell and Ir complex for water splitting are following points 4 through 6.

1. The polymer wells (30-60 nm id) can be created in the one side of aligned MWCNT membrane by electrochemically oxidizing the parts of conductive MWCNTs at 2.5 V vs Ag/AgCl. These polymer wells are helpful to stabilize nanoscale bubbles generated on the tips of MWCNTs.

2. The sine potentials applied on MWCNT membrane can generate nm-scale bubbles at the tips of MWCNTs that can temporarily block the membrane. A 92% blocking efficiency is achieved when the bubbles are stabilized in a 30-60 nm diameter 'wells' at the tips of MWCNTs. Meanwhile, the nanoscale bubbles can be removed with 0.004 atm pressure to recover the transport through the MWCNT membrane.

3. The novel pretreated MWCNT membrane with gold electrodes coated on both sides has been used for storing the electrochemical energy. The self-discharge rate of the membrane by storing the neutral molecular HClO is much better than that by storing the charge ion $Fe(CN)_6^{3-}/Fe^{3+}$. A model was developed to account for built in potential to drive charged species but not neutral species to explain the observed discharge rates. The

nanoscale bubbles can slightly improve self-discharge rate of the membrane but are not sufficient for practical applications with charged species.

4. Uniform ultrathin Pt films were electrodeposited onto the aligned MWCNT array as methanol fuel cell anodes with high-area chemical stability. Electrochemical treatment of the graphitic MWCNTs' surface by diazoniumbenzoic acid allowed for uniform Pt electroplating. The mass activity of the Pt thin film can reach 400 A/g at a scan rate of 20 mV/s and in a solution of 1 M CH_3OH/0.5 M H_2SO_4. A programmed pulse potential at 0V was also seen to nearly eliminate the effects of carbon monoxide poisoning. The mass activity of Pt for methanol oxidation can be maintained at 300 A/g for more than 3000 s, which is 19 times of that under a constant potential of 0.7 V (vs Ag/AgCl).

5. The ideal geometry of a Pt monolayer deposited onto a high surface area chemically inert substrate (buckypaper) was achieved by replacing a precursor Cu monolayer coated on CNTs by the underpotential deposition. The electrochemical surface modification of graphite CNTs by fluorinated benzoic acid was critical to coordinate Cu ions for monolayer formation. The mass activity of Pt monolayer can be improved to 2711 A/g at the same conditions above. This is about 13 times higher than that of the ~10 nm thick Pt film coated on MWCNTs and is the highest known reported mass activity of Pt. Besides the high mass activity, the Pt monolayer coated on buckypaper can be used as excellent catalyst for fuel cells with several other advantages like low cost, high surface area, flexibility, mechanical robusticity and enhanced pressure flow.

6. A new strategy has been developed toward electrochemical water oxidation with Ir complexes catalyst. The catalyst activity of Ir complex grafted on buckypaper by direct binding is much better than that loaded on buckypaper by indirect binding. The TOF of the Ir catalyst for water splitting was 7.9 s^{-1} at the constant potential of 1.4 V vs Ag/AgCl.

In summary, this dissertation is the first time to turn on/off CNT membranes with nanoscale bubbles as a valve and applied it in an electrochemical energy storage system. Meanwhile it is the first time to deposit the uniform Pt film/monolayer on aligned CNT substrate/buckypaper by electrochemical method. The thickness of the Pt film was tuned from 10 nm to monolayer to achieve the record value of the Pt mass activity. The catalyst activity of Ir complex was also evaluated in this dissertation, which was loaded on carbon support by direct and indirect binding method. It was the first time found that the catalyst activity of the catalyst loaded by direct pi-bond coupling was much better than that of the catalyst loaded by indirect binding.

The nanoscale bubbles have been used as valve to turn on/off the transport through the pretreated CNT membrane in this dissertation. It would be interesting to use the nanoscale bubbles for pumping the nanofluid in CNTs as the nanopump of CNT membrane. Surface modification of CNTs by electrochemical method is critical to Pt film/monolayer coating on them. It not only adjusts the wet ability of CNTs but also offers the coordinate force between CNTs and ions in the solution. Thus this could offer a facile way to coat other materials on buckypaper, like titania and silicon, which can be used for the lithium ion battery and solar cells. For Ir complex catalyst for the heterogeneous catalytic water oxidization, the direct binding method for loading the

catalyst can significantly improve its catalyst activity. Unfortunately the carbon support for Ir complex catalyst was destroyed during catalytic water oxidization process, which made the sample lose activity and not be of practical use as the anode in water splitting. However, the discovery about the influence of the ligand binding method on the catalyst activities can be used for improving the other catalysts' activity driven by electrochemical potential.

Reference

1. Glaser, P.E., *Solar energy-alternative source for power generation* Futures, 1969. **1**(4): p. 304.
2. Teske, S., Pregger, T., Simon, S., Naegler, T., Graus, W., Lins, C., *Energy Revolution 2010-a sustainable world energy outlook.* Energy Efficiency, 2011. **4**(3): p. 409.
3. Fischer, G., Schrattenholzer, L., *Global bioenergy potentials through 2050.* Biomass and Bioenergy, 2001. **20**(3): p. 151.
4. Lewis, N.S., Nocera, D. G., *Powering the planet: Chemical challenges in solar energy utilization.* Proceedings of the National Academy of Sciences, 2006. **103**(43): p. 15729.
5. Goldewijk, K.K., *Three Centuries of Global Population Growth: A Spatial Referenced Population (Density) Database for 1700–2000.* Population & Environment, 2005. **26**(4): p. 343.
6. Mattick, C.S., Williams, E., Allenby, B. R., *Historical Trends in Global Energy Consumption.* IEEE Technology and Society Magazine, 2010. **29**(3): p. 22.
7. Siddiqi, T.A., *Natural gas reserves/total energy consumption: A useful new ratio for addressing global climate change concerns.* Energy Policy, 2002. **30**(13): p. 1145.
8. Smeets, E.M.W., Faaij, A. P. C., Lewandowski, I. M., Turkenburg, W. C., *A bottom-up assessment and review of global bio-energy potentials to 2050.* Progress in Energy and Combustion Science, 2007. **33**(1): p. 56.
9. Edmonds, J., Reilly, J., *Global energy production and use to the year 2050.* Energy, 1983. **8**(6): p. 419.
10. Orr, L., *Changing the World's Energy systems.* Stanford University Global Climate& Energy Project.
11. Owen, N.A., Inderwildi, O. R., King, D. A., *The status of conventional world oil reserves—Hype or cause for concern?* Energy Policy, 2010. **38**(8): p. 4743.
12. Solangi, K.H., Islam, M. R., Saidur, R., Rahim, N. A., Fayaz, H., *A review on global solar energy policy.* Renewable and Sustainable Energy Reviews, 2011. **15**(4): p. 2149.
13. Bormann, F.H., Smith, K. R., Bormann, B. T., *Earth to Hearth - a Microcomputer Model for Comparing Biofuel Systems.* Biomass & Bioenergy, 1991. **1**(1): p. 17.
14. Amann C. A., *Alternative fuels and power systems in the long term.* International Journal of Vehicle Design, 1996. **17**(5-6): p. 510.
15. Keating, R., *Hydrogen-alternative energy source for the next century* Omni, 1989. **11**(9): p. 66.
16. Feibelman, P.J., *Partial dissociation of water on Ru(0001).* Science, 2002. **295**(5552): p. 99.
17. Reddington, E., Sapienza, A., Gurau, B., Viswanathan, R., Sarangapani, S., Smotkin, E. S., Mallouk, T. E., *Combinatorial electrochemistry: A highly parallel, optical screening method for discovery of better electrocatalysts.* Science, 1998. **280**(5370): p. 1735.
18. Betts, R.A., Collins, M., Hemming, D. L., Jones, C. D., Lowe, J. A., Sanderson, M. G., *When could global warming reach 4 degrees C?* Philosophical

Transactions of the Royal Society a-Mathematical Physical and Engineering Sciences, 2011. **369**(1934): p. 67.
19. Meinshausen, M., Meinshausen, N., Hare, W., Raper, S. C. B., Frieler, K., Knutti, R., Frame, D. J., Allen, M. R., *Greenhouse-gas emission targets for limiting global warming to 2 degree C.* Nature, 2009. **458**(7242): p. 1158.
20. Cox, P.M., Betts, R. A., Jones, C. D., Spall, S. A., Totterdell, I. J., *Acceleration of global warming due to carbon-cycle feedbacks in a coupled climate model.* Nature, 2000. **408**(6809): p. 184.
21. Rosa, L.P., Ribeiro, S. K., *The present, past, and future contributions to global warming of CO2 emissions from fuels.* Climatic Change, 2001. **48**(2-3): p. 289.
22. Root, T.L., Price, J. T., Hall, K. R., Schneider, S. H., Rosenzweig, C., Pounds, J. A., *Fingerprints of global warming on wild animals and plants.* Nature, 2003. **421**(6918): p. 57.
23. Schindler, D.W., *Effects of Acid Rain on Freshwater Ecosystems.* Science, 1988. **239**(4836): p. 149.
24. Keith, D.W., DeCarolis, J. F., Denkenberger, D. C., Lenschow, D. H., Malyshev, S. L., Pacala, S., Rasch, P. J., *The influence of large-scale wind power on global climate.* Proceedings of the National Academy of Sciences of the United States of America, 2004. **101**(46): p. 16115.
25. Holttinen, H., Meibom, P., Orths, A., Lange, B., O'Malley, M., Tande, J. O., Estanqueiro, A., Gomez, E., Söder, L., Strbac, G., Smith, J. C., Van, H. F., *Impacts of large amounts of wind power on design and operation of power systems, results of IEA collaboration.* Wind Energy, 2011. **14**(2): p. 179.
26. Blaabjerg, F., Lov, F., Teodorescu, R., Chen, Z. *Power Electronics in Renewable Energy Systems*. in *Power Electronics and Motion Control Conference, 2006. EPE-PEMC 2006. 12th International*. 2006.
27. Sawin, L.J., Martinot, E., Sonntag-OBrien, V., McCrone, A., Roussell, J., Barnes, D., Flavin, C. , *Renewables 2010 global status report.* Renewable Energy Policy Network for the 21st Century, 2010: p. 1.
28. Tsur, Y., Zemel, A., *On the dynamics of competing energy sources.* Automatica, 2011. **47**(7): p. 1357.
29. Asif, M., Muneer, T., *Energy supply, its demand and security issues for developed and emerging economies.* Renewable & Sustainable Energy Reviews, 2007. **11**(7): p. 1388.
30. Jager-Waldau, A., Ossenbrink, H., *Progress of electricity from biomass, wind and photovoltaics in the European Union.* Renewable & Sustainable Energy Reviews, 2004. **8**(2): p. 157.
31. Lund, P.D., *Fast market penetration of energy technologies in retrospect with application to clean energy futures.* Applied Energy, 2010. **87**(11): p. 3575.
32. Chou, S.L., Wang, J. Z., Chen, Z. X., Liu, H. K., Dou, S. X., *Hollow hematite nanosphere/carbon nanotube composite: mass production and its high-rate lithium storage properties.* Nanotechnology, 2011. **22**(26).
33. Yang, Z.G., Zhang, J. L., Kintner-Meyer, M. C. W., Lu, X. C., Choi, D. W., Lemmon, J. P., Liu, J., *Electrochemical Energy Storage for Green Grid.* Chemical Reviews, 2011. **111**(5): p. 3577.

34. Cheng, F.Y., Liang, J., Tao, Z. L., Chen, J., *Functional Materials for Rechargeable Batteries.* Advanced Materials, 2011. **23**(15): p. 1695.
35. Cho, A., *Renewable energy - Hydrogen from ethanol goes portable.* Science, 2004. **303**(5660): p. 942.
36. Lim, B., Jiang, M. J., Camargo, P. H. C., Cho, E. C., Tao, J., Lu, X. M., Zhu, Y. M., Xia, Y. A., *Pd-Pt Bimetallic Nanodendrites with High Activity for Oxygen Reduction.* Science, 2009. **324**(5932): p. 1302.
37. Kohl, S.W., Weiner, L., Schwartsburd, L., Konstantinovski, L., Shimon, L. J. W., Ben-David, Y., Iron, M. A., Milstein, D., *Consecutive Thermal H(2) and Light-Induced O(2) Evolution from Water Promoted by a Metal Complex.* Science, 2009. **324**(5923): p. 74.
38. Fthenakis, V., Mason, J. E., Zweibel, K., *The technical, geographical, and economic feasibility for solar energy to supply the energy needs of the US.* Energy Policy, 2009. **37**(2): p. 387.
39. Hummer, G., Rasaiah, J. C., Noworyta, J. P., *Water conduction through the hydrophobic channel of a carbon nanotube.* Nature, 2001. **414**(6860): p. 188.
40. Majumder, M., Chopra, N., Andrews, R., Hinds, B. J., *Nanoscale hydrodynamics: Enhanced flow in carbon nanotubes.* Nature, 2005. **438**(7064): p. 44.
41. Sun, L., Crooks, R. M., *Single Carbon Nanotube Membranes: A Well-Defined Model for Studying Mass Transport through Nanoporous Materials.* Journal of the American Chemical Society, 2000. **122**(49): p. 12340.
42. Holt, J.K., Park, H. G., Wang, Y., Stadermann, M., Artyukhin, A. B., Grigoropoulos, C. P., Noy, A., Bakajin, O., *Fast Mass Transport Through Sub-2-Nanometer Carbon Nanotubes.* Science, 2006. **312**(5776): p. 1034.
43. Dong, L., Tao, X., Hamdi, M., Zhang, L., Zhang, X., Ferreira, A., Nelson, B. J., *Nanotube Fluidic Junctions: Internanotube Attogram Mass Transport through Walls.* Nano Letters, 2008. **9**(1): p. 210.
44. Sokhan, V.P., Nicholson, D., Quirke, N., *Fluid flow in nanopores: Accurate boundary conditions for carbon nanotubes.* Journal of Chemical Physics, 2002. **117**(18): p. 8531.
45. Skoulidas, A.I., Ackerman, D. M., Johnson, J. K., Sholl, D. S., *Rapid Transport of Gases in Carbon Nanotubes.* Physical Review Letters, 2002. **89**(18): p. 185901.
46. Newsome, D.A., Sholl, D. S., *Influences of Interfacial Resistances on Gas Transport through Carbon Nanotube Membranes.* Nano Letters, 2006. **6**(9): p. 2150.
47. Verweij, H., Schillo, M. C, Li, J., *Fast Mass Transport Through Carbon Nanotube Membranes.* Small, 2007. **3**(12): p. 1996.
48. Lee, K.H., Sinnott, S. B., *Computational Studies of Non-Equilibrium Molecular Transport through Carbon Nanotubes.* The Journal of Physical Chemistry B, 2004. **108**(28): p. 9861.
49. Chen, H., Johnson, J. K., Sholl, D. S., *Transport Diffusion of Gases Is Rapid in Flexible Carbon Nanotubes.* The Journal of Physical Chemistry B, 2006. **110**(5): p. 1971.
50. Kim, S., Jinschek, J. R., Chen, H., Sholl, D. S., Marand, E., *Scalable Fabrication of Carbon Nanotube/Polymer Nanocomposite Membranes for High Flux Gas Transport.* Nano Letters, 2007. **7**(9): p. 2806.

51. Wei, C., Srivastava, D., *Theory of Transport of Long Polymer Molecules through Carbon Nanotube Channels.* Physical Review Letters, 2003. **91**(23): p. 235901.
52. Chen, H., Sholl, D. S., *Rapid Diffusion of CH4/H2 Mixtures in Single-Walled Carbon Nanotubes.* Journal of the American Chemical Society, 2004. **126**(25): p. 7778.
53. Mao, Z., Sinnott, S. B., *A Computational Study of Molecular Diffusion and Dynamic Flow through Carbon Nanotubes.* The Journal of Physical Chemistry B, 2000. **104**(19): p. 4618.
54. Sokhan, V.P., Nicholson, D., Quirke, N., *Fluid flow in nanopores: An examination of hydrodynamic boundary conditions.* Journal of Chemical Physics, 2001. **115**(8): p. 3878.
55. Hinds, B.J., Chopra, N., Rantell, T., Andrews, R., Gavalas, V., Bachas, L. G., *Aligned Multiwalled Carbon Nanotube Membranes.* Science, 2004. **303**(5654): p. 62.
56. Whitby, M., Cagnon, L., Thanou, M., Quirke, N., *Enhanced Fluid Flow through Nanoscale Carbon Pipes.* Nano Letters, 2008. **8**(9): p. 2632.
57. Andrews, R., Jacques, D., Qian, D. L., Rantell, T. , *Multiwall Carbon Nanotubes: Synthesis and Application.* Accounts of Chemical Research, 2002. **35**(12): p. 1008.
58. Wu, J., Paudel, K. S., Strasinger, C., Hammell, D., Stinchcomb, A. L., Hinds, B. J., *Programmable transdermal drug delivery of nicotine using carbon nanotube membranes.* Proceedings of the National Academy of Sciences, 2010. **107**(26): p. 11698.
59. Lee, C.Y., Choi, W., Han, J. H., Strano, M. S., *Coherence Resonance in a Single-Walled Carbon Nanotube Ion Channel.* Science, 2010. **329**(5997): p. 1320.
60. Sun, X.H., Su, X., Wu, J., Hinds, B. J., *Electrophoretic Transport of Biomolecules through Carbon Nanotube Membranes.* Langmuir, 2011. **27**(6): p. 3150.
61. Gethard, K., Sae-Khow, O., Mitra, S., *Water Desalination Using Carbon-Nanotube-Enhanced Membrane Distillation.* Acs Applied Materials & Interfaces, 2011. **3**(2): p. 110.
62. Corry, B., *Designing Carbon Nanotube Membranes for Efficient Water Desalination.* The Journal of Physical Chemistry B, 2007. **112**(5): p. 1427.
63. Kalra, A., Garde, S., Hummer, G., *Osmotic water transport through carbon nanotube membranes.* Proceedings of the National Academy of Sciences, 2003. **100**(18): p. 10175.
64. Majumder, M., Zhan, X., Andrews, R., Hinds, B. J., *Voltage Gated Carbon Nanotube Membranes.* Langmuir, 2007. **23**(16): p. 8624.
65. Majumder M., C.N., Hinds B. J.,, *Effect of Tip Functionalization on Transport through Vertically Oriented Carbon Nanotube Membranes.* Journal of the American Chemical Society, 2005. **127**(25): p. 9062.
66. Majumder, M., Keis, K., Zhan, X., Meadows, C., Cole, J., Hinds, B. J., *Enhanced Electrostatic Modulation of Ionic Diffusion Through Carbon Nanotube Membranes by Diazonium Grafting Chemistry.* Journal of Membrane Science, 2008. **316**(1-2): p. 89.

67. Majumder, M., Stinchcomb, A., Hinds, B. J., *Towards mimicking natural protein channels with aligned carbon nanotube membranes for active drug delivery.* Life Sciences, 2010. **86**(15-16): p. 563.
68. Meng, D.D., Kim C. J., , *Micropumping of liquid by directional growth and selective venting of gas bubbles.* Lab on a Chip, 2008. **8**(6): p. 958.
69. Jun, T.K., Kim, C. J., *Valveless pumping using traversing vapor bubbles in microchannels.* Journal of Applied Physics, 1998. **83**(11): p. 5658.
70. Ljunggren, S., Eriksson, J. C., *The lifetime of a colloid-sized gas bubble in water and the cause of the hydrophobic attraction.* Colloids and Surfaces a-Physicochemical and Engineering Aspects, 1997. **130**: p. 151.
71. Ishida, N., Inoue, T., Miyahara, M., Higashitani, K., *Nano bubbles on a hydrophobic surface in water observed by tapping-mode atomic force microscopy.* Langmuir, 2000. **16**(16): p. 6377.
72. Zhang, X.H., Khan, A., Ducker, W. A., *A nanoscale gas state.* Physical Review Letters, 2007. **98**(13).
73. Ducker, W.A., *Contact Angle and Stability of Interfacial Nanobubbles.* Langmuir, 2009. **25**(16): p. 8907.
74. Tyrrell, J.W.G., Attard, P., *Images of nanobubbles on hydrophobic surfaces and their interactions.* Physical Review Letters, 2001. **87**(17): p. 176104.
75. Zhang, X.H., Quinn, A., Ducker, W. A., *Nanobubbles at the Interface between Water and a Hydrophobic Solid.* Langmuir, 2008. **24**(9): p. 4756.
76. Huang, C.W., Jiang, J. C., Lu, M. Y., Sun, L., Meletis, E. I., Hao, Y. W., *Capturing Electrochemically Evolved Nanobubbles by Electroless Deposition. A Facile Route to the Synthesis of Hollow Nanoparticles.* Nano Letters, 2009. **9**(12): p. 4297.
77. Zhang, L.J., Zhang, Y., Zhang, X. H., Li, Z. X., Shen, G. X., Ye, M., Fan, C. H., Fang, H. P., Hu, J., *Electrochemically Controlled Formation and Growth of Hydrogen Nanobubbles.* Langmuir, 2006. **22**(19): p. 8109.
78. Tas, N.R., Berenschot, J. W., Lammerink, T. S. J., Elwenspoek, M., van den Berg, A., *Nanofluidic Bubble Pump Using Surface Tension Directed Gas Injection.* Analytical Chemistry, 2002. **74**(9): p. 2224.
79. Sun, L., Karanjgaokar, N., Sun, K., Chasiotis, I., Carter, W. C., Dillon, S., *High-strength All-solid Lithium Ion Electrodes Based on Li(4)Ti(5)O(12).* Journal of Power Sources, 2011. **196**(15): p. 6507.
80. Leung, P.K., de Leon, C. P., Low, C. T. J., Walsh, F. C., *Ce(III)/Ce(IV) in methanesulfonic acid as the positive half cell of a redox flow battery.* Electrochimica Acta, 2011. **56**(5): p. 2145.
81. Wang, Q., Wen, Z., Li, J., *Solvent-controlled synthesis and electrochemical lithium storage of one-dimensional TiO2 nanostructures.* Inorganic Chemistry, 2006. **45**(17): p. 6944.
82. Weissbach, R.S., Teodorescu, R. E., Sonnenmeier, J. R. . *Comparison of Time-Based Probability Methods for Estimating Energy Storage Requirements for an Off-Grid Residence*. in *Energy 2030 Conference, 2008. ENERGY 2008. IEEE*. 2008.
83. Chen, D., Wang, S., Xiao, M., Han, D., Meng, Y., *Sulfonated Poly (fluorenyl ether ketone) Membrane with Embedded Silica Rich Layer and Enhanced Proton*

Selectivity for Vanadium Redox Flow Battery. Journal of Power Sources, 2010. **195**(22): p. 7701.
84. Schulte, D., Drillkens, J., Schulte, B., Sauer, D. U., *Nafion Hybrid Membranes for Use in Redox Flow Batteries.* Journal of the Electrochemical Society, 2010. **157**(9): p. A989.
85. Merle, G., Wessling, M., Nijmeijer, K., *Anion exchange membranes for alkaline fuel cells: A review.* Journal of Membrane Science, 2011. **377**(1-2): p. 1.
86. Mai, Z.S., Zhang, H. M., Li, X. F., Xiao, S. H., Zhang, H. Z., *Nafion/polyvinylidene fluoride blend membranes with improved ion selectivity for vanadium redox flow battery application.* Journal of Power Sources, 2011. **196**(13): p. 5737.
87. Hwang, G.J., Ohya, H., *Preparation of cation exchange membrane as a separator for the all-vanadium redox flow battery.* Journal of Membrane Science, 1996. **120**(1): p. 55.
88. Mohammadi, T., Skyllas-Kazacos, M., *Preparation of sulfonated composite membrane for vanadium redox flow battery applications.* Journal of Membrane Science, 1995. **107**(1-2): p. 35.
89. Xi, J., Wu, Z., Qiu, X., Chen, L., *Nafion/SiO2 hybrid membrane for vanadium redox flow battery.* Journal of Power Sources, 2007. **166**(2): p. 531.
90. Ponce de León, C., Frías-Ferrer, A., González-García, J., Szánto, D. A., Walsh, F. C., *Redox flow cells for energy conversion.* Journal of Power Sources, 2006. **160**(1): p. 716.
91. Jones, I.W., *The Sodium-Sulphur Battery.* Philosophical Transactions of the Royal Society of London. Series A, Mathematical and Physical Sciences, 1981. **302**(1468): p. 339.
92. Zumdahl, S.S., Zumdahl S. A., *Chemistry.* 1999: p. 750.
93. Su, X., Wu, J., Hinds, B. J., *Catalytic activity of ultrathin Pt films on aligned carbon nanotube arrays.* Carbon, 2011. **49**(4): p. 1145.
94. Jung, I., Kim, D., Yun, Y., Chung, S., Lee, J., Tak, Y., *Electro-oxidation of methanol diffused through proton exchange membrane on Pt surface: crossover rate of methanol.* Electrochimica Acta, 2004. **50**(2-3): p. 607.
95. Mu, Y.Y., Liang, H. P., Hu, J. S., Jiang, L., Wan, L. J., *Controllable Pt Nanoparticle Deposition on Carbon Nanotubes as an Anode Catalyst for Direct Methanol Fuel Cells.* The Journal of Physical Chemistry B, 2005. **109**(47): p. 22212.
96. Tian, N., Zhou, Z. Y., Sun, S. G., Ding, Y., Wang, Z. L., *Synthesis of Tetrahexahedral Platinum Nanocrystals with High-Index Facets and High Electro-Oxidation Activity.* Science, 2007. **316**(5825): p. 732.
97. McDaniel, N.D., Coughlin, F. J., Tinker, L. L., Bernhard, S., *Cyclometalated iridium(III) aquo complexes: Efficient and tunable catalysts for the homogeneous oxidation of water.* Journal of the American Chemical Society, 2008. **130**(1): p. 210.
98. Hull, J.F., Balcells, D., Blakemore, J. D., Incarvito, C. D., Eisenstein, O., Brudvig, G. W., Crabtree, R. H., *Highly Active and Robust Cp* Iridium Complexes for Catalytic Water Oxidation.* Journal of the American Chemical Society, 2009. **131**(25): p. 8730.

99. Iwasita, T., *Electrocatalysis of methanol oxidation.* Electrochimica Acta, 2002. **47**(22-23): p. 3663.
100. Hull, R.V., Li, L., Xing, Y. C., Chusuei, C. C., *Pt Nanoparticle Binding on Functionalized Multiwalled Carbon Nanotubes.* Chemistry of Materials, 2006. **18**(7): p. 1780.
101. Yang, H., Yang, Y., Zou, S., *In Situ Surface-Enhanced Raman Spectroscopic Studies of CO Adsorption and Methanol Oxidation on Ru-Modified Pt Surfaces.* The Journal of Physical Chemistry C, 2007. **111**(51): p. 19058.
102. Surampudi, S., Narayanan, S. R., Vamos, E., Frank, H., Halpert, G., LaConti, A., Kosek, J., Prakash, G. K. Surya, Olah, G. A., *Advances in direct oxidation methanol fuel cells.* Journal of Power Sources, 1994. **47**(3): p. 377.
103. Hamnett A., *Mechanism and electrocatalysis in the direct methanol fuel cell.* Catalysis Today, 1997. **38**(4): p. 445.
104. Ren, X., Zelenay, P., Thomas, S., Davey, J., Gottesfeld, S., *Recent advances in direct methanol fuel cells at Los Alamos National Laboratory.* Journal of Power Sources, 2000. **86**(1-2): p. 111.
105. Baldauf, M., Preidel, W., *Status of the development of a direct methanol fuel cell.* Journal of Power Sources, 1999. **84**(2): p. 161.
106. Liu, H., Song, C., Zhang, L., Zhang, J., Wang, H., Wilkinson, D. P., *A review of anode catalysis in the direct methanol fuel cell.* Journal of Power Sources, 2006. **155**(2): p. 95.
107. Heinzel, A., Barragán, V. M., *A review of the state-of-the-art of the methanol crossover in direct methanol fuel cells.* Journal of Power Sources, 1999. **84**(1): p. 70.
108. Gurau, B., Smotkin, E. S., *Methanol crossover in direct methanol fuel cells: a link between power and energy density.* Journal of Power Sources, 2002. **112**(2): p. 339.
109. Kamarudin, S.K., Daud, W. R. W., Ho, S. L., Hasran, U. A., *Overview on the challenges and developments of micro-direct methanol fuel cells (DMFC).* Journal of Power Sources, 2007. **163**(2): p. 743.
110. Cacciola, G., Antonucci, V., Freni, S., *Technology up date and new strategies on fuel cells.* Journal of Power Sources, 2001. **100**(1-2): p. 67.
111. Cruickshank, J., Scott, K., *The degree and effect of methanol crossover in the direct methanol fuel cell.* Journal of Power Sources, 1998. **70**(1): p. 40.
112. Heinzel, A., Hebling, C., Müller, M., Zedda, M., Müller, C., *Fuel cells for low power applications.* Journal of Power Sources, 2002. **105**(2): p. 250.
113. Kreuer K.D., *On the development of proton conducting polymer membranes for hydrogen and methanol fuel cells.* Journal of Membrane Science, 2001. **185**(1): p. 29.
114. Breen, J.P., Ross, J. R. H., *Methanol reforming for fuel-cell applications: development of zirconia-containing Cu–Zn–Al catalysts.* Catalysis Today, 1999. **51**(3-4): p. 521.
115. Liu, Y., Chen, J., Zhang, W. M., Ma, Z. F., Swiegers, G. F., Too, C. O., Wallace, G. G., *Nano-Pt modified aligned carbon nanotube arrays are efficient, robust, high surface area. Electrocatalysts.* Chemistry of Materials, 2008. **20**(8): p. 2603.

116. Prehn, K., Adelung, R., Heinen, M., Nunes, S. P., Schulte, K., *Catalytically active CNT-polymer-membrane assemblies: From synthesis to application.* Journal of Membrane Science, 2008. **321**(1): p. 123.
117. Pozio, A., De Francesco, M., Cemmi, A., Cardellini, F., Giorgi, L., *Comparison of high surface Pt/C catalysts by cyclic voltammetry.* Journal of Power Sources, 2002. **105**(1): p. 13.
118. Kim, Y.T., Mitani, T., *Surface thiolation of carbon nanotubes as supports: A promising route for the high dispersion of Pt nanoparticles for electrocatalysts.* Journal of Catalysis, 2006. **238**(2): p. 394.
119. Mu, Y.Y., Liang, H. P., Hu, J. S., Jiang, L., Wan, L. J., *Controllable Pt nanoparticle deposition on carbon nanotubes as an anode catalyst for direct methanol fuel cells.* Journal of Physical Chemistry B, 2005. **109**(47): p. 22212.
120. Yang, D.Q., Sun, S. H., Dodelet, J. P., Sacher, E., *A facile route for the self-organized high-density decoration of Pt nanoparticles on carbon nanotubes.* Journal of Physical Chemistry C, 2008. **112**(31): p. 11717.
121. Guo, Y.G., Hu, J. S., Zhang, H. M., Liang, H. P., Wan, L. J., Bai, C. L., *Tin/platinum bimetallic nanotube array and its electrocatalytic activity for methanol oxidation.* Advanced Materials, 2005. **17**(6): p. 746.
122. Tang, H., Chen, J. H., Huang, Z. P., Wang, D. Z., Ren, Z. F., Nie, L. H., Kuang, Y. F., Yao, S. Z., *High dispersion and electrocatalytic properties of platinum on well-aligned carbon nanotube arrays.* Carbon, 2004. **42**(1): p. 191.
123. Ficicioglu, F., Kadirgan, F., *Electrooxidation of methanol on platinum doped polyaniline electrodes: deposition potential and temperature effect.* Journal of Electroanalytical Chemistry, 1997. **430**(1-2): p. 179.
124. Ye, J.H., Fedkiw, P. S., *Electrodeposition of high-surface area platinum in a well adherent Nafion film on glassy carbon.* Electrochimica Acta, 1996. **41**(2): p. 221.
125. Wu, G., Chen, Y. S., Xu, B. Q., *Remarkable support effect of SWNTs in Pt catalyst for methanol electro oxidation.* Electrochemistry Communications, 2005. **7**(12): p. 1237.
126. Tsai, M.C., Yeh, T. K., Juang, Z. Y., Tsai, C. H., *Physical and electrochemical characterization of platinum and platinum-ruthenium treated carbon nanotubes directly grown on carbon cloth.* Carbon, 2007. **45**(2): p. 383.
127. Tang, H., Chen, J. H., Huang, Z. P., Wang, D. Z., Ren, Z. F., Nie, L. H., Kuang, Y. F., Yao, S. Z., *High dispersion and electrocatalytic properties of platinum nanoparticles on graphitic carbon nanofibers (GCNFs).* Journal of Colloid and Interface Science, 2004. **269**(1): p. 26.
128. Xu, Y.H., Lin, X. Q., *Selectively attaching Pt-nano-clusters to the open ends and defect sites on carbon nanotubes for electrochemical catalysis.* Electrochimica Acta, 2007. **52**(16): p. 5140.
129. Guha, A., Lu, W. J., Zawodzinski, T. A., Schiraldi, D. A., *Surface-modified carbons as platinum catalyst support for PEM fuel cells.* Carbon, 2007. **45**(7): p. 1506.
130. Brandl, W., Marginean, G., *Functionalisation of the carbon nanofibres by plasma treatment.* Thin Solid Films, 2004. **447**: p. 181.
131. Moreno-Castilla, C., Ferro-Garcia, M. A., Joly, J. P., Bautista-Toledo, I., Carrasco-Marin, F., Rivera-Utrilla, J., *Activated Carbon Surface Modifications by*

Nitric Acid, Hydrogen Peroxide, and Ammonium Peroxydisulfate Treatments. Langmuir, 1995. **11**(11): p. 4386.

132. Bahr, J.L., Yang, J. P., Kosynkin, D. V., Bronikowski, M. J., Smalley, R. E., Tour, J. M., *Functionalization of Carbon Nanotubes by Electrochemical Reduction of Aryl Diazonium Salts: A Bucky Paper Electrode.* Journal of the American Chemical Society, 2001. **123**(27): p. 6536.
133. Combellas, C., Kanoufi, F., Pinson, J., Podvorica, F. I., *Time-of-flight secondary ion mass spectroscopy characterization of the covalent bonding between a carbon surface and aryl groups.* Langmuir, 2005. **21**(1): p. 280.
134. Wang, C.H., Shih, H. C., Tsai, Y. T., Du, H. Y., Chen, L. C., Chen, K. H., *High methanol oxidation activity of electrocatalysts supported by directly grown nitrogen-containing carbon nanotubes on carbon cloth.* Electrochimica Acta, 2006. **52**(4): p. 1612.
135. Prabhuram, J., Zhao, T. S., Liang, Z. X., Chen, R., *A simple method for the synthesis of PtRu nanoparticles on the multi-walled carbon nanotube for the anode of a DMFC.* Electrochimica Acta, 2007. **52**(7): p. 2649.
136. Tong, Y.Y., Kim, H. S., Babu, P. K., Waszczuk, P., Wieckowski, A., Oldfield, E., *An NMR Investigation of CO Tolerance in a Pt/Ru Fuel Cell Catalyst.* Journal of the American Chemical Society, 2001. **124**(3): p. 468.
137. Frelink, T., Visscher, W., van Veen, J. A. R., *Measurement of the Ru Surface Content of Electrocodeposited PtRu Electrodes with the Electrochemical Quartz Crystal Microbalance: Implications for Methanol and CO Electrooxidation.* Langmuir, 1996. **12**(15): p. 3702.
138. Park, I.S., Lee, K. S., Cho, Y. H., Park, H. Y., Sung, Y. E., *Methanol electro-oxidation on carbon-supported and Pt-modified Au nanoparticles.* Catalysis Today, 2008. **132**(1-4): p. 127.
139. Zhang, J., Sasaki, K., Sutter, E., Adzic, R. R., *Stabilization of Platinum Oxygen-Reduction Electrocatalysts Using Gold Clusters.* Science, 2007. **315**(5809): p. 220.
140. Service, R.F., *Platinum in Fuel Cells Gets a Helping Hand.* Science, 2007. **315**(5809): p. 172.
141. Choi, J.H., Park, K. W., Kwon, B. K., Sung, Y. E., *Methanol Oxidation on Pt/Ru, Pt/Ni, and Pt/Ru/Ni Anode Electrocatalysts at Different Temperatures for DMFCs.* Journal of the Electrochemical Society, 2003. **150**(7): p. A973.
142. Liu, Y., Chen, J., Zhang, W. M., Ma, Z. F., Swiegers, G. F., Too, C. O., Wallace, G. G., *Nano-Pt Modified Aligned Carbon Nanotube Arrays Are Efficient, Robust, High Surface Area Electrocatalysts.* Chemistry of Materials, 2008. **20**(8): p. 2603.
143. Prehn, K., Adelung, R., Heinen, M., Nunes, S. P., Schulte, K., *Catalytically active CNT–polymer-membrane assemblies: From synthesis to application.* Journal of Membrane Science, 2008. **321**(1): p. 123.
144. Wu, G., Chen, Y. S., Xu, B. Q., *Remarkable support effect of SWNTs in Pt catalyst for methanol electrooxidation.* Electrochemistry Communications, 2005. **7**(12): p. 1237-1243.
145. Tang, J.M., Jensen, K., Waje, M., Li, W., Larsen, P., Pauley, K., Chen, Z., Ramesh, P., Itkis, M. E., Yan, Y., Haddon, R. C., *High Performance Hydrogen*

Fuel Cells with Ultralow Pt Loading Carbon Nanotube Thin Film Catalysts†. The Journal of Physical Chemistry C, 2007. **111**(48): p. 17901.

146. Liu, Z., Lin, X., Lee, J. Y., Zhang, W., Han, M., Gan, L. M., *Preparation and Characterization of Platinum-Based Electrocatalysts on Multiwalled Carbon Nanotubes for Proton Exchange Membrane Fuel Cells.* Langmuir, 2002. **18**(10): p. 4054.
147. Gaebler, W., Jacobi, K., Ranke, W., *The structure and electronic properties of thin palladium films on zinc oxide studied by AES and UPS.* Surface Science, 1978. **75**(2): p. 355.
148. Jelic, J., Meyer, R. J., *A DFT study of pseudomorphic monolayer Pt and Pd catalysts for NOx storage reduction applications.* Catalysis Today, 2008. **136**(1-2): p. 76.
149. Lorenz, W.J., Hermann, H. D., Wuthrich, N., Hilbert, F. , *The Formation of Monolayer Metal Films on Electrodes.* Journal of the Electrochemical Society, 1974. **121**(9): p. 1167.
150. Brankovic, S.R., Wang, J. X., Adžić, R. R., *Metal monolayer deposition by replacement of metal adlayers on electrode surfaces.* Surface Science, 2001. **474**(1-3): p. L173.
151. Brunt, T.A., Rayment, T., O'Shea, S. J., Welland, M. E., *Measuring the Surface Stresses in an Electrochemically Deposited Metal Monolayer: Pb on Au(111).* Langmuir, 1996. **12**(24): p. 5942.
152. Herrero, E., Buller, L. J., Abruña, H. D., *Underpotential Deposition at Single Crystal Surfaces of Au, Pt, Ag and Other Materials.* Chemical Reviews, 2001. **101**(7): p. 1897.
153. Chen, C.H., Vesecky, S. M., Gewirth, A. A., *In situ atomic force microscopy of underpotential deposition of silver on gold(111).* Journal of the American Chemical Society, 1992. **114**(2): p. 451.
154. Markovic, N., Ross, P.N., *Effect of anions on the underpotential deposition of Cu on Pt(111) and Pt(100) surfaces.* Langmuir, 1993: p. 580.
155. Kolb, D.M., Przasnyski, M., Gerischer, H., *Underpotential deposition of metals and work function differences.* Journal of Electroanalytical Chemistry and Interfacial Electrochemistry, 1974. **54**(1): p. 25.
156. Hachiya, T., Honbo, H., Itaya, K., *Detailed underpotential deposition of copper on gold(III) in aqueous solutions.* Journal of Electroanalytical Chemistry and Interfacial Electrochemistry, 1991. **315**(1-2): p. 275.
157. Personick, M.L., Langille, M. R., Zhang, J., Mirkin, C. A., *Shape Control of Gold Nanoparticles by Silver Underpotential Deposition.* Nano Letters, 2011. **11**(8): p. 3394.
158. Kim, Y.G., Kim, J. Y., Vairavapandian, D., Stickney, J. L.,, *Platinum Nanofilm Formation by EC-ALE via Redox Replacement of UPD Copper: Studies Using in-Situ Scanning Tunneling Microscopy.* The Journal of Physical Chemistry B, 2006. **110**(36): p. 17998.
159. Wang, R.Y., Wang, C., Cai, W. B., Ding, Y., *Ultralow-Platinum-Loading High-Performance Nanoporous Electrocatalysts with Nanoengineered Surface Structures.* Advanced Materials, 2010. **22**(16): p. 1845.

160. Lima, F., Profeti, D., Chatenet, M., Riello, D., Ticianelli, E., Gonzalez, E., *Electro-oxidation of Ethanol on Rh/Pt and Ru/Rh/Pt Sub-monolayers Deposited on Au/C Nanoparticles.* Electrocatalysis, 2010. **1**(1): p. 72.
161. Adzic, R., Zhang, J., Sasaki, K., Vukmirovic, M., Shao, M., Wang, J., Nilekar, A., Mavrikakis, M., Valerio, J., Uribe, F. , *Platinum Monolayer Fuel Cell Electrocatalysts.* Topics in Catalysis, 2007. **46**(3): p. 249.
162. Liu, P., Ge, X., Wang, R., Ma, H., Ding, Y., *Facile Fabrication of Ultrathin Pt Overlayers onto Nanoporous Metal Membranes via Repeated Cu UPD and in Situ Redox Replacement Reaction.* Langmuir, 2008. **25**(1): p. 561.
163. Eisenberg, R., Gray, H. B., *Preface on making oxygen.* Inorganic Chemistry, 2008. **47**(6): p. 1697.
164. Concepcion, J.J., Jurss, J. W., Brennaman, M. K., Hoertz, P. G., Patrocinio, A. O. T., Iha, N. Y. M., Templeton, J. L., Meyer, T. J., *Making Oxygen with Ruthenium Complexes.* Accounts of Chemical Research, 2009. **42**(12): p. 1954.
165. Gust, D., Moore, T. A., Moore, A. L., *Solar Fuels via Artificial Photosynthesis.* Accounts of Chemical Research, 2009. **42**(12): p. 1890.
166. Hashimoto, A., Ettinger, W. F., Yamamoto, Y., Theg, S. M., *Assembly of Newly Imported Oxygen-Evolving Complex Subunits in Isolated Chloroplasts: Sites of Assembly and Mechanism of Binding.* The Plant Cell Online, 1997. **9**(3): p. 441.
167. Gersten, S.W., Samuels, G. J., Meyer, T. J., *Catalytic-Oxidation of Water by an Oxo-Bridged Ruthenium Dimer.* Journal of the American Chemical Society, 1982. **104**(14): p. 4029.
168. Liu, F., Concepcion, J. J., Jurss, J. W., Cardolaccia, T., Templeton, J. L., Meyer, T. J., *Mechanisms of Water Oxidation from the Blue Dimer to Photosystem II.* Inorganic Chemistry, 2008. **47**(6): p. 1727.
169. Duan, L.L., Fischer, A., Xu, Y. H., Sun, L. C., *Isolated Seven-Coordinate Ru(IV) Dimer Complex with [HOHOH](-) Bridging Ligand as an Intermediate for Catalytic Water Oxidation.* Journal of the American Chemical Society, 2009. **131**(30): p. 10397.
170. Zong, R., Thummel, R. P., *A new family of Ru complexes for water oxidation.* Journal of the American Chemical Society, 2005. **127**(37): p. 12802.
171. Ellis, W.C., McDaniel, N. D., Bernhard, S., Collins, T. J., *Fast water oxidation using iron.* Journal of the American Chemical Society. **132**(32): p. 10990.
172. Geletii, Y.V., Huang, Z. Q., Hou, Y., Musaev, D. G., Lian, T. Q., Hill, C. L., *Homogeneous Light-Driven Water Oxidation Catalyzed by a Tetraruthenium Complex with All Inorganic Ligands.* Journal of the American Chemical Society, 2009. **131**(22): p. 7522.
173. Yin, Q.S., Tan, J. M., Besson, C., Geletii, Y. V., Musaev, D. G., Kuznetsov, A. E., Luo, Z., Hardcastle, K. I., Hill, C. L., *A Fast Soluble Carbon-Free Molecular Water Oxidation Catalyst Based on Abundant Metals.* Science, 2010. **328**(5976): p. 342.
174. Kanan, M.W., Nocera, D. G., *In situ formation of an oxygen-evolving catalyst in neutral water containing phosphate and Co2+.* Science, 2008. **321**(5892): p. 1072.
175. Jiao, F., Frei, H., *Nanostructured Cobalt Oxide Clusters in Mesoporous Silica as Efficient Oxygen-Evolving Catalysts.* Angewandte Chemie-International Edition, 2009. **48**(10): p. 1841.

176. Kanan, M.W., Surendranath, Y., Nocera, D. G., *Cobalt-phosphate oxygen-evolving compound.* Chemical Society Reviews, 2009. **38**(1): p. 109.
177. Yagi, M., et al., *Self-assembly of active IrO2 colloid catalyst on an ITO electrode for efficient electrochemical water oxidation.* Journal of Physical Chemistry B, 2005. **109**(46): p. 21489-21491.
178. Nakagawa, T., Bjorge, N. S., Murray, R. W., *Electrogenerated IrOx Nanoparticles as Dissolved Redox Catalysts for Water Oxidation.* Journal of the American Chemical Society, 2009. **131**(43): p. 15578.
179. Youngblood, W.J., Lee, S. H. A., Maeda, K., Mallouk, T. E., *Visible Light Water Splitting Using Dye-Sensitized Oxide Semiconductors.* Accounts of Chemical Research, 2009. **42**(12): p. 1966.
180. Zhong, D.K., Sun, J. W., Inumaru, H., Gamelin, D. R., *Solar Water Oxidation by Composite Catalyst/alpha-Fe2O3 Photoanodes.* Journal of the American Chemical Society, 2009. **131**(17): p. 6086.
181. Youngblood, W.J., Lee, S. H., Kobayashi, Y., Hernandez-Pagan, E. A., Hoertz, P. G., Moore, T. A., Moore, A. L., Gust, D., Mallouk, T. E., *Photoassisted overall water splitting in a visible light-absorbing dye-sensitized photoelectrochemical cell.* Journal of the American Chemical Society, 2009. **131**(3): p. 926.
182. Metz W. D., *Energy-Storage and Solar Power-Exaggerated Problem* Science, 1978. **200**(4349): p. 1471.
183. Li, X.J., Xiao, Y., Shao, Z. G., Yi, B. L. , *Mass minimization of a discrete regenerative fuel cell (RFC) system for on-board energy storage.* Journal of Power Sources, 2010. **195**(15): p. 4811.
184. Kamel, R.M., Chaouachi, A., Nagasaka, K. , *Wind power smoothing using fuzzy logic pitch controller and energy capacitor system for improvement Micro-Grid performance in islanding mode.* Energy, 2010. **35**(5): p. 2119.
185. Swinnen S., N.V.S., Nguyen M. T. , *Potential hydrogen storage of lithium amidoboranes and derivatives.* Chemical Physics Letters, 2010. **489**(4-6): p. 148.
186. Che, G.L., Lakshmi, B. B., Fisher, E. R. , Martin, C. R., *Carbon nanotubule membranes for electrochemical energy storage and production.* Nature, 1998. **393**(6683): p. 346.
187. Ljunggren S., E.J.C., *The lifetime of a colloid-sized gas bubble in water and the cause of the hydrophobic attraction.* Colloids and Surfaces A: Physicochemical and Engineering Aspects, 1997. **129-130**: p. 151.
188. Ishida N., I., T., Miyahara, M., Higashitani, K., *Nano Bubbles on a Hydrophobic Surface in Water Observed by Tapping-Mode Atomic Force Microscopy.* Langmuir, 2000. **16**(16): p. 6377.
189. Zhang, X.H., Khan, A., Ducker, W. A., *A Nanoscale Gas State.* Physical Review Letters, 2007. **98**(Copyright (C) 2010 The American Physical Society): p. 136101.
190. Connick, R.E., Chia, Y. T., *The Hydrolysis of Chlorine and Its Variation With Temperature* Journal of the American Chemical Society, 1959. **81**(6): p. 1280.
191. Morris, J.C., *The Mechanism of the Hydrolysis of Chlorine.* Journal of the American Chemical Society, 1946. **68**(9): p. 1692.
192. Leaist, D.G., *Absorption of chlorine into water.* Journal of Solution Chemistry, 1986. **15**(10): p. 827.

193. Silov, E.A., Solodusenkov, S. M., *The velocity of hydrolysis of chlorine.* Comptes Rendus De L Academie Des Sciences De L Urss, 1936. **12**: p. 15.
194. Silov, E.A., Kupinskaja, G. V., *On the rate of hydrolysis of chlorine.* Comptes Rendus De L Academie Des Sciences De L Urss, 1935. **7**: p. 222.
195. Tang, A., Sandall, O. C., *Diffusion coefficient of chlorine in water at 25-60 degree C.* Journal of Chemical & Engineering Data, 1985. **30**(2): p. 189.
196. Leaist, D.G., *Isothermal diffusion in aqueous-solutions of chlorine a ternary process* Journal of Physical Chemistry, 1985. **89**(8): p. 1486.
197. Motomizu, S., Takayanagi, T., *Electrophoretic mobility study on ion–ion interactions in an aqueous solution.* Journal of Chromatography A, 1999. **853**(1-2): p. 63.
198. Wang, T.X., Margerum, D. W., *Kinetics of Reversible Chlorine Hydrolysis: Temperature Dependence and General-Acid/Base-Assisted Mechanisms.* Inorganic Chemistry, 1994. **33**(6): p. 1050.
199. Jafvert, C.T., Valentine, R. L., *Reaction scheme for the chlorination of ammoniacal water.* Environmental Science & Technology, 1992. **26**(3): p. 577.
200. McGrath, K.M., Prakash, G. K. S., Olah, G. A., *Direct methanol fuel cells.* Journal of Industrial and Engineering Chemistry, 2004. **10**(7): p. 1063.
201. Li, H.Q., Wang, Y. G., Na, H. T., Liu, H. M., Zhou, H. S., *Rechargeable Ni-Li Battery Integrated Aqueous/Nonaqueous System.* Journal of the American Chemical Society, 2009. **131**(42): p. 15098.
202. Li, Z.J., Yan, W. F., Dai, S., *Surface functionalization of ordered mesoporous carbons - A comparative study.* Langmuir, 2005. **21**(25): p. 11999.
203. Ye, J.L., Liu, J. G., Zhou, Y., Zou, Z. G., Gu, J., Yu, T., *High catalytic performance and stability of Pt/C using acetic acid functionalized carbon.* Journal of Power Sources, 2009. **194**(2): p. 683.
204. Yang, H., Yang, Y., Zou, S., *In situ surface-enhanced Raman spectroscopic studies of CO adsorption and methanol oxidation on Ru-modified Pt surfaces.* Journal of Physical Chemistry C, 2007. **111**(51): p. 19058.
205. D'Amours, M., Belanger, D., *Stability of substituted phenyl groups electrochemically grafted at carbon electrode surface.* Journal of Physical Chemistry B, 2003. **107**(20): p. 4811.
206. Huang, S.D., Liming M., Albert W. H., *Patterned Growth and Contact Transfer of Well-Aligned Carbon Nanotube Films.* The Journal of Physical Chemistry B, 1999. **103**(21): p. 4223.
207. Wilde, P., Mändle, M., Murata, M., Berg, N., *Structural and Physical Properties of GDL and GDL/BPP Combinations and their Influence on PEMFC Performance.* Fuel Cells, 2004. **4**(3): p. 180.
208. Yang, H., Tu, H. C., Chiang, I. L., *Carbon cloth based on PAN carbon fiber practicability for PEMFC applications.* International Journal of Hydrogen Energy, 2010. **35**(7): p. 2791.
209. Murray, E.P., Tsai, T., Barnett, S. A., *A direct-methane fuel cell with a ceria-based anode.* Nature, 1999. **400**(6745): p. 649.
210. Tadanaga, K., Furukawa, Y., Hayashi, A., Tatsumisago, M., *Direct Ethanol Fuel Cell Using Hydrotalcite Clay as a Hydroxide Ion Conductive Electrolyte.* Advanced Materials, 2010. **22**(39): p. 4401.

211. Fu, Q., Li, W. X., Yao, Y. X., Liu, H. Y., Su, H. Y., Ma, D., Gu, X. K., Chen, L. M., Wang, Z., Zhang, H., Wang, B., Bao, X. H., *Interface-Confined Ferrous Centers for Catalytic Oxidation.* Science, 2010. **328**(5982): p. 1141.
212. Iwasita, T., *Electrocatalysis of methanol oxidation* Electrochimica Acta, 2002. **48**(3): p. 289.
213. Sun, S.H., Jaouen, F., Dodelet, J. P., *Controlled Growth of Pt Nanowires on Carbon Nanospheres and Their Enhanced Performance as Electrocatalysts in PEM Fuel Cells.* Advanced Materials, 2008. **20**(20): p. 3900.
214. Mu, Y., Liang, H., Hu, J., Jiang, L., Wan, L., *Controllable Pt Nanoparticle Deposition on Carbon Nanotubes as an Anode Catalyst for Direct Methanol Fuel Cells.* The Journal of Physical Chemistry B, 2005. **109**(47): p. 22212.
215. Silien, C., Lahaye, D., Caffio, M., Schaub, R., Champness, N. R., Buck, M., *Electrodeposition of Palladium onto a Pyridine-Terminated Self-Assembled Monolayer.* Langmuir, 2011. **27**(6): p. 2567.
216. Damian, A., Maroun, F., Allongue, P., *Electrochemical growth and dissolution of Ni on bimetallic Pd/Au(111) substrates.* Electrochimica Acta, 2010. **55**(27): p. 8087.
217. Yang, W., Wang, X. L., Yang, F., Yang, C., Yang, X. R., *Carbon nanotubes decorated with Pt nanocubes by a noncovalent functionalization method and their role in oxygen reduction.* Advanced Materials, 2008. **20**(13): p. 2579.
218. Lee, J.R.I., O'Malley, R. L., O'Connell, T. J., Vollmer, A., Rayment, T., *X-ray absorption spectroscopy characterization of Zn underpotential deposition on Au(111) from phosphate supporting electrolyte.* Electrochimica Acta, 2010. **55**(28): p. 8532.
219. de Oca, M.G.M., Fermin, D. J., *Electrochemical deposition of Te adlayers onto 3D networks of gold nanoparticles.* Electrochimica Acta, 2010. **55**(28): p. 8986.
220. Wu, J., Paudel, K. S., Strasinger, C., Hammell, D., Stinchcomb, A. L., Hinds, B. J., *Programmable transdermal drug delivery of nicotine using carbon nanotube membranes.* Proceedings of the National Academy of Sciences of the United States of America, 2010. **107**(26): p. 11698.
221. Liu, J., Cheng, L., Liu, B., Dong, S., *Covalent Modification of a Glassy Carbon Surface by 4-Aminobenzoic Acid and Its Application in Fabrication of a Polyoxometalates-Consisting Monolayer and Multilayer Films.* Langmuir, 2000. **16**(19): p. 7471.
222. Yang, L., Chen, J., Wei, X., Liu, B., Kuang, Y., *Ethylene diamine-grafted carbon nanotubes: A promising catalyst support for methanol electro-oxidation.* Electrochimica Acta, 2007. **53**(2): p. 777.
223. Deinhammer, R.S., Ho, M., Anderegg, J. W., Porter, M. D., *Electrochemical Oxidation of Amine-Containing Compounds: A Route to the Surface Modification of Glassy-Carbon Electrodes* Langmuir, 1994. **10**(4): p. 1306.
224. Lu, J.P., Albert, M. R., Bernasek, S. L., *The Decopostion of Methanol on the Sulfur Modified Fe (100) Surface.* Surface Science, 1991. **258**(1-3): p. 269.
225. Shulga, O.V., Jefferson, K., Khan, A. R., D'Souza, V. T., Liu, J., Demchenko, A. V., Stine, K. J., *Preparation and Characterization of Porous Gold and Its Application as a Platform for Immobilization of Acetylcholine Esterase.* Chemistry of Materials, 2007. **19**(16): p. 3902.

226. Xu, G.H., Zhang, Q., Zhou, W. P., Huang, J. Q., Wei, F., *The feasibility of producing MWCNT paper and strong MWCNT film from VACNT array.* Applied Physics a-Materials Science & Processing, 2008. **92**(3): p. 531.
227. Kim, Y.A., Muramatsu, H., Hayashi, T., Endo, M., Terrones, M., Dresselhaus, M. S., *Fabrication of high-purity, double-walled carbon nanotube buckypaper.* Chemical Vapor Deposition, 2006. **12**(6): p. 327.
228. Yu, M., Funke, H. H., Falconer, J. L., Noble, R. D., *High Density, Vertically-Aligned Carbon Nanotube Membranes.* Nano Letters, 2008. **9**(1): p. 225.
229. Lewis, N.S., Nocera, D. G., *Powering the planet: Chemical challenges in solar energy utilization.* Proceedings of the National Academy of Sciences of the United States of America, 2006. **103**(43): p. 15729.
230. Turner, J.A., *Sustainable hydrogen production.* Science, 2004. **305**(5686): p. 972.
231. Le Goff, A., Artero, V., Jousselme, B., Tran, P. D., Guillet, N., Metaye, R., Fihri, A., Palacin, S., Fontecave, M., *From Hydrogenases to Noble Metal-Free Catalytic Nanomaterials for H-2 Production and Uptake.* Science, 2009. **326**(5958): p. 1384.
232. Karunadasa, H.I., Chang, C. J., Long, J. R., *A molecular molybdenum-oxo catalyst for generating hydrogen from water.* Nature, 2010. **464**(7293): p. 1329.
233. Yagi, M., Tomita, E., Sakita, S., Kuwabara, T., Nagai, K., *Self-Assembly of Active IrO2 Colloid Catalyst on an ITO Electrode for Efficient Electrochemical Water Oxidation.* The Journal of Physical Chemistry B, 2005. **109**(46): p. 21489.

Vita

Xin Su was born on February 5th 1981 in Fuqing China. He obtained the bachelor degree (Inorganic Nonmmetallic Materials) from Jilin University in 2003 with the scholarships for outstanding student every year. Then he entered to Tsinghua University for master degree (Material Science and Engineering) with scholarships for outstanding graduate every year and performed the research in Dr Zhang's lab. After he got the master degree in 2006, he joined the Dr Hinds' group in University of Kentucky for Ph.D. degree.

1. Xin Su, Ji Wu and Bruce J Hinds, 'Nanoscale bubble valves on CNT membranes for chemical energy storage' on writing to Advanced Materials
2. Xin Su, Xin Zhan and Bruce J Hinds, 'High electrochemical activity of Pt monolayer on bukypaper electrodes' accepted by Journal of Materials Chemistry
3. Xin Su, Ji Wu and Bruce J Hinds, 'Catalytic Activity of Ultrathin Pt Films on Aligned Carbon Nanotube Arrays', Carbon, 2011, 49, 1145.
4. Xin Su, Zhengjun Zhang, and Minmin Zhu, 'Melting and the optical properties of ZnO nanorods', Applied Physics Letters, 2006, 88, 061913.
5. Xin Su, Zhengjun Zhang, Yuquan Wang and Minmin Zhu, 'Synthesis and photoluminescence of aligned ZnO nanorods by thermal decomposition of zinc acetate at a substrate temperature of ~250℃', Journal of Physics D: Applied Physics, 2005, 38, 3934.
6. Xinghua Sun, Xin Su, Ji Wu and Bruce J. Hinds, 'Electrophoretic Transport of Biomolecules through Carbon Nanotube Membranes', Langmuir, 2011, 27, 3150.
7. Navaladian Subramanian, Xin Su, Qing Liu Wu, Bruce Hinds and Stephen E.Rankin, "Preparation and photocatalytical properties of carbon nanotube coated with mesoporous titania thin films", on writing for The Journal of Physical Chemistry C.
8. Chunyu Pan, Zhengjun Zhang, Xin Su, and Ye Zhao, 'Characterization of Fe nanorods grown directly from submicron-sized iron grain by thermal evaporation', Physical Review B, 2004, 70, 233404.
9. Jingguo Liu, Zhengjun Zhang, Xin Su, and Ye Zhao, 'Zinc Nanowires to Zinc Oxide Nanowires: A Low-temperature Process', Journal of Physics D: Applied Physics, 2005, 38, 1068.
10. Jingguo Liu, Zhengjun Zhang, Ye Zhao, Xin Su, and Shuang Liu,' Tuning the field emission properties of tungsten oxide nanorods', Small, 2005, 1, 310-313.
11. Kathryn E. deKrafft, Cheng Wang, Zhigang Xie, Xin Su, Bruce J. Hinds, and Wenbin Lin, 'Electrochemical Water Oxidation with Carbon-Grafted Iridium Complexes' accepted by ACS Applied Materials & Interfaces.
12. Jingguo Liu, Zhengjun Zhang, Chunyu Pan, Ye Zhao, Xin Su, Ya Zhou, Dapeng Yu, 'Enhanced field emission properties Of MoO_2 nanorods with controllable shape and orientation' , Materials. Letters. 2004, 58 (29), 3812-3815.